AD-A170 072 COMPUTATIONAL ASPECTS OF THE ARA THREE INVARIANT CONSTITUTIVE MODEL(U) APPLIED RESEARCH ASSOCIATES INC ALBUQUERQUE NM W C DASS ET AL. 29 MAY 86 5934 1/2

UNCLASSIFIED AFOSR-TR-86-0463 F49620-84-C-0066 F/G 8/13 NL

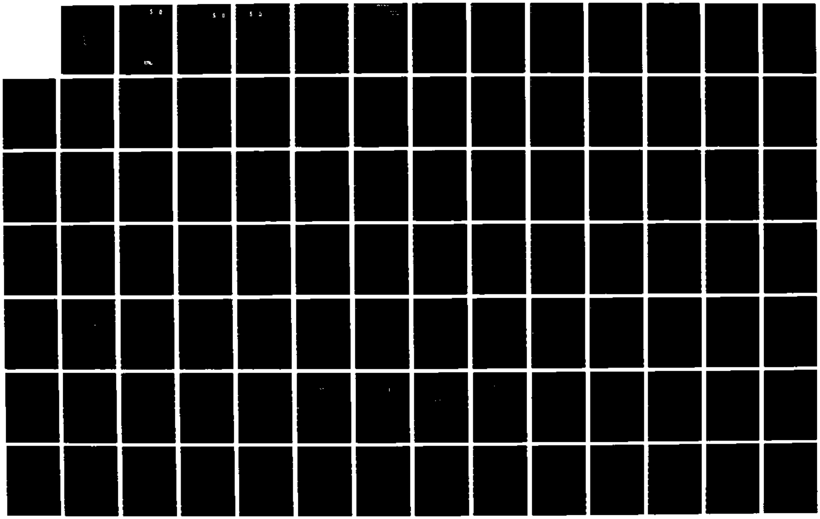

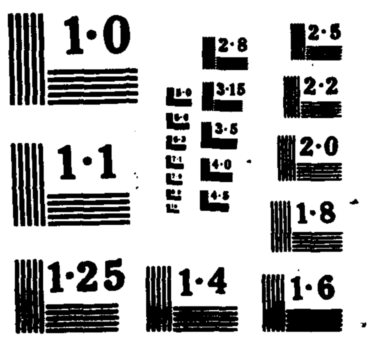
1·0
2·8
2·5
3·15
2·2
3·5
2·0
1·1
4·0
4·5
1·8
1·25
1·4
1·6

AFOSR-TR- 86-0463

DTIC
ELECTE
JUL 24 1986
S D
D

COMPUTATIONAL ASPECTS OF THE ARA
THREE INVARIANT CONSTITUTIVE MODEL

AD-A170 072

DTIC FILE COPY

Approved for public release;
distribution unlimited.

APPLIED RESEARCH ASSOCIATES, INC.

Engineering and Applied Science

86 7 23 244

(2)

COMPUTATIONAL ASPECTS OF THE ARA THREE INVARIANT CONSTITUTIVE MODEL

By

William C. Dass
Douglas H. Merkle

May 1986

Applied Research Associates, Inc.
4300 San Mateo Blvd., NE, Suite A220
Albuquerque, New Mexico 87110

Prepared for

Air Force Office of Scientific Research
Bolling Air Force Base
Washington, DC 20332

Final Report

Contract No. F49620-84-C-0066

UNCLASSIFIED
SECURITY CLASSIFICATION OF THIS PAGE

REPORT DOCUMENTATION PAGE

Form Approved
OMB No. 0704-0188
Exp. Date: Jun 30, 1986

1a. REPORT SECURITY CLASSIFICATION: UNCLASSIFIED

1b. RESTRICTIVE MARKINGS:

2a. SECURITY CLASSIFICATION AUTHORITY:

2b. DECLASSIFICATION/DOWNGRADING SCHEDULE:

3. DISTRIBUTION/AVAILABILITY OF REPORT: DISTRIBUTION STATEMENT A — Approved for public release; Distribution Unlimited

4. PERFORMING ORGANIZATION REPORT NUMBER(S): 5934

5. MONITORING ORGANIZATION REPORT NUMBER(S): AFOSR-TR- 86-0463

6a. NAME OF PERFORMING ORGANIZATION: Applied Research Associates, Inc.

6b. OFFICE SYMBOL (If applicable):

7a. NAME OF MONITORING ORGANIZATION: Air Force Office of Scientific Research/NA

6c. ADDRESS (City, State, and ZIP Code): 4300 San Mateo Blvd., NE, Suite A220, Albuquerque, NM 87110

7b. ADDRESS (City, State, and ZIP Code): Bolling AFB, DC 20332

8a. NAME OF FUNDING/SPONSORING ORGANIZATION: AFOSR

8b. OFFICE SYMBOL (If applicable): NA

9. PROCUREMENT INSTRUMENT IDENTIFICATION NUMBER: Contract F49620-84-C-0066

8c. ADDRESS (City, State, and ZIP Code): Bolling AFB, DC 20332

10. SOURCE OF FUNDING NUMBERS

PROGRAM ELEMENT NO	PROJECT NO	TASK NO	WORK UNIT ACCESSION NO
61102F	2307	C1	

11. TITLE (Include Security Classification): Computational Aspects of the ARA Three-Invariant Constitutive Model (U)

12. PERSONAL AUTHOR(S): Dass, William C., and Merkle, Douglas H.

13a. TYPE OF REPORT	13b. TIME COVERED	14. DATE OF REPORT (Year, Month, Day)	15. PAGE COUNT
Final	FROM 840801 TO 850731	860529	124

16. SUPPLEMENTARY NOTATION:

17. COSATI CODES

FIELD	GROUP	SUB-GROUP

18. SUBJECT TERMS (Continue on reverse if necessary and identify by block number): Constitutive Models; Dry Alluvium; Soil Dynamics; Wave Propagation; Finite Difference Calculations

19. ABSTRACT (Continue on reverse if necessary and identify by block number)

The three invariant elasto-plastic constitutive model developed by Applied Research Associates, Inc. (ARA) has been implemented for use in finite difference blast and shock calculations. The model employs two yield surfaces with an independent plastic potential to control shear-induced dilatancy. The model is conceptually similar to Lade's cohesionless soil model. Several improvements in the original ARA model have been incorporated during the course of implementation including tensile strength, expansive strain tracking during tensile failure, optional elimination of work-softening, and a high pressure-temperature equation of state. Strain subcycling has been used to prevent violation of the consistency condition. Results are given for planar, spherical, and cylindrical one-dimensional wave propagation, and are compared with results using several other currently available constitutive models. Two dimensional DIHEST calculation results are also shown. These calculations employed a newly developed interface between the Soil Element Model (SEM) subroutines and STEALTH 2D. This approach allows the SEM to act as a central bank of

20. DISTRIBUTION/AVAILABILITY OF ABSTRACT: ☐ UNCLASSIFIED/UNLIMITED ☒ SAME AS RPT ☐ DTIC USERS

21. ABSTRACT SECURITY CLASSIFICATION: UNCLASSIFIED

22a. NAME OF RESPONSIBLE INDIVIDUAL: Lt. Col. Lawrence D. Hokanson

22b. TELEPHONE (Include Area Code): (202) 767-4934

22c. OFFICE SYMBOL: AFOSR/NA

DD FORM 1473, 84 MAR — 83 APR edition may be used until exhausted. All other editions are obsolete.

SECURITY CLASSIFICATION OF THIS PAGE
UNCLASSIFIED

19. ABSTRACT (Continued)

material models for potentially any number of continuum codes. Overall, the new constitutive model is physically realistic, somewhat expensive to run, and promising for future application. Steps which remain to make the model more useful in practice include parameter sensitivity studies to help dynamic insitu behavior prediction, improved algorithms for eliminating numerical errors, a rezoning procedure, and more two-dimensional calculational experience.

UNCLASSIFIED

SECURITY CLASSIFICATION OF THIS PAGE

AD-A170 072

REPORT DOCUMENTATION PAGE

Form Approved
OMB No. 0704-0188
Exp. Date: Jun 30, 1986

1a. REPORT SECURITY CLASSIFICATION: UNCLASSIFIED	1b. RESTRICTIVE MARKINGS
2a. SECURITY CLASSIFICATION AUTHORITY	3. DISTRIBUTION/AVAILABILITY OF REPORT: DISTRIBUTION STATEMENT A. Approved for public release; Distribution Unlimited
2b. DECLASSIFICATION/DOWNGRADING SCHEDULE	
4. PERFORMING ORGANIZATION REPORT NUMBER(S): 5934	5. MONITORING ORGANIZATION REPORT NUMBER(S)
6a. NAME OF PERFORMING ORGANIZATION: Applied Research Associates, Inc. — 6b. OFFICE SYMBOL (If applicable)	7a. NAME OF MONITORING ORGANIZATION: Air Force Office of Scientific Research/NA
6c. ADDRESS (City, State, and ZIP Code): 4300 San Mateo Blvd., NE, Suite A220, Albuquerque, NM 87110	7b. ADDRESS (City, State, and ZIP Code): Bolling AFB, DC 20332
8a. NAME OF FUNDING/SPONSORING ORGANIZATION: AFOSR — 8b. OFFICE SYMBOL (If applicable): NA	9. PROCUREMENT INSTRUMENT IDENTIFICATION NUMBER: Contract F49620-84-C-0066
8c. ADDRESS (City, State, and ZIP Code): Bolling AFB, DC 20332	10. SOURCE OF FUNDING NUMBERS

PROGRAM ELEMENT NO	PROJECT NO	TASK NO.	WORK UNIT ACCESSION NO
61102F	2307	C1	

11. TITLE (Include Security Classification): Computational Aspects of the ARA Three-Invariant Constitutive Model (U)

12. PERSONAL AUTHOR(S): Dass, William C., and Merkle, Douglas H.

13a. TYPE OF REPORT	13b. TIME COVERED	14. DATE OF REPORT (Year, Month, Day)	15. PAGE COUNT
Final	FROM 840801 TO 850731	860529	124

16. SUPPLEMENTARY NOTATION

17. COSATI CODES		
FIELD	GROUP	SUB-GROUP

18. SUBJECT TERMS (Continue on reverse if necessary and identify by block number): Constitutive Models; Dry Alluvium; Soil Dynamics; Wave Propagation; Finite Difference Calculations

19. ABSTRACT (Continue on reverse if necessary and identify by block number)

The three invariant elasto-plastic constitutive model developed by Applied Research Associates, Inc. (ARA) has been implemented for use in finite difference blast and shock calculations. The model employs two yield surfaces with an independent plastic potential to control shear-induced dilatancy. The model is conceptually similar to Lade's cohesionless soil model. Several improvements in the original ARA model have been incorporated during the course of implementation including tensile strength, expansive strain tracking during tensile failure, optional elimination of work-softening, and a high pressure-temperature equation of state. Strain subcycling has been used to prevent violation of the consistency condition. Results are given for planar, spherical, and cylindrical one-dimensional wave propagation, and are compared with results using several other currently available constitutive models. Two dimensional DIHEST calculation results are also shown. These calculations employed a newly developed interface between the Soil Element Model (SEM) subroutines and STEALTH 2D. This approach allows the SEM to act as a central bank of

20. DISTRIBUTION/AVAILABILITY OF ABSTRACT: ☐ UNCLASSIFIED/UNLIMITED ☒ SAME AS RPT ☐ DTIC USERS	21. ABSTRACT SECURITY CLASSIFICATION: UNCLASSIFIED
22a. NAME OF RESPONSIBLE INDIVIDUAL: Lt. Col. Lawrence D. Hokanson	22b. TELEPHONE (Include Area Code): (202) 767-4934 — 22c. OFFICE SYMBOL: AFOSR/NA

DD FORM 1473, 84 MAR — 83 APR edition may be used until exhausted. All other editions are obsolete.

SECURITY CLASSIFICATION OF THIS PAGE

UNCLASSIFIED

19. ABSTRACT (Continued)

material models for potentially any number of continuum codes. Overall, the new constitutive model is physically realistic, somewhat expensive to run, and promising for future application. Steps which remain to make the model more useful in practice include parameter sensitivity studies to help dynamic insitu behavior prediction, improved algorithms for eliminating numerical errors, a rezoning procedure, and more two-dimensional calculational experience.

PREFACE

This report is the fifth in a series of reports on constitutive modeling by Applied Research Associates, Inc. (ARA) which have been funded by the Air Force Office of Scientific Research (AFOSR). The research described by these reports and other publications has been directed toward improved calculational modeling of soils under complex dynamic loadings, specifically those produced by explosive sources. The following summary of these ARA reports is intended to provide background and perspective for the current report.

The first report [Dass, Bratton, and Higgins (1981)] was primarily a review of constitutive modeling requirements for dynamic modeling of soil behavior. A literature review of existing models was presented to show which models or parts of models might be applied to the specific problem of explosive loadings. The Soil Element Model (SEM), a utility computer program used to study and develop material models, was also introduced. The second report [Dass, Merkle, and Bratton (1983)] dealt with the capability of several selected models to predict the behavior of soils under one-dimensional planar, cylindrical, and spherical geometry explosive loadings. The important behavioral differences between models whose parameters were fit to laboratory data and those fit to insitu data were illustrated. The third report [Merkle and Dass (1983)] focused on modeling the dynamic response of saturated soil and a review of some widely-applied plasticity concepts. It provided substantial theoretical background toward development of an improved constitutive model, described in the fourth report [Merkle and Dass (1985)]. The new model was based on work by Lade at UCLA with improvements aimed at better response in a single-phase finite difference calculation of explosively-driven wave propagation. In the fourth report, the detailed theoretical background of this model and important aspects of several other models were presented, and its single-element behavior was directly compared, using the SEM, to other models currently in use in the ground shock community.

This report describes the first calculational tests of the new model (now referred to as the ARA Three-Invariant Model) for one- and two-dimensional wave propagation. It addresses many of the computational issues which need to be considered when fully implementing a constitutive model. The theory behind the model is not presented in detail and the reader may find it necessary to consult the previous reports, particularly the fourth report, for additional background information.

TABLE OF CONTENTS

LIST OF FIGURES

LIST OF FIGURES (Continued)

LIST OF TABLES

1.0 INTRODUCTION

The area of constitutive modeling in soil mechanics and dynamics has evolved to the point where many kinds of models have been proposed, fewer have been implemented, and still fewer are actually being used. There are several reasons for this:

(1) Models which have been around for a while are used more often because they are familiar, ready to use, their limitations are known, and organizations have developed an experience base over the course of many projects.

(2) Complicated models are harder to understand and therefore it is often hard to attach physical significance to their features and parameters.

(3) When implemented, complex models sometimes do not produce appreciably better calculated results.

(4) Involved laboratory testing for determining model parameters is beyond the scope of many projects.

By way of analogy, the selection of a constitutive model for use in an engineering calculation can be compared to the purchase of an automobile. The engineer is faced with choices, many of which are similar to those faced by the car-buyer (see Table 1). The actual choice usually boils down to budget, prior experience, or the advice of a helpful friend. For a model to gain acceptance in the marketplace, the model developer must be aware of what model-users are looking for and what they need.

The purpose of this research has been to test a material model (developed under a prior AFOSR contract) in much the same fashion as a car manufacturer would test a new model before making it available to the consumer. The model has been taken over some bumpy calculational roads to be sure the doors won't fall off in the process. Its usability and speed have been tested and compared with some other models.

The result is a model with no known bugs, some improvements, and initial computational experience. The model's future now depends to a large degree on its attractiveness to potential consumers (i.e., calculators). Many of its features have never, to the authors' knowledge, actually been implemented in calculations of blast effects. There is promise that this model will produce better calculations of dynamic problems involving complex loading paths.

TABLE 1. PARALLELS IN MODEL EVALUATION

Choosing An Automobile[1]		Choosing A Constitutive Model	
Performance	Fuel Economy Driveability Acceleration Braking Handling/Roadholding	Computer Funds Economy Useability Speed Theoretical Soundness Predictive Accuracy	Performance
Driver	Driving Position Instruments/Controls Visibility Heating/Ventilation	Installed in Right Code Parameter Determination Physical Insight into Model Source for Help in Problems	User
Passenger	Seat Comfort Passenger Room Ride Noise	Confidence in Model Physical Insight into Model Quality of Results Model Induced Errors	Client
Convenience	Entry/Exit Cargo Room Serviceability Equipment	Learning Time Expandability Serviceability Available Behavioral Features	Convenience
Workmanship	Body Construction Paint/Exterior Interior	Model Construction Implementation Coding Simplicity/Accuracy	Workmanship

[1] Consumer Guide: 1985 Cars, Publications International, Ltd., 1985, p. 376.

2.0 ARA THREE INVARIANT MODEL

2.1 Model Background

The ARA three invariant model was developed by Applied Research Associates, Inc. (ARA) under funding from the Air Force Office of Scientific Research (AFOSR). The model is described in detail and compared with several other models under laboratory loading conditions by Merkle and Dass (1985). The model owes its beginnings and concept to a plasticity model developed by Lade and Nelson (1981) at UCLA. The ARA model is called a three invariant model because the controlling surfaces in principal stress space are functions of three independent stress invariants (octahedral normal and shear stress and Lode's angle). Figure 1 shows several views of the model's surfaces.

The ARA model is a strain hardening/softening elastoplastic model with two independent yield surfaces, one associative and the other nonassociative. The compressive yield surface is an ellipsoid with its center at the origin in principal stress space. It is associative, only strain hardens, and the strain hardening parameter is the corresponding plastic work. The expansive yield surface is a hyperboloid with its apex on the hydrostatic axis in principal stress space. It is nonassociative, both strain hardens and softens, and the strain hardening/softening parameter is the corresponding plastic work. The expansive plastic potential surface is also a hyperboloid.

The ARA model computational strategy involves four independent conditions for each yield surface:

(1) Yield Condition - This is a necessary, but not sufficient condition for yielding to occur.

(2) Flow Rule - If yielding occurs, the plastic strain increment is normal to the plastic potential surface.

(3) Consistency Condition - If yielding occurs, the yield condition must be satisfied throughout yielding.

(4) Dissipation Condition - Yielding must generate positive plastic work.

The basic equations of the ARA model without tensile strength are given below. The compressive yield criterion is

$$f_c = f'_c - f''_c = 0 \qquad (1)$$

where

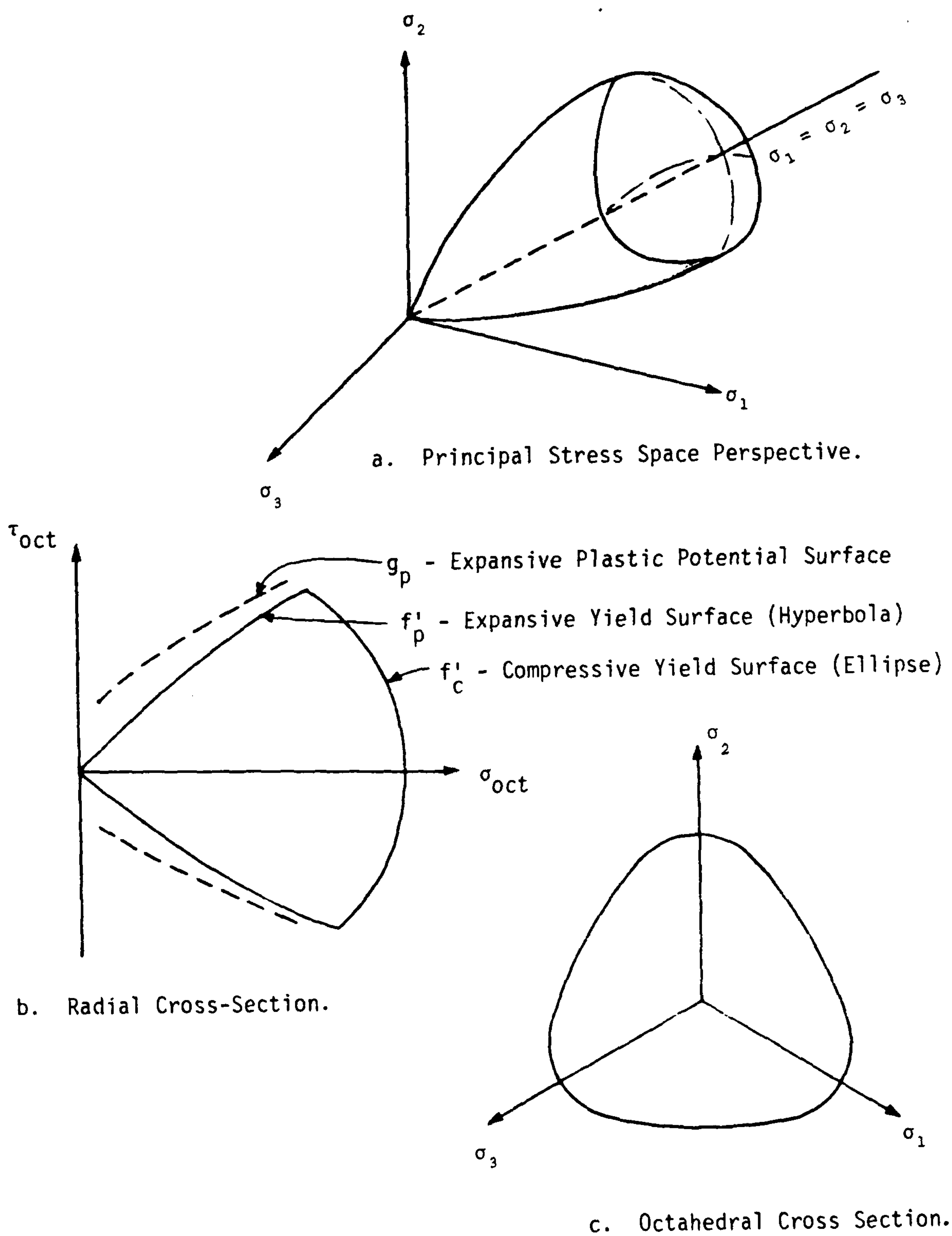

Figure 1. ARA Three-Invariant Model Yield and Plastic Potential Surfaces.

$$f'_c = 3(\sigma^2_{oct} + r^2\, \tau^2_{oct}) \qquad (2)$$

$$f''_c = P_a{}^2 \left(\frac{W_c}{C\, P_a}\right)^{1/P} \qquad (3)$$

where f'_c = compressive yield stress function, f''_c = compressive yield hardening function, σ_{oct} = octahedral normal stress, τ_{oct} = octahedral shear stress, P_a = atmospheric pressure, W_c = compressive plastic work (defined below), and r, C, P = model parameters. The compressive flow rule is

$$\{d\varepsilon_c\} = d\lambda_c \left\{\frac{\partial f'_c}{\partial \sigma}\right\} \qquad (4)$$

where $\{d\varepsilon_c\}$ = column vector of compressive plastic strain increments, $d\lambda_c$ = compressive yield proportionality constant, $\{\sigma\}$ = column vector of effective stress components. The compressive plastic work increment is

$$dW_c = \{\sigma\}^T \{d\varepsilon_c\} > 0 \qquad (5)$$

The expansive yield criterion is

$$f_p = f'_p - f''_p = 0 \qquad (6)$$

where

$$f'_p = \left(\frac{\tau_{oct}}{P_a}\right) (1 - E \cos 3\omega) \left(\frac{P_a}{\tau_{oct}} + m\right) \qquad (7)$$

$$f''_p = a\, e^{-bW_p} \left(\frac{W_p}{P_a}\right)^{1/q} \qquad (8)$$

$$f''_{p,max} = \eta_1 \qquad (9)$$

where ω = Lode's angle, and E, m, η_1, a, b, q = model parameters. The expansive flow rule is

$$\{d\varepsilon_p\} = d\lambda_p \left\{\frac{\partial g_p}{\partial \sigma}\right\} \qquad (10)$$

where $\{d\varepsilon_p\}$ = column vector of expansive plastic strain increments, $d\lambda_p$ = expansive yield proportionality constant. The expansive plastic potential function is

$$g_p = \left(\frac{\tau_{oct}}{P_a}\right)(1 - E\cos 3\omega) - \frac{\eta_2\left(\frac{\sigma_{oct}}{P_a}\right)}{1 + m\left(\frac{\sigma_{oct}}{P_a}\right)} \tag{11}$$

where η_2 = model parameter. The expansive plastic work increment is

$$dW_p = \{\sigma\}^T \{d\varepsilon_p\} > 0 \tag{12}$$

The effective stress increments are determined by the elastic strain increments

$$\{d\sigma\} = \underline{C}_e \{d\varepsilon_e\} \tag{13}$$

where

$$\{d\varepsilon_e\} = \{d\varepsilon\} - \{d\varepsilon_c\} - \{d\varepsilon_p\} \tag{14}$$

where $\underline{C}_e$ = elastic stiffness matrix, $\{d\varepsilon_e\}$ = column vector of elastic strain increments, and $\{d\varepsilon\}$ = column vector of total strain increments.

2.2 Low Stress Improvements

During the course of the continuum code checkout, the ARA model was improved in several ways. One of the improvements is an option for tensile strength (cohesion). Originally, the expansive failure surface had its apex at the origin in principal stress space. This precluded modeling tensile strength, which is exhibited by some soils and most rocks. Tension capacity was added by shifting the entire model down the hydrostatic axis, as shown in Figure 2.

The new equation for the expansive yield surface is then

$$f_p' = \left(\frac{\tau_{oct}}{P_a}\right)(1 - E\cos 3\omega)\left(\frac{P_a}{\sigma_{oct}+T} + m\right) \tag{15}$$

where T is tensile strength measured along the octahedral normal stress axis. The revised equation for the expansive plastic potential is

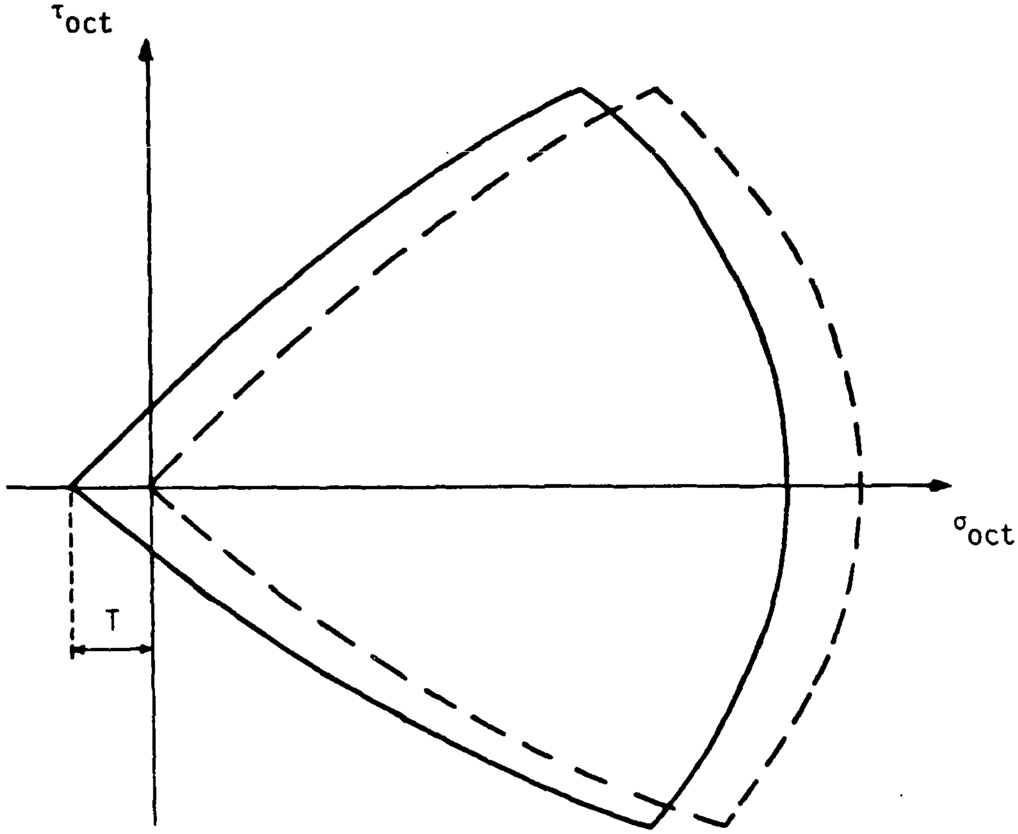

Figure 2. Introduction of Tensile Strength.

$$g_p = \left(\frac{\tau_{oct}}{P_a}\right) (1 - E \cos 3\omega) - \frac{\eta_2 \left(\frac{\sigma_{oct}+T}{P_a}\right)}{1+m \left(\frac{\sigma_{oct}+T}{P_a}\right)} \tag{16}$$

The compressive yield surface is also shifted:

$$f_c' = 3(\sigma_{oct} + T)^2 + 3\, r^2\, \tau_{oct}^2 \tag{17}$$

The net effect is a simple translation of the principal stress axes. Equations which involve the derivatives of the above quantities are also affected and have been modified.

Figure 3 compares the response of the model using zero tension capacity with that using 2.0 MPa tension capacity for an element exercised along an arbitrary strain path. The strain path is representative of those experienced in spherical wave propagation [Akers (1985)].

When soil is subjected to large tensile strains, the soil particles separate and the material behaves less and less like a continuum as large voids develop. This kind of behavior is modeled in the ARA model by tracking the total volume strain which occurs while the element is failed in tension. An element is not allowed to rejoin (develop compressive stress) until the volumetric strain is equal to that at which tensile failure occurred. Specifically, the strain tracked is

$$\epsilon_{spall} = \epsilon_1 + \epsilon_2 + \epsilon_3 \tag{18}$$

While the material is in a spalled condition, each principal stress is set equal to -T, and all shear stresses are set equal to zero. Thus, the stress point remains at the apex of the expansive yield surface and rejoin always initiates from this point. Figure 4 shows the behavior of an element which has failed in tension (using the same strain path shown in Figure 3) and is then forced to rejoin under subsequent uniaxial loading ($\epsilon_1 = \epsilon_3 = 0$, ϵ_2 = compressive).

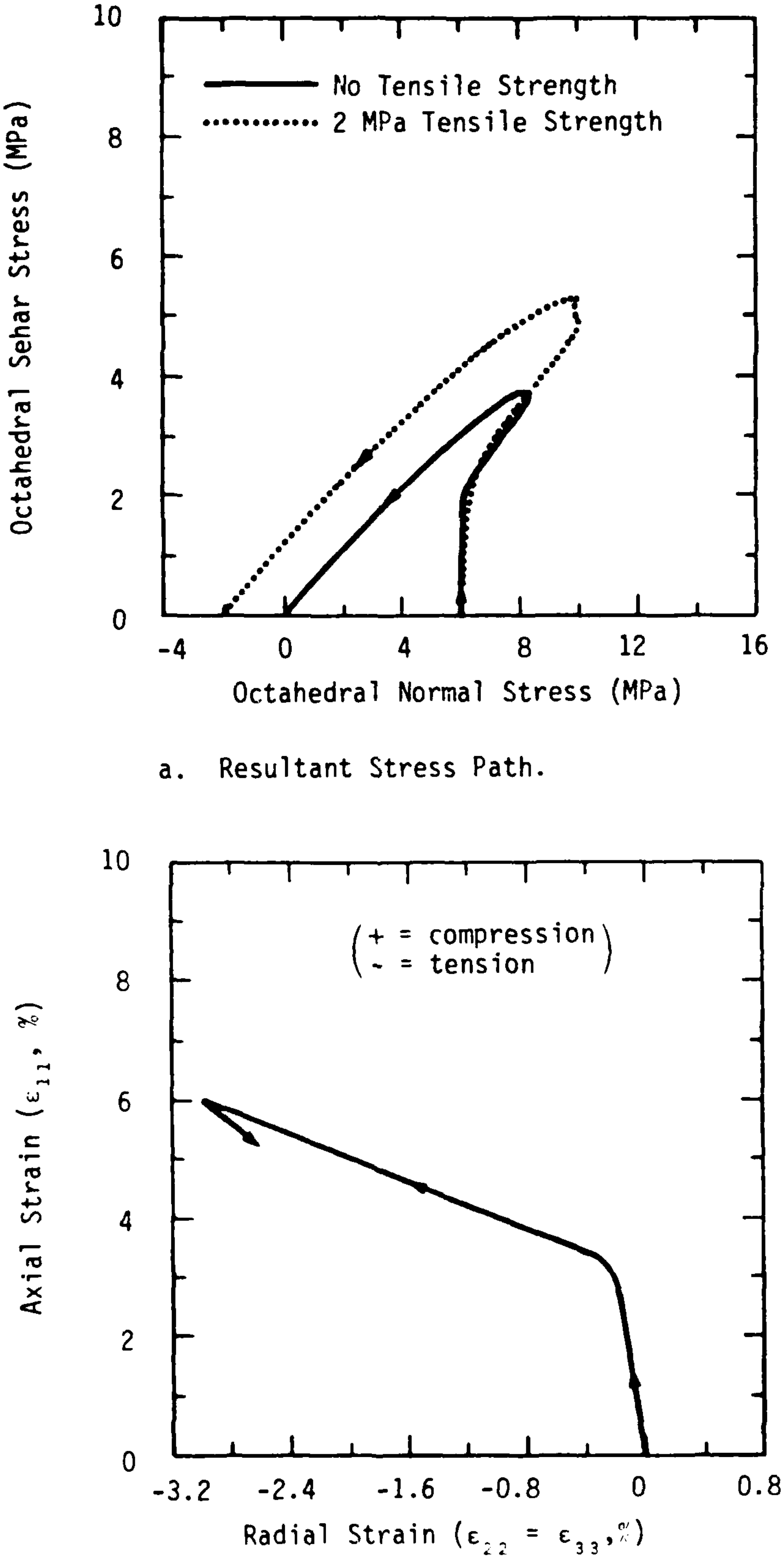

a. Resultant Stress Path.

b. Input Strain Path.

Figure 3. Effect of Tensile Capacity on Stress Path Response.

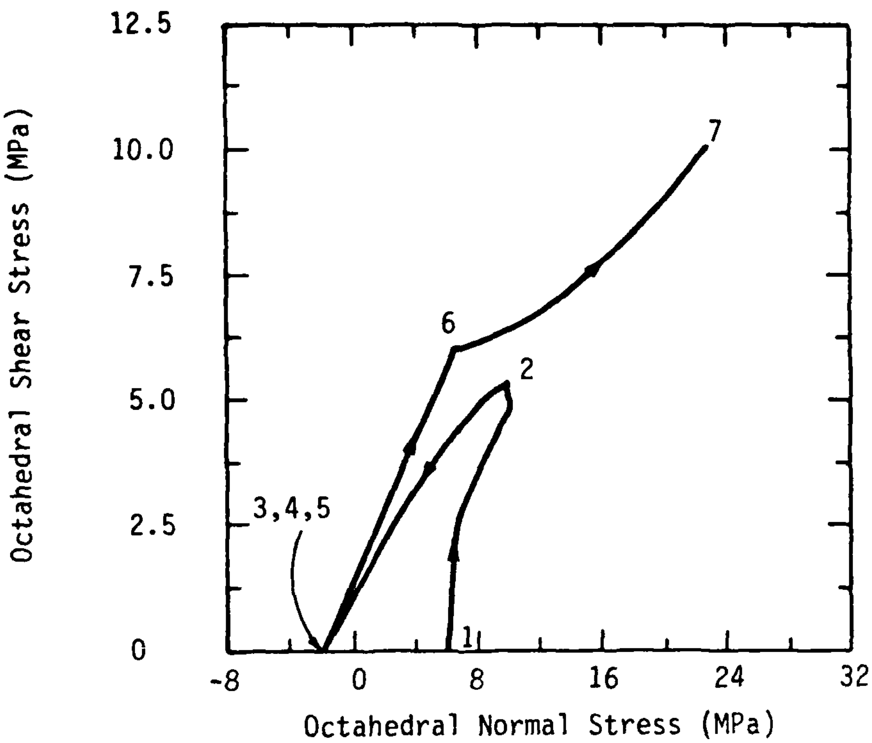

a. Stress Path Response.

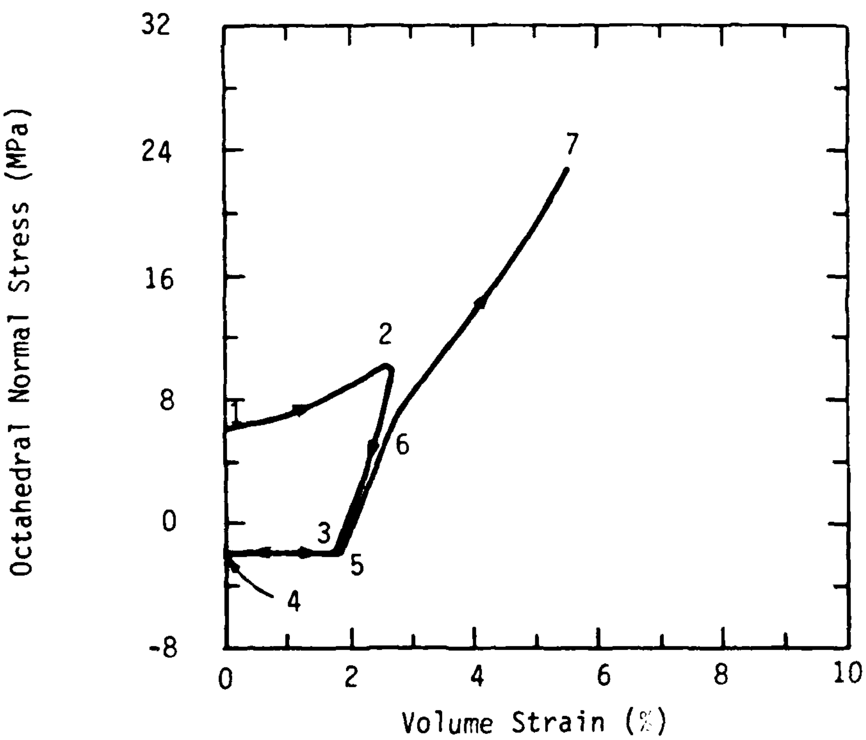

b. Pressure-Volume Response.

Figure 4. Tensile Failure Followed by Forced Rejoin.

2.3 High Stress Improvements

Another substantial improvement to the ARA model is the addition of an equation of state for the high pressure and temperature regime. This allows the model to be used very near an explosive source where melting and/or vaporization may be important phenomena. The form of the high pressure equation of state adopted for the ARA model has seen widespread use in the ground shock community. Its development here essentially follows that given by Shuster and Isenberg (1972) and Schuster (1981). At lower stresses (below the initiation of melting) material behavior is controlled by the ARA three invariant model.

The high pressure equation of state computes the hydrostatic component of effective stress, P, as a function of specific internal energy, E, and elastic volumetric strain ε_{ve}. Specific internal energy is the difference between heat added to a material and elastic volumetric work done by it, per unit mass. The First Law of Thermodynamics yields

$$dE = dQ - P\, dV_e \qquad (19)$$

where dQ = increment of heat added to the substance, per unit mass and dV_e = elastic increment of specific volume. The volumetric strain is given by the expression

$$\varepsilon_v = \frac{V_o - V}{V_o} = 1 - \frac{V}{V_o} = 1 - \rho_o V \qquad (20)$$

so that

$$dV_e = - \frac{1}{\rho_o} d\varepsilon_{ve} \qquad (21)$$

and therefore substitution of Equation (21) into Equation (19) yields

$$dE = dQ + \frac{P}{\rho_o} d\varepsilon_{ve} \qquad (22)$$

For an initial internal energy deposition at constant volume, Equation (22) yields

$$dE = dQ \qquad (23)$$

and during subsequent adiabatic deformation, Equation (22) yields

$$dE = \frac{P}{\rho_0} d\varepsilon_{ve} \tag{24}$$

The hydrostatic stress, P, is assumed to be the sum of a solid/liquid pressure, σ, plus a vapor pressure, p,

$$P = \sigma + p \tag{25}$$

where the vapor pressure, p, remains zero until the specific internal energy, E, reaches the value, E_m, required to initiate melting. When $E > E_m$, an increase in E contributes to the heat of fusion (melting) and vaporization, as well as to increases in both σ and p.

Because elastic volumetric strain, ε_{ve}, and specific internal energy, E, are the two variables which determine the solid/liquid pressure, σ, we can write

$$d\sigma = \left(\frac{\partial\sigma}{\partial\varepsilon_{ve}}\right)_E d\varepsilon_{ve} + \left(\frac{\partial\sigma}{\partial E}\right)_{\varepsilon_{ve}} dE \tag{26}$$

The first partial derivative in Equation (26) is the isothermal elastic bulk modulus, K,

$$K = \left(\frac{\partial\sigma}{\partial\varepsilon_{ve}}\right)_E \tag{27}$$

The second partial derivative in Equation (26) is the rate of increase of solid/liquid pressure with respect to specific internal energy at constant elastic volumetric strain. It can be expressed in terms of familiar quantities by noting that the condition of constant elastic volumetric strain can be expressed in the form

$$d\varepsilon_{ve} = \left(\frac{\partial\varepsilon_{ve}}{\partial\sigma}\right)_E d\sigma + \left(\frac{\partial\varepsilon_{ve}}{\partial E}\right)_\sigma dE = 0 \tag{28}$$

where Equation (27) yields

$$\left(\frac{\partial\varepsilon_{ve}}{\partial\sigma}\right)_E = \frac{1}{K} \tag{29}$$

and also

$$\left(\frac{\partial \varepsilon_{ve}}{\partial E}\right)_\sigma = \left(\frac{\partial \varepsilon_{ve}}{\partial T}\right)_\sigma \left(\frac{\partial T}{\partial E}\right)_\sigma = - \frac{\alpha_p}{C_p} \tag{30}$$

where T = temperature, and

$$\alpha_p = - \left(\frac{\partial \varepsilon_{ve}}{\partial T}\right)_\sigma \tag{31}$$

$$C_p = \left(\frac{\partial E}{\partial T}\right)_\sigma \tag{32}$$

The quantity α_p is the coefficient of thermal expansion at constant pressure, and the quantity C_p is the specific heat at constant pressure. Substitution of Equations (29) and (30) into Equation (28) yields

$$\frac{1}{K} d\sigma - \frac{\alpha_p}{C_p} dE = 0 \tag{33}$$

so that

$$\left(\frac{\partial \sigma}{\partial E}\right)_{\varepsilon_{ve}} = \frac{K \alpha_p}{C_p} \tag{34}$$

For an initial energy deposition at constant volume, substitution of Equation (34) into Equation (26) yields

$$d\sigma = \frac{K \alpha_p}{C_p} dE = K \, d\varepsilon_{ve}^{*} \tag{35}$$

where

$$d\varepsilon_{ve}^{*} = \frac{\alpha_p}{C_p} dE \tag{36}$$

During subsequent adiabatic deformation prior to melting, substitution of Equations (24), (25), (27), and (34) into Equation (26) yields

$$d\sigma = K \, d\varepsilon_{ve} + \frac{K \alpha_p}{C_p} \frac{\sigma}{\rho_0} d\varepsilon_{ve} = K \left[1 + \left(\frac{\alpha_p}{C_p \rho_0}\right) \sigma\right] d\varepsilon_{ve} \tag{37}$$

When $E > E_m$, the vapor pressure, p, is calculated by an expression similar to that for adiabatic compression of a perfect gas, for which

$$pV^{\gamma} = k \tag{38}$$

where

$$\gamma = \frac{C_p}{C_V} \tag{39}$$

C_V = specific heat at constant volume and k = constant. Now under adiabatic conditions,

$$dE = - p\ dV = - pV^{\gamma} \frac{dV}{V^{\gamma}} = - k \frac{dV}{V^{\gamma}} \tag{40}$$

so that

$$E = \int dE = - k \int_{\infty}^{V} \frac{dx}{X^{\gamma}} = - k \left[\frac{x^{-\gamma+1}}{-\gamma+1} \right]_{\infty}^{V} = \frac{pV}{\gamma-1} \tag{41}$$

and therefore

$$p = (\gamma-1)\ \rho\ E \tag{42}$$

The expression used to calculate the vapor pressure, p, is identical to Equation (42), except a reduced specific energy is used to account for melting and vaporization. The equation is

$$p = (\gamma-1)\ \rho\ E' \qquad (E > E_m) \tag{43}$$

where

$$E' = (E - E_m) \left[1 - e^{-\left(\frac{E-E_m}{E_m}\right)} \right] (E > E_m) \tag{44}$$

and γ-1 is given by the dimensionless empirical expression

$$\gamma - 1 = 0.4 + 0.052 \ln G + 0.023 \ln^2 \left(\frac{H}{G}\right) \tag{45}$$

where $G = \rho/\rho_0$, $H = E^*/E_0^*$, ρ_0 = reference mass density (1.0 g/cm^3), and E_0^* = reference specific internal energy (21.171 Te/g). E^* is defined as

$$E^* = E_m \quad (E' \le E_m) \tag{46a}$$

$$E^* = E' \quad (E' > E_m) \tag{46b}$$

Equation (46) is necessary to avoid a logarithmic singularity in Equation (45). It can be shown, starting from Equation (44), that $E' > E_m$ when $E > 2.35\ E_m$.

The deviator stresses are reduced by the factor $1 - E/E_m$ when $E \le E_m$, so when $E \ge E_m$, the material is a fluid or a gas, and there are no plastic strain increments. Thus, there is no distinction between total and elastic volume change whenever the vapor pressure is calculated.

The high pressure equation of state has been implemented and is included in the model version listed in Appendix A. The hydrostatic behavior of the model to 5×10^5 MPa (5 Mbar) is shown in Figure 5, both with and without activation of the high pressure equation of state. Uniaxial strain compression behavior of the model with the high pressure equation of state is shown in Figure 6. The material melts at a pressure of about 2×10^5 MPa. At this point the deviator stresses (and the expansive yield surface) have been fully reduced to zero (Figure 6b).

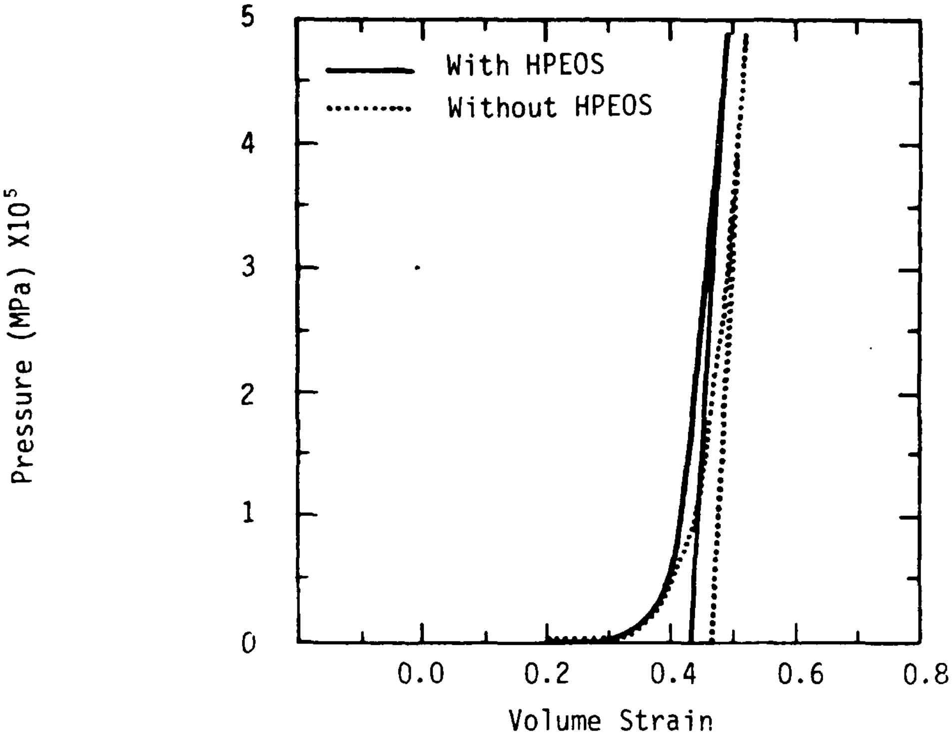

a. Hydrostat.

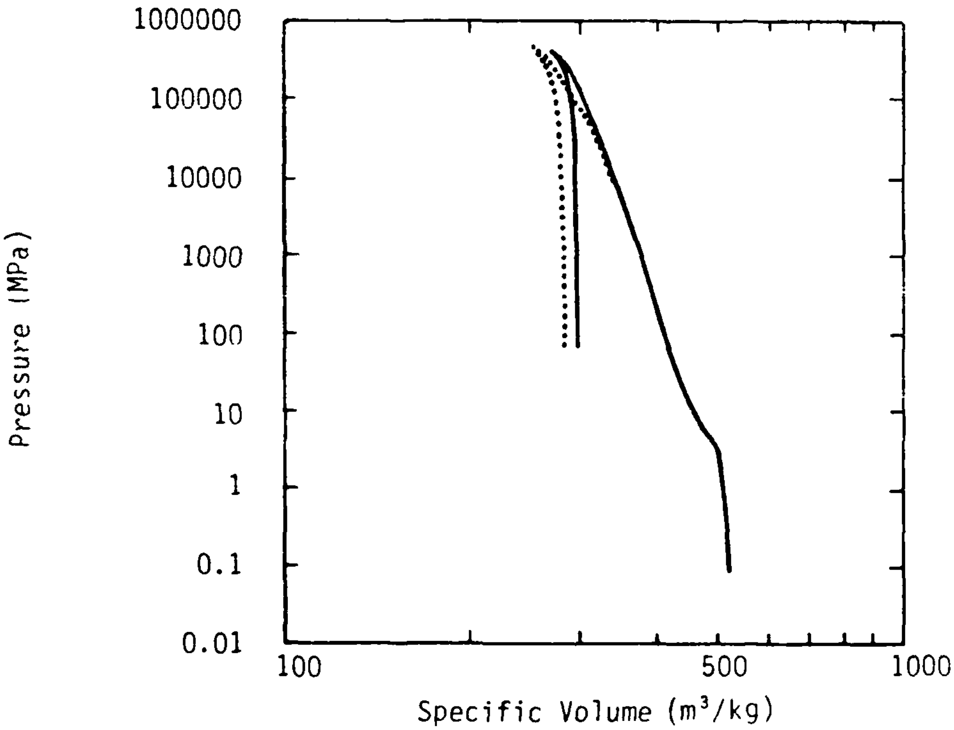

b. Specific Volume.

Figure 5. High Pressure EOS Behavior in Isotropic Consolidation.

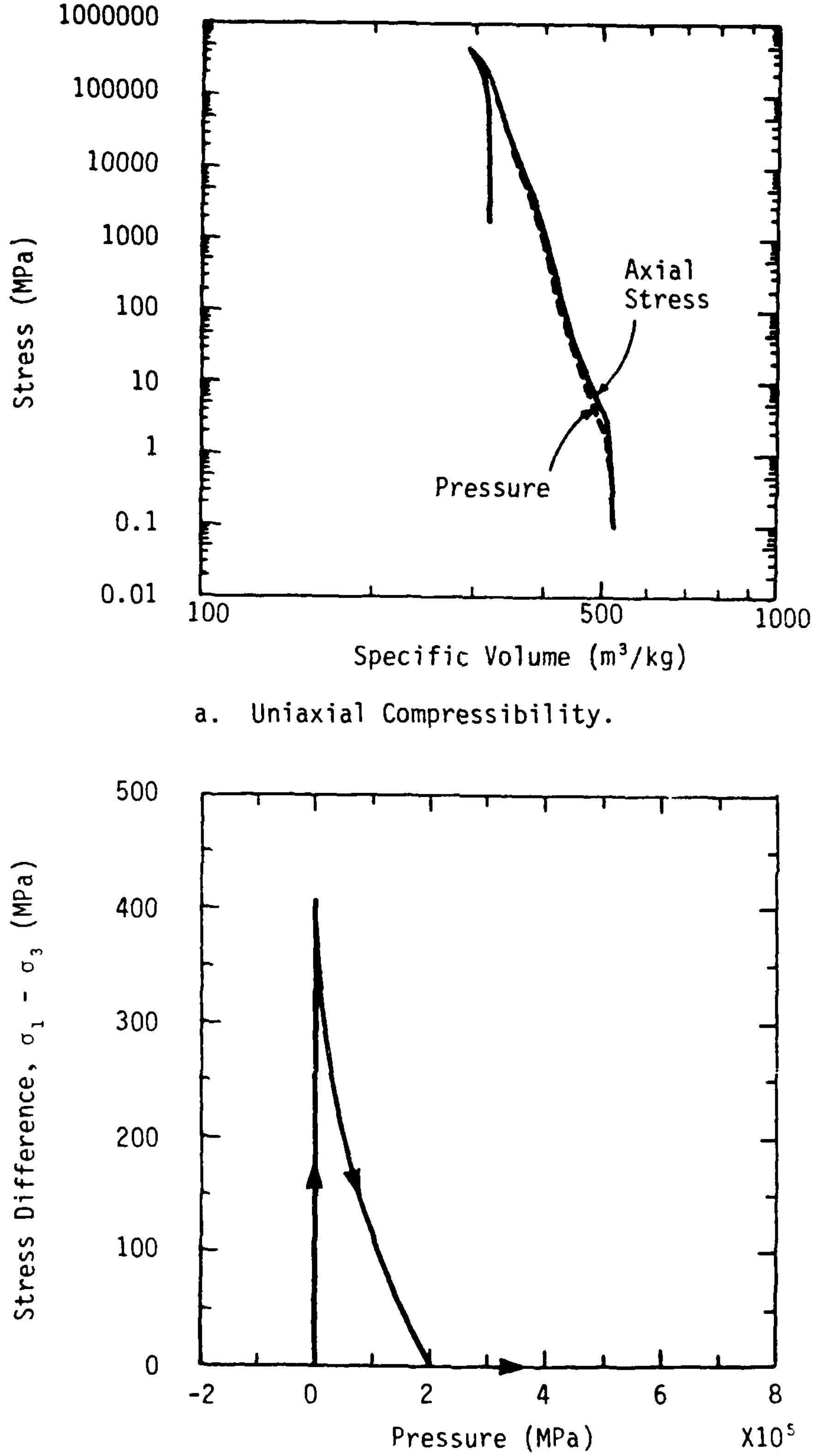

a. Uniaxial Compressibility.

b. Stress Difference Reduction Due to Melting.

Figure 6. High Pressure EOS Behavior in Uniaxial Strain Compression.

3.0 COMPUTATIONAL ISSUES IN CONSTITUTIVE MODELING

3.1 Timestep

The timestep in time-marching finite difference or finite element solutions is often determined based on the Courant condition. Simply put, this condition permits a stress wave to travel no more than one zone thickness in one timestep. Thus, for a given zone:

$$\Delta t \leq F \frac{D_{min}}{C_p} \tag{47}$$

where Δt = calculational timestep, C_p = current compressional wavespeed, D_{min} = minimum distance across the zone, and F = a safety factor ($\leq$ 1.0) which can further restrict the timestep. When the Courant condition is employed, the material model is required to report the current wavespeed in each zone. For an elastic compressional wave,

$$C_p = \sqrt{\frac{M}{\rho}} \tag{48}$$

where M = constrained modulus and ρ = mass density. Because a zone may be deforming plastically, the above elastic relationship will not always yield the fastest signal propagation speed. Therefore, the approximate wavespeed across a zone is then taken to be:

$$C = \sqrt{\frac{M_e}{\rho}} \tag{49}$$

where M_e = the maximum of [$C_{ep}(1,1)$, $C_{ep}(2,2)$, $C_{ep}(3,3)$] and C_{ep} is the 6x6 incremental elastoplastic stiffness matrix. Using this wavespeed allows the Courant condition to be closely followed. An additional safety factor of F = 0.9 is typically applied.

3.2 Numerical Errors

The types of numerical errors discussed here are primarily those which occur within the constitutive model itself. Of the other errors in a finite difference or finite element calculation which occur outside the material model, those which are controlled by artificial viscosity are most pertinent. Artificial viscosity is intended to damp high frequency oscillations. The damping is ignored when computing stress increments within the constitutive model. In conjunction with a rate-dependent model, its use may hamper the evaluation of strain-rate effects. Because the ARA three invariant model is not strain-rate dependent, typical values of artificial viscosity may be employed to smear shock fronts and limit grid oscillations.

Numerical errors produced in the ARA model are primarily the result of its incremental stiffness formulation. The first kind of numerical error is the tendency for the stress point to overshoot the expansive yield surface at low values of expansive plastic work. Since this occurs when the stress point is on the yield surface and pushing it out, it is called "plastic" overshoot. Plastic overshoot results in a violation of the expansive consistency condition, which states that

$$f'_p = f''_p \tag{50}$$

throughout yielding. Plastic overshoot is most likely to occur as the stress point leaves the hydrostatic axis, because the derivative of the expansive hardening function with respect to expansive plastic work is infinite when $W_p = 0$:

$$\frac{df''_p}{dW_p} = f''_p \left(\frac{1}{q\, W_p} - b \right) \tag{51}$$

Because the value of f''_p at the end of an increment is computed from the slope (df''_p/dW_p) at the beginning of the increment, it tends to be over-estimated and the consistency condition therefore violated. This phenomenon can be held in check if the strain increments are kept very small in this region. A strain subcycling scheme was devised which evaluates the change in df''_p/dW_p over a strain increment found to have violated the consistency condition along the expansive yield surface. This change in slope is used to break down the total current strain increment into n equal subincrements, where

$$n = 1 + 50 \left[\frac{\left(\frac{df''_p}{dW_p} \right)_{start}}{\left(\frac{df''_p}{dW_p} \right)_{end}} - 1 \right] \leq 1000 \qquad (52)$$

The model is then internally cycled using these smaller increments. Compatability is more closely enforced, eliminating plastic overshoot.

Another kind of error which occurs in the ARA model (as well as in other models) is associated with the large strain increments which can occur in one timestep under explosive loading. When the stress point is initially in the elastic region of the model, a large strain increment can drive the stress point past one or both yield surfaces. There are several ways of correcting this, including: (1) pulling the stress point back to the yield surface, either at constant octahedral normal stress or normal to the yield surface, (2) correcting back at either constant f'_c or constant f'_p, depending upon which surface has been violated, (3) breaking down the total strain increment into two parts (the first elastic and just sufficient to initiate yielding) based on the ratio of f'/f'', or (4) breaking down the total strain increment into many smaller increments and subcycling within the model. This last method is currently employed in the ARA model. Proper treatment of "elastic" overshoot was observed to be very important in the wave propagation calculations, because of the tendency of the stress point to violate the yield surface upon unloading and reloading, especially from a spalled condition.

A different kind of numerical problem, but not an error, was encountered while using the ARA model on a VAX 11/750 computer, which is a much smaller machine than the CRAY, on which the ARA model was developed. The problem was the occurrence of very large numbers associated with the compressive yield surface; numbers larger than the computer could handle. Although the expansive yield surface expression,

$$f'_p = \left(\frac{\tau_{oct}}{Pa} \right) (1 - E \cos 3\omega) \left(\frac{Pa}{\sigma_{oct}} + m \right) \qquad (53)$$

has been made dimensionless through the use of atmospheric pressure, the compressive yield surface expression,

$$f_c' = 3\,\sigma_{oct}^2 + r^2\,\tau_{oct}^2 \tag{54}$$

has not been. So when, for example, units of Pascals are being used with stress levels typical of blast loading, a quantity using $(f_c')^2$ will be extremely large. The problem has been circumvented by using units of MPa instead of Pa on the VAX. There are several ways to make the compressive yield function dimensionless. One possibility is to simply use atmospheric pressure again to cancel units:

$$f_c' = 3\left[\left(\frac{\sigma_{oct}}{Pa}\right)^2 + \left(r\,\frac{\tau_{oct}}{Pa}\right)^2\right] \tag{55}$$

3.3 Efficiency

Evaluating the efficiency of a constitutive model involves answering three questions:

1. How long does it take the computer to execute the model?
2. How much information does the model require to be stored for each element?
3. Are the increases in run time and storage required by a more complicated model over a simpler model offset by improved calculational results?

The ARA model is a fairly long model in terms of coding, as can be seen in Appendix A. The time it takes a typical mini-computer to run through the model is compared with several other models in Table 2. It is to be expected that more calculational steps will require a somewhat longer execution time. So, the results in Table 2 are not surprising. However, as will be seen for the one-dimensional wave propagation calculations, the real run time differences arise from the strain subcycling scheme used to minimize the numerical errors discussed above. Therefore, it is not necessarily true that a complicated model will be significantly more expensive to run. What is needed is a more efficient computational strategy.

TABLE 2. MODEL EXECUTION TIMES-SINGLE ELEMENT STUDIES

Model	CPU Time[1] to Simulate Laboratory Test (sec)		
	Uniaxial Strain Compression[2]	Standard Triaxial Compression[3]	Arbitrary Strain Path[4]
ARA[5]	239 (εa = 13.5%)	301	34
CAP	32 (εa = 17.5%)	48	6
AFWL Engineering	14 (εa = 17.4%)	16	4
Elastic	18 (εa = 57.0%)	12	2

[1] CPU times are to the nearest second for the entire calculation with no plotting. The computer used was a Digital VAX 11/750.

[2] Sample loaded to an axial stress of 40 MPa and unloaded to an axial stress of 10 MPa using equal axial strain increments of 0.0025%. Note that each model resulted in a different maximum εa, as noted.

[3] Sample initially confined to 3.45 MPa, loaded to 10% axial strain in equal increments of 0.0025%. Unloaded to 0.25 MPa stress difference.

[4] Strain path shown in Figure 35, simulating insitu spherical wave propagation.

[5] Note that the execution times achieved for the ARA model are heavily influenced by the numerical correction scheme and can be substantially improved by using improved computational strategies.

As coded in the Soil Element Model (SEM), the ARA model (without the high pressure equation of state) has six state variables: (1) maximum past octahedral normal stress, (2) compressive plastic work, (3) expansive plastic work, (4) expansive yield surface activation switch, (5) volume expansion since last tensile failure, and (6) initial confining pressure. This is compared with no state variables for the elastic model, three for the modified AFWL Engineering model, and one for the cap model. Each state variable must be stored for each calculational zone. The use of six state variables in the ARA model has not yet caused any storage-related problems, either on a large computer (CRAY) or a mini-computer (VAX 11/750). Calculational costs may be increased due to expanded core space requirements, but this will not be the case if space is being utilized which was already available in the code (as was the case for the STEALTH implementation).

3.4 Uniqueness and Work-Softening

Uniqueness in the context of constitutive modeling is concerned with the possibility of more than one solution for a given set of stress or strain conditions. For example, is it possible that a total strain increment can produce more than one stress increment? If the answer for a particular model is yes, then uniqueness is violated and confidence in the results generated by that model is greatly diminished. For models with two yield surfaces meeting at a corner, the question of uniqueness at that corner is particularly relevant. The ARA model employs a method of choosing yield modes which was formulated to insure uniqueness [see Merkle and Dass (1985: Appendix I)]. If a nonunique situation is possible, the calculation is stopped. In this way, a unique solution has been assured for all loading cases.

The tendency of some geologic materials to work-soften, i.e., to display a decreasing load capacity with increasing strain, has been demonstrated many times in laboratory tests. There remains debate over the interpretation of these tests and whether or not a soil sample is undergoing homogeneous deformation at later times in these tests. What is sometimes interpreted as work-softening may actually be a consequence of testing method, boundary conditions, or localized shear failure. However, there are clearly some cases where soil materials exhibit a peak shearing resistance followed by a lesser residual resistance. The transition between the two is referred to as work-softening.

The expansive yield surface in the ARA model has been formulated to account for work-softening. Currently, a material is allowed to soften until zero shearing resistance remains (see Figure 7). This is not a good representation for most geologic materials well beyond peak stress because they tend to display substantial residual shear strength. An expansive yield function which allows residual strength has been formulated and tested in the model but is not fully implemented.

During the early stages of the wave propagation calculations, it was observed that the ARA model frequently shut itself off because it had encountered the possibility of a nonunique solution in the mode decision algorithm at the corner of the yield surfaces. This problem often coincided with the onset of work-softening.

To expedite the continuum code checkout of the model, a modification was made to allow work-softening to be deactivated. Thus, the yield surface can now achieve a maximum value at which it becomes stationary (Figure 7). The consequences of work-softening in dynamic wave propagation certainly deserve further study, but it was felt that a complete treatment of this issue was beyond the scope of this effort.

3.5 Rezoning

Rezoning is an important computational issue which is often encountered in finite difference calculations of blast and shock events which employ a Lagrangian grid. The need for rezoning arises when distortion of the grid around an explosive source, in a crater, or at a stress concentration point becomes so severe that it either (1) drives the timestep to zero, or (2) turns the grid inside-out. Rezoning is the process of rearranging the grid (at one instant of time or over several cycles) so that it is again fairly uniformly spaced, and all zones resemble quadrilaterals. Because the numerical grid is being remapped onto the material, as it would be in an Eulerian grid, a calculation employing this process is sometimes called arbitrary Eulerian-Lagrangian (ALE). Rezoning is an approximate process and does not always conserve both mass and momentum. The reason it involves (and is dependent on) the constitutive model is that as material is transported and mixed from one zone to another, the state variables which define each zone's material must also be consistently redefined.

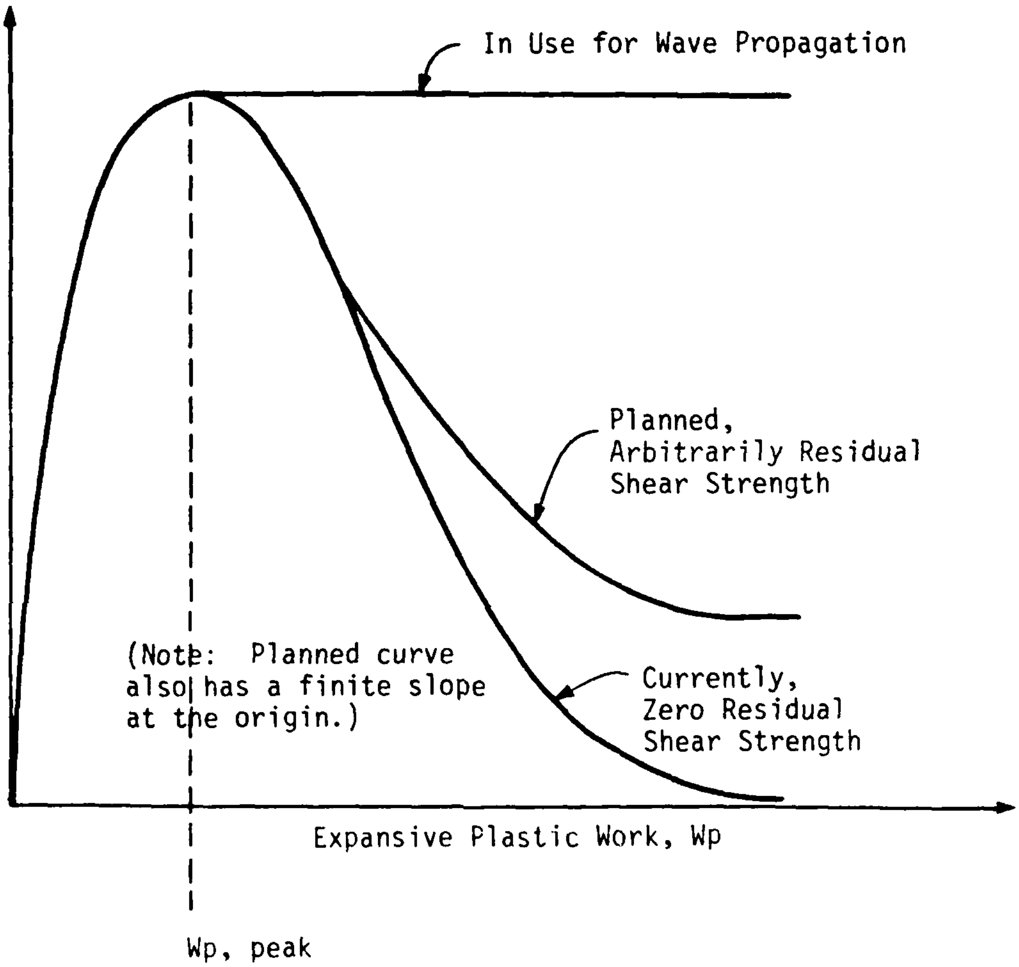

Figure 7. Expansive Yield Surface Hardening Functions.

Figure 8 shows what physically happens for one type of internal point rezone, using STEALTH numbering conventions. The interior point common to four surrounding zones is adjusted to a more central location. In the process, mass and volume are exchanged among old zones to create new zones. The quantity V_{ij} is introduced, defined to be the volume contributed from old zone i to new zone j. If, in creating new zone j, no material is gained from old zone i, then $V_{ij} = 0$. A matrix of weighting factors is created for the four new zones created by relocation of an interior point:

$$F_{ij} = \begin{bmatrix} F_{11} & F_{12} & F_{13} & F_{14} \\ F_{21} & F_{22} & F_{23} & F_{24} \\ F_{31} & F_{32} & F_{33} & F_{34} \\ F_{41} & F_{42} & F_{43} & F_{44} \end{bmatrix} \quad (56)$$

where

$$F_{ij} = \max\left(\frac{V_{ij}}{V_{j,new}}, 0\right) \quad (57)$$

F_{ij} is defined as the positive volume fraction of new zone j, which came from old zone, i. The "max" operation in Equation (57) is needed because V_{ij} can be negative due to extreme distortion before rezoning. For each rezone case, there will be a total of nine non-zero weighting factors. Zone centered variables, such as mass and internal energy, are then redistributed using these weighting factors. Material model state variables must also be distributed and a new stress state determined for each new zone. For the ARA model, the parameters which must be distributed are the initial confining pressure, the maximum past pressure, compressive and expansive plastic work, and volume expansion since last tensile failure (if any). For adjacent zones, redistributing initial pressure and reinitializing confining pressure -dependent properties is not critical. However, the new stress state and state variables must be consistent with the new strain state, which is a known quantity upon reconfiguring the zone.

A scheme for achieving a consistent state has not yet been formulated for the ARA model, but will be necessary for its eventual use in ground shock calculations involving severe environments.

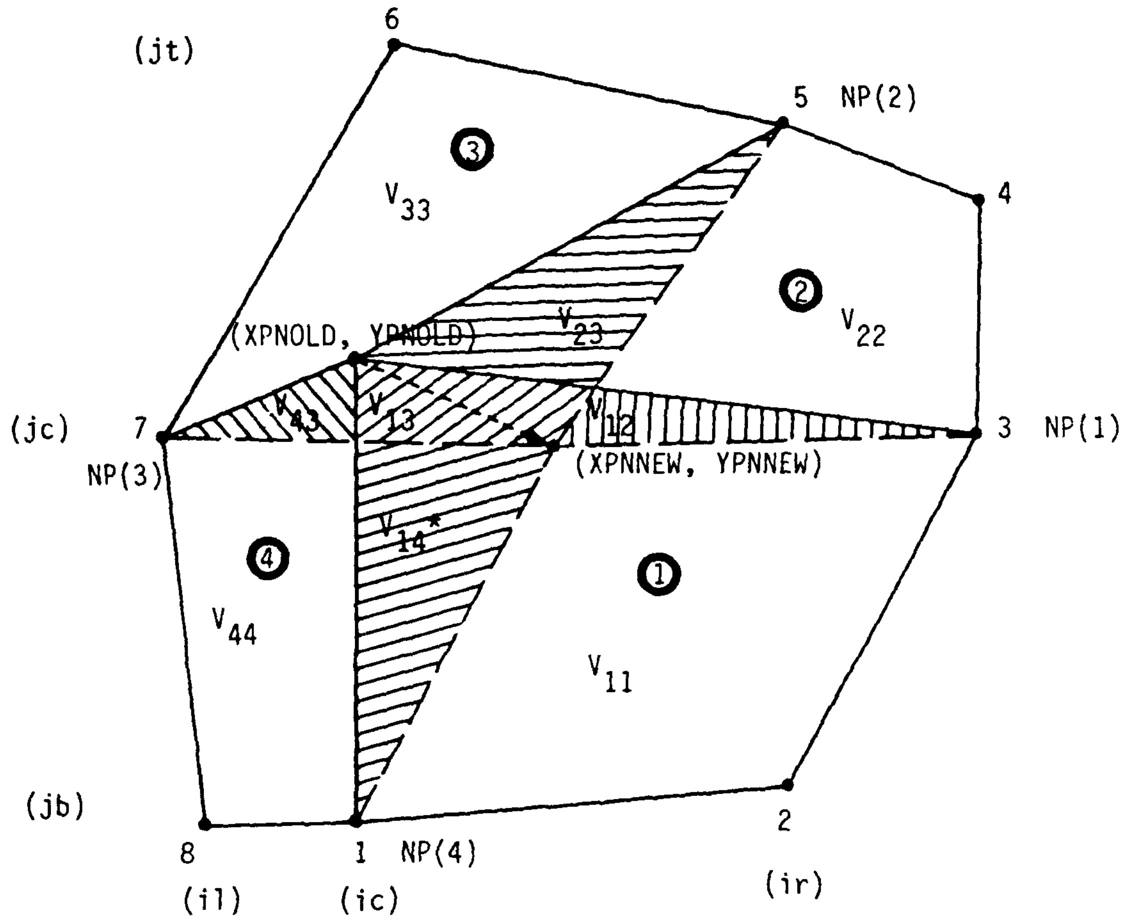

* V_{ij} = Volume Contributed from Old Zone I to New Zone j.

Figure 8. The Interior Point Rezone Problem.

3.6 Strain Conventions

A large class of finite difference codes (including TOODY, HEMP, STEALTH, and SNEAKY) do not track displacement of grid points. Instead, they use current strain rates

$$\dot{\varepsilon} = \frac{\partial \varepsilon}{\partial t} = \frac{1}{\ell}\left(\frac{\partial \ell}{\partial t}\right) = \frac{\dot{\ell}}{\ell} \tag{58}$$

which, when multiplied by the current timestep yields

$$\Delta\varepsilon = \frac{\Delta \ell}{\ell} \tag{59}$$

where ℓ = current zone length. These strains are commonly known as true strains and are based on current dimensions. The properties of the constitutive models, however, are typically formulated from laboratory data using engineering strains,

$$\Delta\bar{\varepsilon} = \frac{\Delta \ell}{\ell_0} \tag{60}$$

where ℓ_0 = original zone length. The difference between the two strains is small at small strains. But at strains greater than about ten percent, the difference becomes significant and can affect calculated results. Therefore, it has been necessary to add variables in the finite difference codes employed in this study to track original zone dimensions and to calculate actual engineering strains. These strains are then used in the material models and are consistent with the development of the models and their parameters.

4.0 WAVE PROPAGATION CALCULATIONS

4.1 ARA Model Implementation

The ARA model has been implemented in a fashion compatible with finite difference or finite element code applications. The model is formulated to operate under strain control, where the total strain increment is known and the resultant stress increment is determined by the model. The incremental elasto-plastic stiffness approach used by the ARA model [Merkle and Dass (1985)], is fundamentally different than the trial and error failure surface correction procedure employed by many current models, including the AFWL Engineering and cap models. The incremental stiffness procedure more accurately tracks plastic strains and plastic work, although some errors are produced by extrapolating stiffness from an old stress state to a new one (see Section 3.2).

Because the ARA model was developed using the Soil Element Model [Dass, Bratton, and Higgins (1981)], its implementation has kept pace with its improvement and change. The model has been extensively tested in a single element mode under many kinds of laboratory stress and strain paths. Applying the model to wave propagation problems, however, did require some modification. The behavioral improvements are discussed in Section 2, and numerical improvements are discussed in Section 3.

4.2 Initial Anisotropic Stress State

The stress field at a point in an earth mass initially at rest under the force of gravity depends on depth, local tectonic conditions, and material properties. If the action of gravity during geologic history is idealized as a uniaxial strain compression process, then calculating the insitu stress field may procede accordingly. The calculation is relatively easy for an elastic material.

The elastic geostatic octahedral normal stress is

$$\sigma_{oct,0} = \left(\frac{1+2\ K_0}{3} \right) \sigma_z \qquad (61)$$

or

$$\sigma_{oct,0} = \frac{1+\nu}{3(1-\nu)} \sigma_z \qquad (62)$$

where σ_z is the vertical effective stress at the depth of interest due to overburden, K_0 is the coefficient of earth pressure at rest, and ν is Poisson's ratio. The insitu stress state is then a point on the elastic uniaxial stress path shown in Figure 9a.

For an elastic-plastic material, which can actually be at incipient shear failure under insitu stress, or for which there can be model state parameters which cannot be directly determined, it is possible to initially load each element in uniaxial strain compression (Figure 9b). At the proper vertical stress, each element is then at equilibrium under gravity with correct horizontal stresses as well as state parameters. If one or more model parameters depend on "initial" confining pressure, however, this process becomes more complicated. These model parameters are used to load the element uniaxially, but the final model parameters actually depend on the at-rest anisotropic stress state. If these parameters cannot be explicitly determined, it would appear that some form of iteration is necessary to arrive at the true "initial" condition.

The ARA model has several parameters which depend on initial confining pressure. These parameters control the work hardening functions and the expansive plastic potential surface, as well as the initial elastic moduli. In order to characterize these parameters correctly, a procedure has been devised to approximate initial anisotropic consolidation. This procedure is exercised for each depth, so that as depth increases, each zone will have unique initial conditions. The steps, shown in Figure 9c, are as follows:

(1) Eliminate the usual model initialization which occurs when parameters are input. Or initialize the model parameters to a very low isotropic pressure, approximately one-tenth of an atmosphere (point a in Figure 9c).

(2) Calculate the stress state which would be achieved due to overburden at the depth of interest if the material were elastic (as was discussed above). Use the unloading-reloading Poisson's ratio, ν_u, to do this (from Point a to Point b).

(3) Reinitialize the model parameters using the octahedral normal stress found in Step 2 (point c).

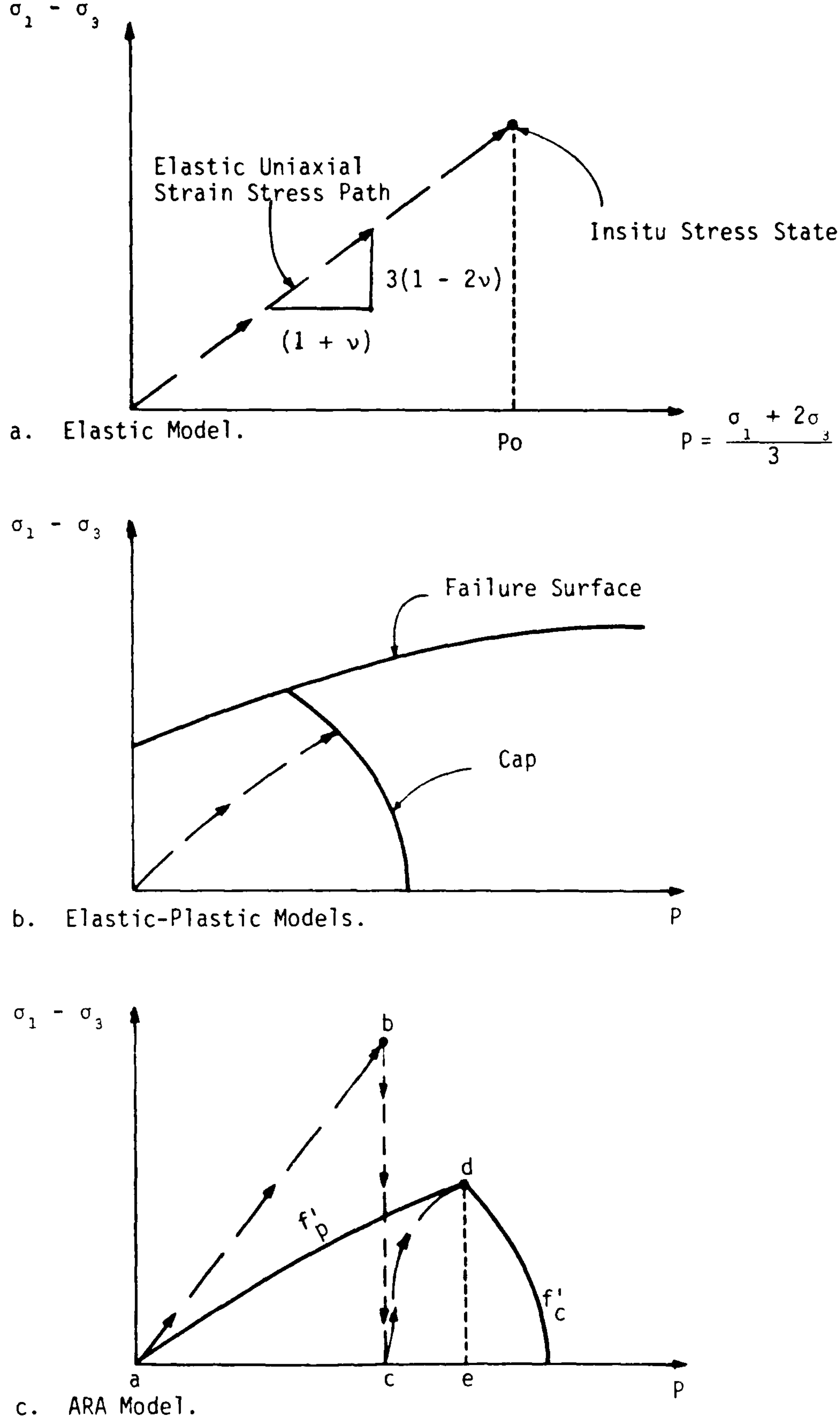

Figure 9. Application of Geostatic Stresses.

(4) Load the model in uniaxial strain compression until the vertical stress reaches the overburden level (from point c to d). Save the insitu stress state and the value of the expansive plastic work, W_p, at this point.

(5) Reinitialize all other model parameters using the pressure level reached in Step 4 (point e).

Achieving an appropriate and consistent insitu stress state is important to a successful calculation for several reasons. First, the calculational grid will be stable under gravity forces prior to arrival of a stress wave. Second, the material behavior of models such as the ARA conic model can be quite sensitive to initial confining pressure. And third, the orientation of the stress wave with respect to the orientation of the insitu stresses is important when the dynamic and static stresses are of the same order of magnitude. Figure 10 illustrates the second and third of these effects. Shown are the stress paths due to a hypothetical insitu spherical strain path. The strain path used here is the same as that used before in Figure 3. Three cases were calculated:

(1) Initial isotropic compression to 6 MPa. Since the initial stresses are equal in the x, y, and z directions, direction of load application does not affect this case.

(2) Initial anisotropic consolidation to σ_x = 6 MPa. The strain path is applied as if the stress wave were traveling in the vertical (x) direction. Behavior is qualitatively similar to Case (1) but quantitatively quite different.

(3) Initial anisotropic consolidation to σ_x = 6 MPa (same as Case (2)). The strain path is applied as if the stress wave were traveling the horizontal (y) direction. Note the difference in initial behavior due to the initial drop in shear stress. This same response will be apparent in Section 4.5 for the two-dimensional DIHEST calculation.

4.3 Description of Modeled Soil

The ARA model is intended to be quite general and is capable of modeling many types of soil, as well as other kinds of materials. Fundamentally different types of soil response can be matched through the parameter determination process. The soil modeled in the wave propagation problems discussed here is a dry alluvium representative of the alluvial materials found across the desert southwest and the basin and range topographies of the United States. Dry alluvium was chosen for several reasons. First, dry alluvium is of great interest to the Air Force because of the ISST test program currently being conducted in Yuma, Arizona. Secondly, there is a good deal of data (both

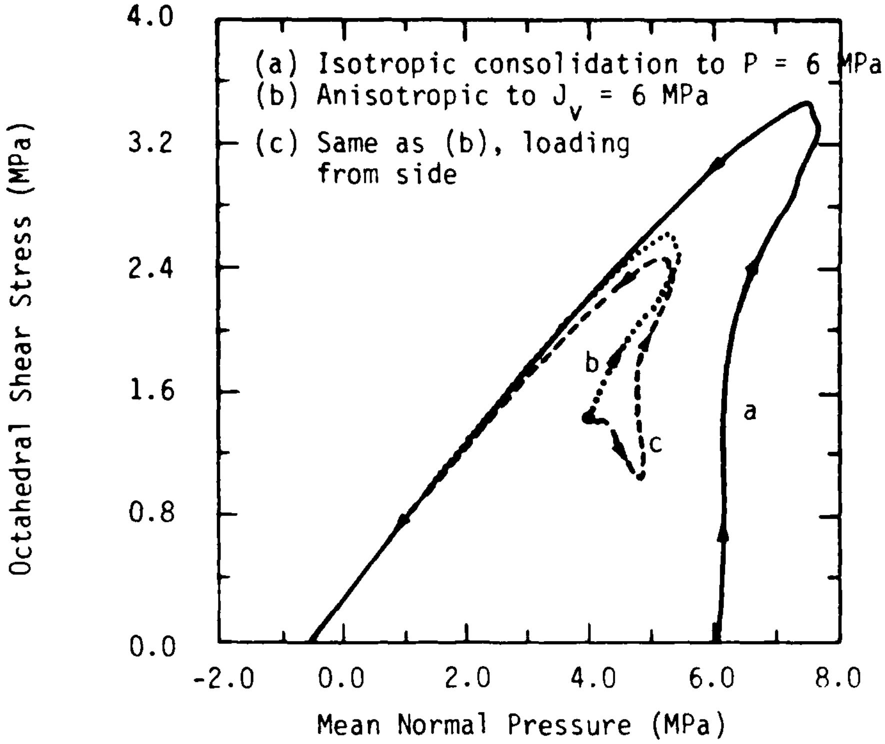

a. Stress Path Response.

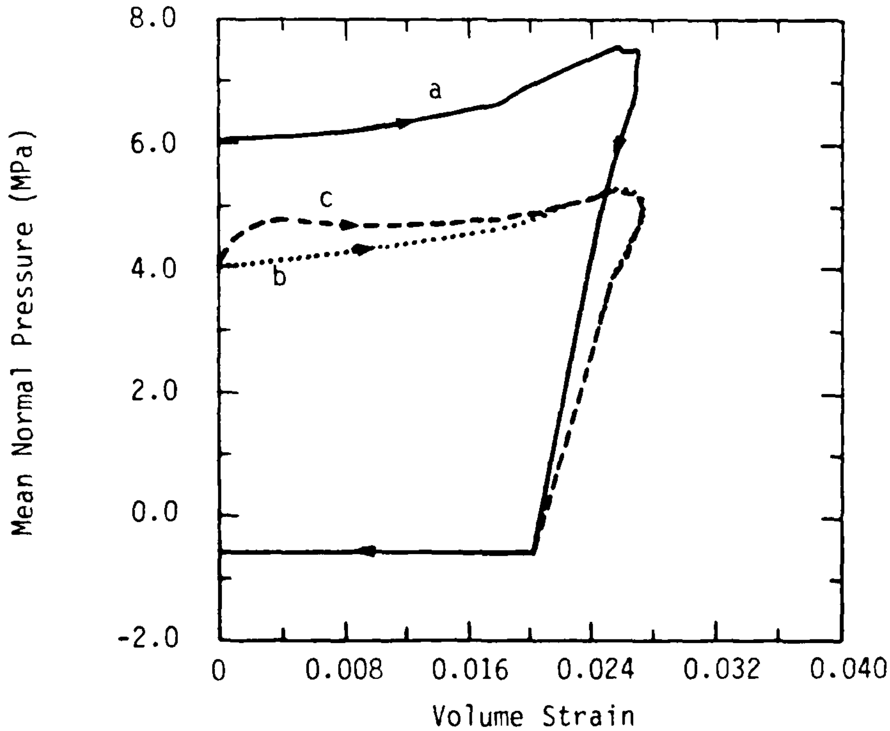

b. Pressure-Volume Response.

Figure 10. Some Effects of Anisotropic Consolidation in the ARA Model.

laboratory and insitu) available from many test programs performed in similar materials. Third, a dry material was necessary to avoid the additional computational issues involved when propagating waves through saturated or partially saturated media. Finally, the dry alluvium used here is the same material used to demonstrate the model against laboratory data by Merkle and Dass (1985).

Table 3 shows the ARA, CAP, AFWL Engineering, and elastic model prameters used for the calculations reported here. The fact that data from remolded laboratory samples was used to fit the model parameters is important because it limits the potential accuracy of the model in predicting insitu test results. Even when undisturbed samples are used to fit a model, the predicted response using a laboratory model is commonly different from the dynamic insitu response, for both simple and complex geometries. When simple models are used, the parameters can be adjusted to yield a best estimate of what insitu response will be. Figure 11 shows preliminary estimates of laboratory and insitu uniaxial strain compressibility for ISST alluvium [Jackson (1984)]. No adjustment of this kind has been utilized for this study. The result will be poor agreement between the calculations and the data from insitu events. Because the observed insitu responses are typically stiffer (at low to intermediate stress levels) than the laboratory response, calculated peak motions based on laboratory-derived properties will be too high and peak stresses will be too low.

Note also that although only one material was used for all the wave propagation calculations, the materials in which the tests were conducted varied significantly. All the insitu tests were in dry alluvium but there were variations from site to site, and with depth within each site. Because the purpose of these calculations was to check out the ARA model in continuum code problems, however, one material was used for all tests at all depths. This allowed a direct comparison of model responses for different geometries and insitu conditions.

4.4 One-Dimensional Calculations

4.4.1 Code Description. The finite difference code used for the one-dimensional calculations is an adaptation of the mechanical-only portion of SNEAKY, written by Hart (1981). It has been incorporated in the ARA Soil Element Model as a boundary condition option along with the laboratory test and arbitrary strain path options. The frame of reference in the code is

TABLE 3. REMOLDED CARES-DRY ALLUVIUM CONSTITUTIVE MODEL PROPERTIES

Symbol	Parameter	SEM Name	Value	Units
(1) ARA Model				
Kur	Elastic Modulus Coefficient	AKUR	363.5	-
n	Elastic Modulus Exponent	AN	0.8412	-
νu	Elastic Poisson's Ratio	APOI	0.20	-
-	Unload-Reload Hysteresis Switch	AHSWITCH	0.0	-
-	No. Collapse Function Segments	ACRV	3.0	-
-	Work Softening Switch	AWSOFT	0.0	-
C1		AACC(1)	4.645E-5	-
P1		AAPC(1)	1.401	-
C2	Compressive Hardening Constant	AACC(2)	6.086E-2	-
P2	Compressive Hardening Exponent	AAPC(2)	0.4667	-
C3		AACC(3)	0.7516	-
P3		AAPC(3)	0.2688	-
r	Elliptical Cap Shape	AR	0.25	-
E	Expansive Yield Constant	AEY	0.1111	-
m	Expansive Yield Constant	AMY	2.875E-4	-
η1	Expansive Failure Constant	AETA1	0.6454	-
P	Expansive Hardening Constant	APBAR	0.5057	-
ℓ	Expansive Hardening Exponent	AL	0.8691	-
α	Expansive Hardening Constant	AALPH	5.000	-
β	Expansive Hardening Constant	ABETA	-2.631E-3	-
t	Plastic Potential Constant	ATG	-0.9646	-
R	Plastic Potential Constant	ARG	2.182E-3	-
s	Plastic Potential Constant	ASG	1.860	-
T	Tensile Strength	APEX	0.0	Pa
ρ	Mass Density	RHOREF	1900.	kg/m3
(2) Cap Model				
KI	Bulk Modulus Parameters	AKI	4.0E9	Pa
K1		AK1	0.0	-
K2		AK2	0.0	-
GI	Shear Modulus Parameters	AGI	3.0E9	Pa
G1		AG1	0.0	-
G2		AK2	0.0	-
C	Failure Surface	AC	0.288E6	Pa
M		AM	0.215	-
c		CCC	0.0	-
b		BB	0.0	-
RI	Cap Shape	ARI	2.5	-
R1		AR1	0.0	-
R2		AR2	0.0	-
w	Cap Hardening Parameters	AW	0.200	-
d		AD	0.018E-6	1/Pa
ρ	Mass Density	RHOREF	1900.	kg/m3
(3) AFWL Engineering Model				
ρ	Mass Density	RHOREF	1900.	kg/m3
T	Tension Cutoff	ST1	-0.288E6	Pa
Y	Yield Intercept	Y1	0.288E6	Pa
S	Failure Surface Slope	S1	0.215	-
VM	von Mises Cutoff	VM1	175E6	Pa

Hydrostat (No. Load Slopes = 8, No. Unload Slopes = 5)

Loading Segments:		1	2	3	4	5	6	7	8
Kℓ	Bulk Modulus (Pa)	9.302E7	6.261E7	1.491E8	3.530E8	1.088E9	3.419E9	9.042E9	7.000E11
εℓ	Strain Breakpoint	0.001181	0.008191	0.1292	0.1642	0.2014	0.2294	0.2516	1.0000
νℓ	Poisson's Ratio	0.32	0.32	0.32	0.32	0.32	0.32	0.32	0.32

Unloading Segments:		1	2	3	4	5
Ku	Bulk Modulus (Pa)	9.000E11	4.500E11	1.39E10	4.725E9	1.000E9
pu	Pressure Breakpoint	3.7E8	2.8E8	3.0E7	2.0E7	-0.288E6
νu	Poisson's Ratio	0.20	0.20	0.20	0.20	0.20

(4) Elastic Model				
K	Bulk Modulus	BULK	80E6	Pa
G	Shear Modulus	SHEAR	31E6	Pa
ρ	Mass Density	RHOREF	1900.	kg/m3

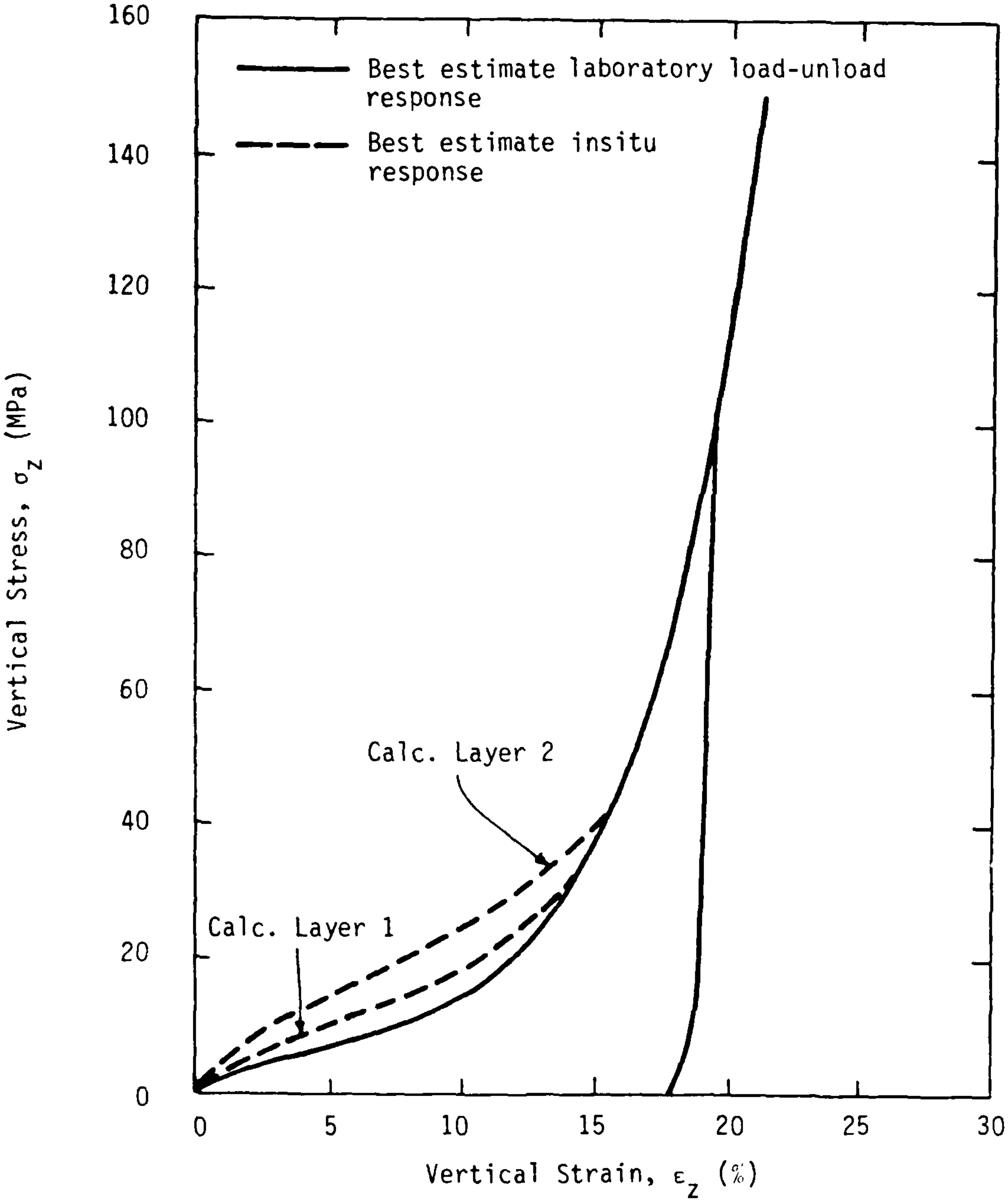

Figure 11. Variations in Laboratory and Insitu Uniaxial Strain Compressibility. (After: Jackson, 1984)

Lagrangian, so no material is transported from zone to zone. (No rezoning was used for these calculations.) The calculational sequence for a time step is shown in Figure 12. The overall formulation of SNEAKY is very similar to STEALTH which was used for the two-dimensional calculations discussed in Section 4.5

Only quadratic artificial viscosity was used for the one-dimensional calculations. Since quadratic artificial viscosity was activated only during compression, the shock fronts were spread out but the zone-to-zone numerical oscillations seen after the peak were not damped. The artificial viscous stress in SNEAKY is given by

$$q_Q = C_Q^2 \rho(h)^2 \left(\frac{\partial \dot{x}}{\partial x} \right)^2 \tag{63}$$

where ρ = current mass density, h = zone thickness, $\partial\dot{x}/\partial x$ = strain rate in the direction of propagation, and C_Q = dimensionless constant. C_Q was set equal to 2.0 for these calculations.

4.4.2 Planar (HEST) Calculations. The HEST (High Explosive Simulation Technique) is commonly used for simulating superseismic airblast effects from a nuclear detonation. Within the working volume and simulation time, which depend on the extent of the HEST cavity, the simulator produces loading conditions which are essentially one-dimensional uniaxial strain compression. Figure 13 shows the experimental layout for SIMCAL 3 (SIMulation CALibration 3), which was a HEST test performed by the Air Force at the HAVE HOST test site near Yuma, Arizona in 1979 [AFWL (1981)]. This test was chosen for analysis here because it was fielded adjacent to the ISST test site, and because it was a fairly successful test in terms of data recovery.

The calculational idealization of this test is shown in Figure 14. One material was used for the entire calculational grid. Layering, which was observed at the site, has been neglected. The mesh consisted of 99 grid points with fairly fine zoning near the surface. The bottom boundary was deep enough to avoid reflections within the time of interest. Acceleration due to gravity was included, and the grid was initially loaded to an anisotropic stress state. Target point depths were chosen to correspond to data locations in SIMCAL 3.

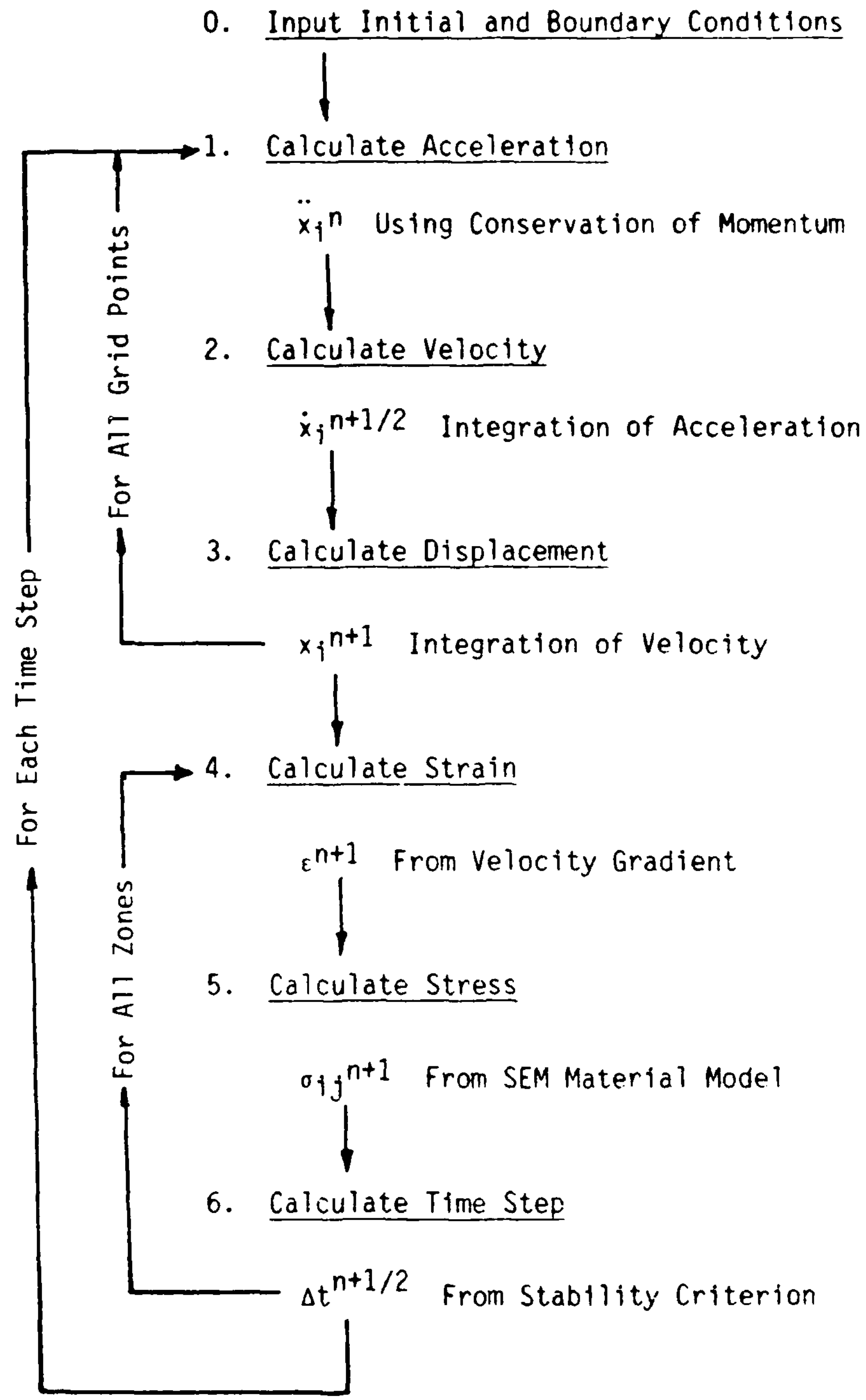

Figure 12. SNEAKY 1-D Calculational Sequence for A Time Step
[Hart (1980:3-27)]

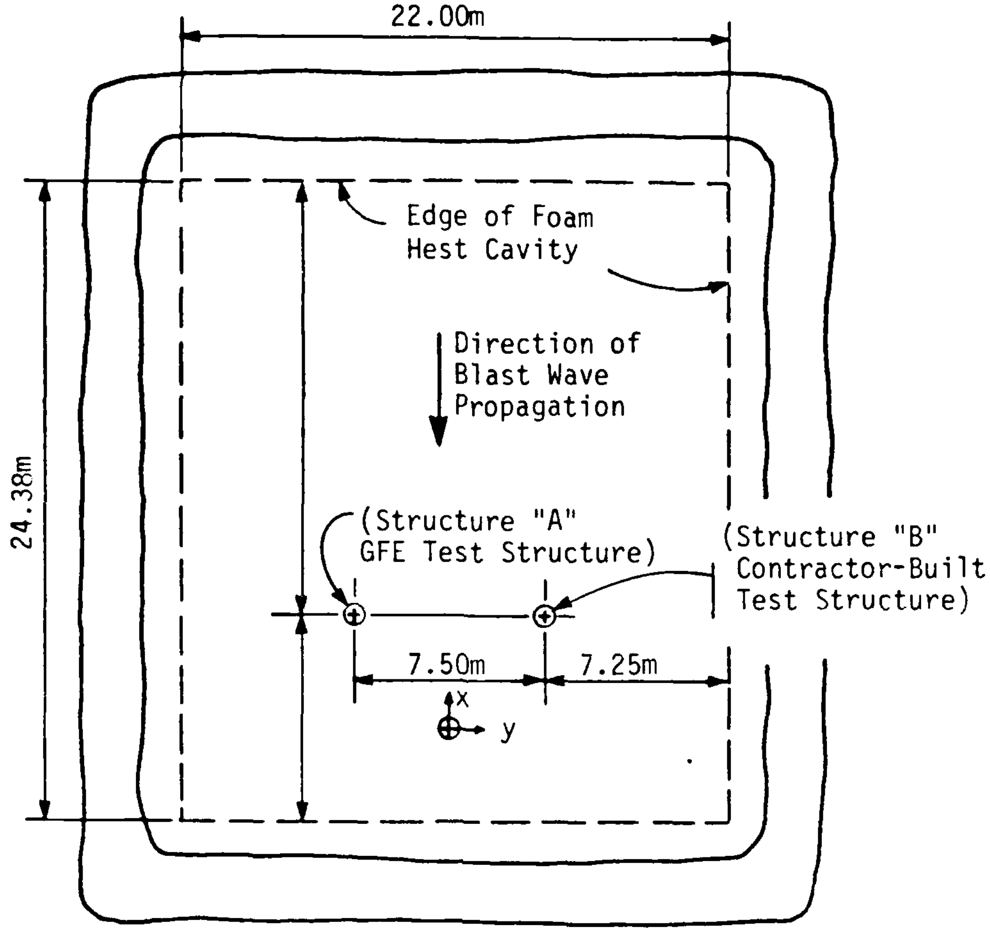

a. Plan.

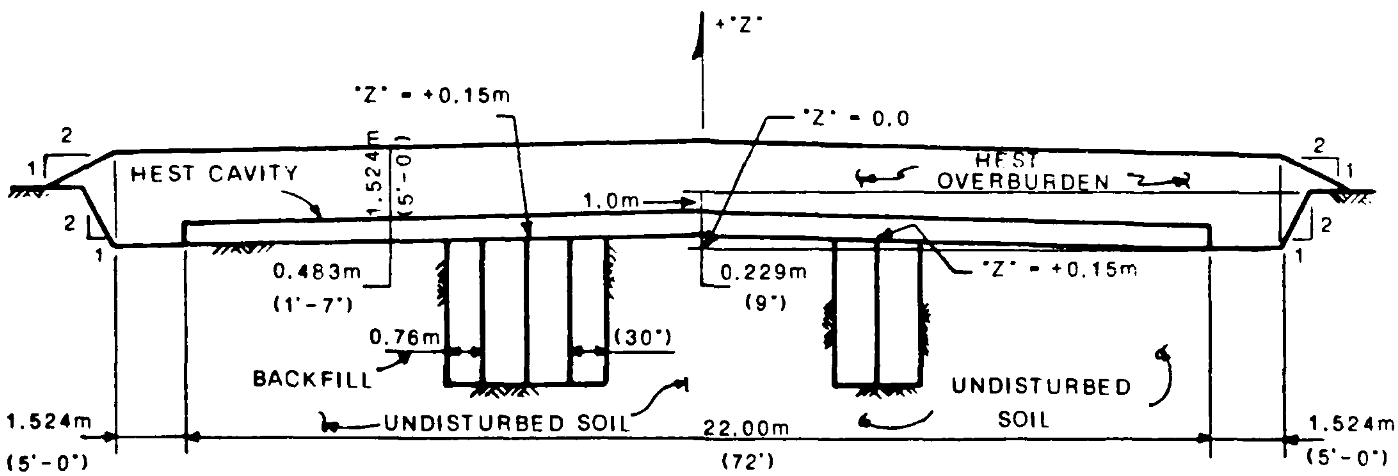

b. Elevation.

Figure 13. SIMCAL 3 Experiment Configuration.

Symmetry: Planar

Applied Load: P(t), Speicher-Brode Nuclear Overpressure

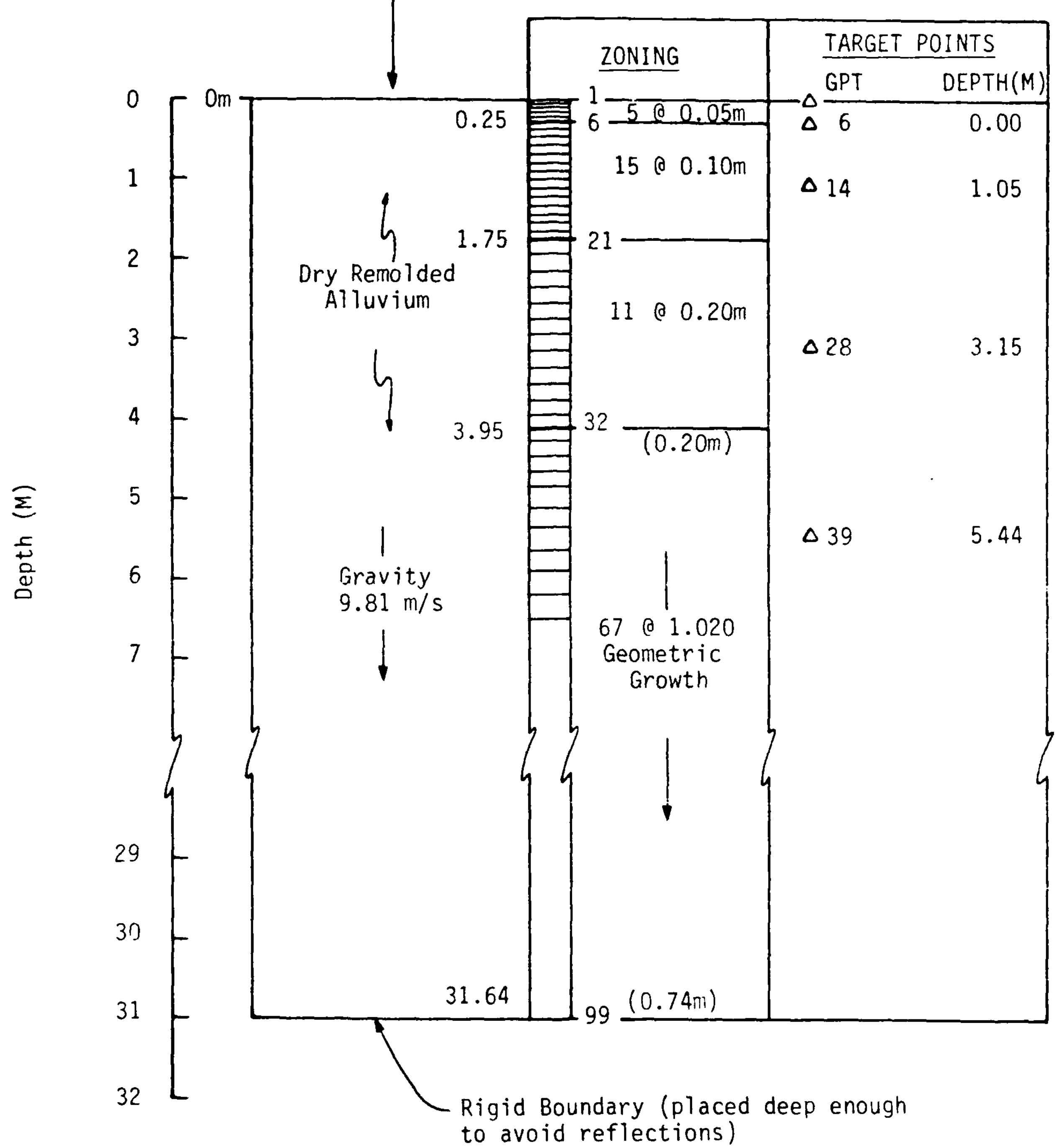

Figure 14. 1-D Planar Wave Propagation Calculational Configuration.

The exponentially-decaying pressure waveform shown in Figure 15 was applied to the ground surface. It corresponds to a 424 kt, 313 m range nuclear airblast loading [Brode and Speicher (1984)]. This is an impulse fit to the recorded HEST overpressures in SIMCAL 3 as developed by the Air Force Weapons Laboratory (1981). The calculation was run out to 40 ms, at which point the impulse had not yet reached its peak. (Impulse peaks at about 1.2 seconds for this yield and range.)

Calculated vertical velocity and displacement at five locations, using the ARA model, are shown in Figures 16a and b, respectively. It is very clear that in this highly compactive media, the entire grid moves downward nearly as a rigid body behind the wave peak. Figures 17a and b show the stress path and pressure-volume response, respectively, for three depths. Because the loading is uniaxial strain compression, this kind of response is entirely predictable from the laboratory uniaxial test simulations run previously with this model.

The calculated results do not predict the test results very well, because the parameters were not fit to match the insitu-based loading hydrostat. This is shown in Figure 18, where it is seen that the calculated velocity peaks are too high, the arrivals too slow, the rise times too fast, and the duration too long.

The identical problem was run using three other models: the AFWL Engineering model, the cap model, and an elastic model. A typical comparison between velocity waveforms is shown in Figure 19 for two depths. The elastic model results are fundamentally different because there is no permanent compaction. The remaining models all give very similar results. The ARA model is a little softer than the AFWL or cap models, as is seen in Figure 20b. This is partly due to its initialization at a very low confining pressure at this depth. Figure 20a demonstrates that all models give similar loading stress paths. And, since they all have identical unload-reload Poisson's ratios, all three compactive models have identical unloading stress paths. Figure 21 compares peak velocity attenuation between the models.

4.4.3 <u>Spherical (Buried HE Sphere) Calculations</u>. The purpose of performing one-dimensional calculations in geometries other than planar is to more fully exercise the ARA model prior to delving into the two-dimensional realm of arbitrary stress and strain paths. Planar wave propagation subjects the model

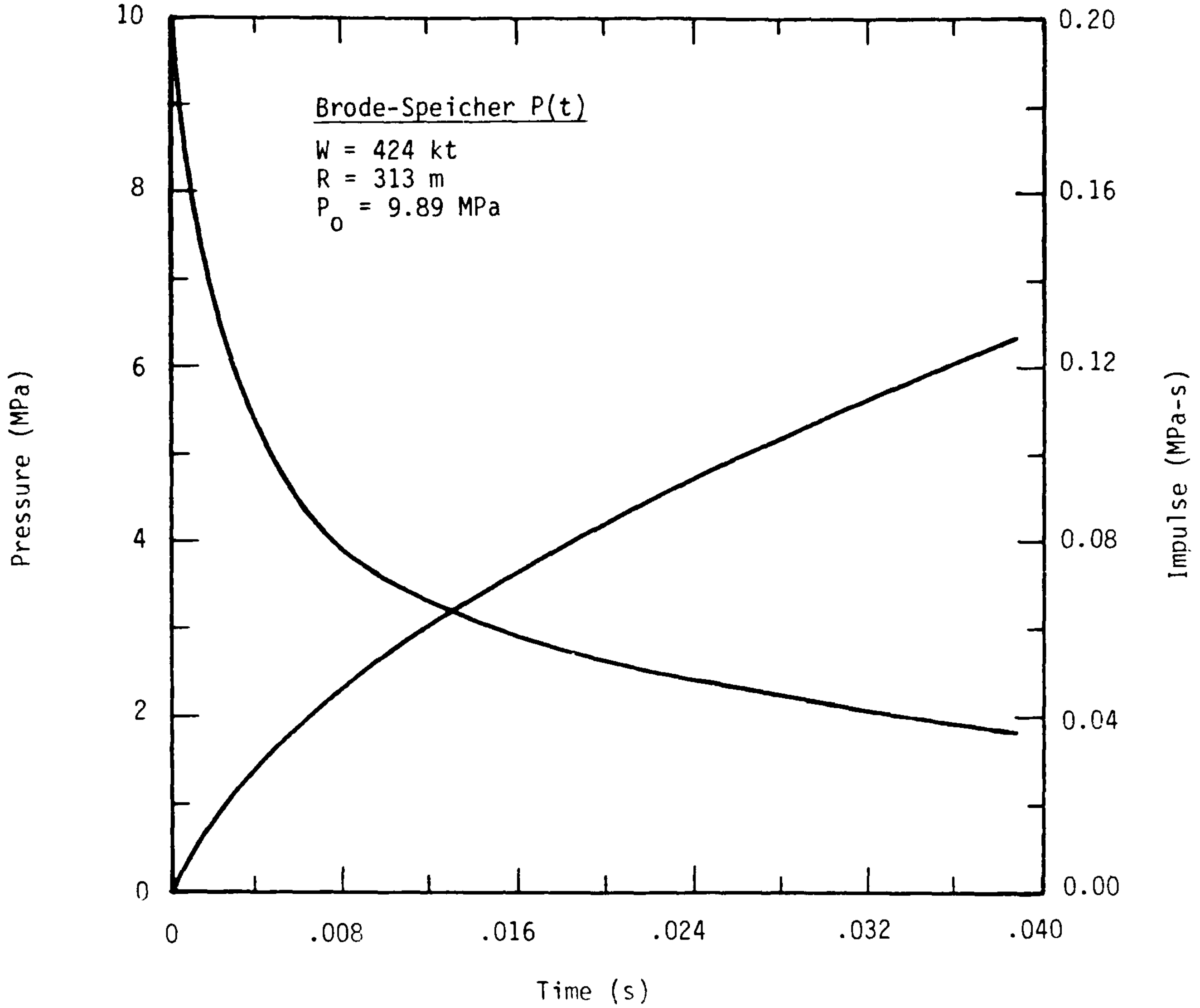

Figure 15. Applied Surface Pressure and Impulse Histories for the 1-D Planar HEST Problem.

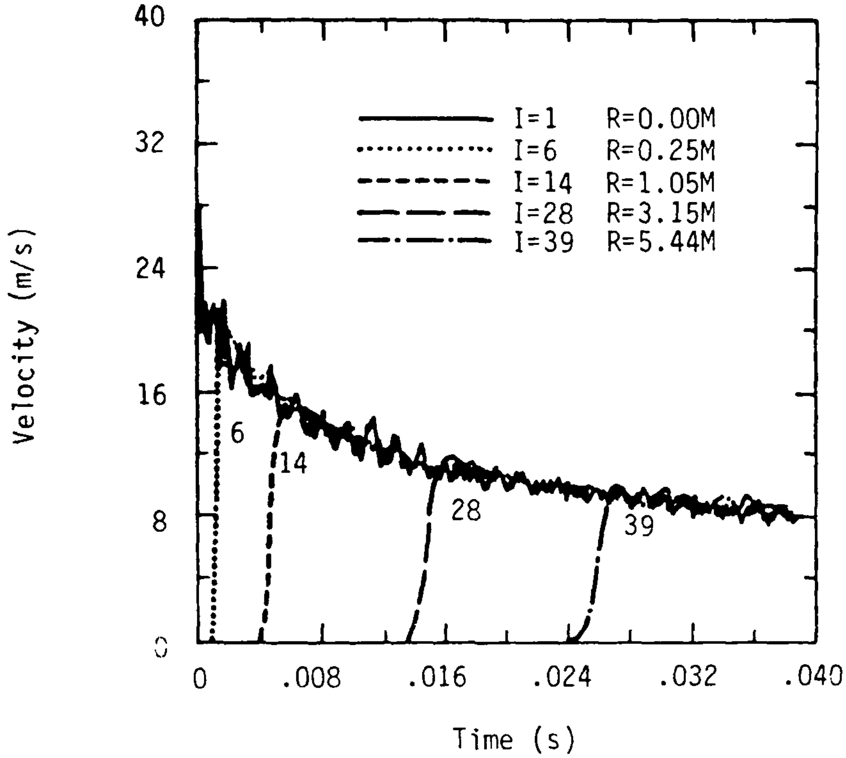

a. Vertical Velocity.

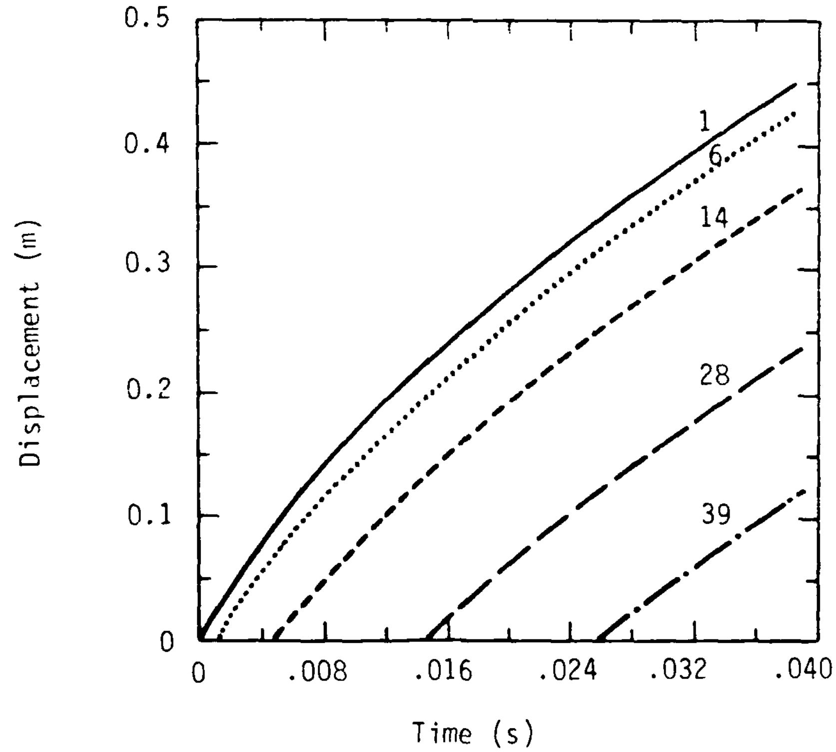

b. Vertical Displacement.

Figure 16. ARA Model 1-D Planar Calculated Motions.

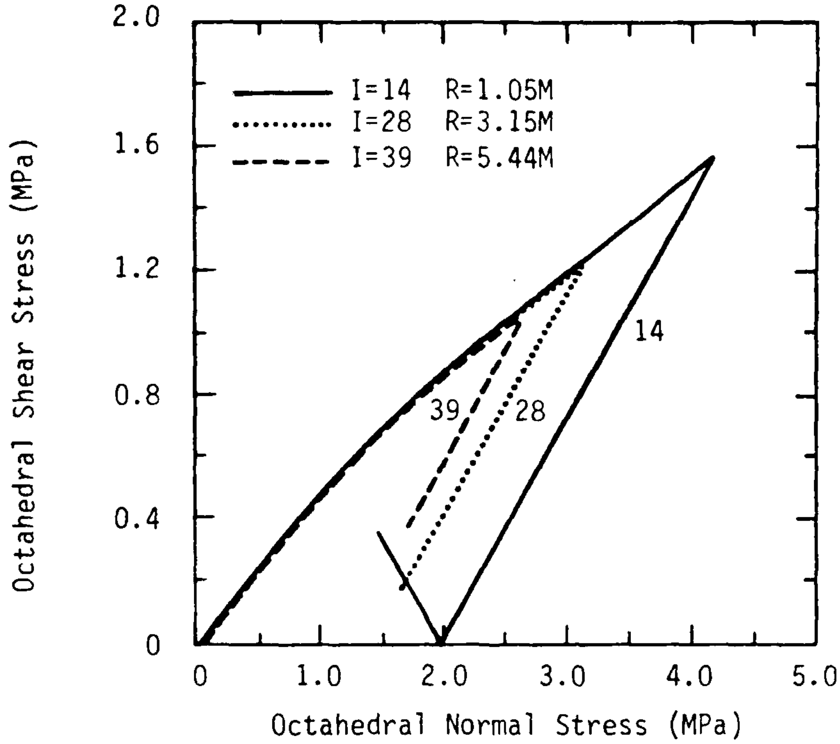

a. Stress Paths.

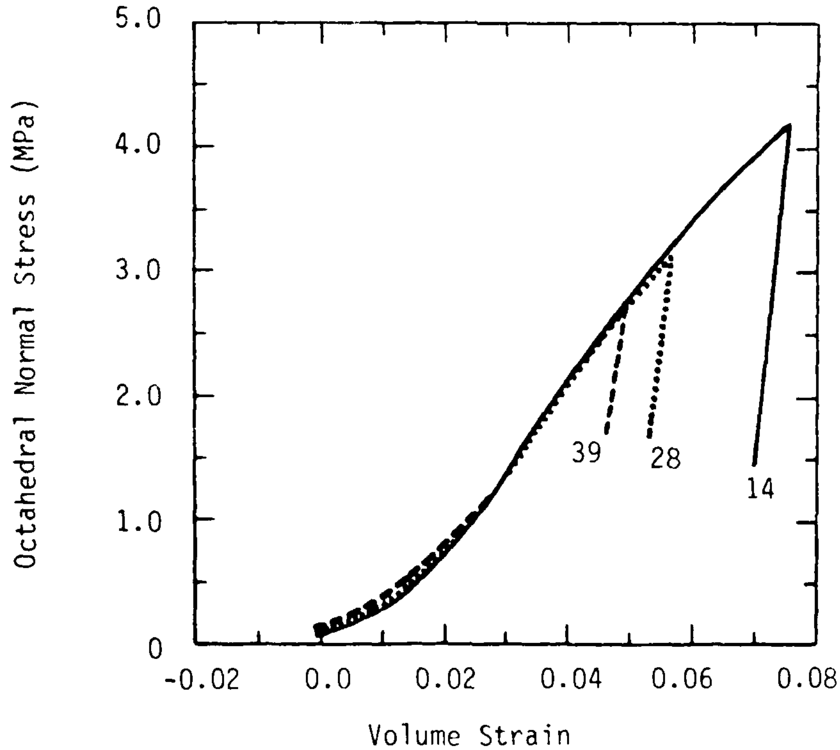

b. Pressure-Volume Response.

Figure 17. ARA Model 1-D Planar Calculated Material Response.

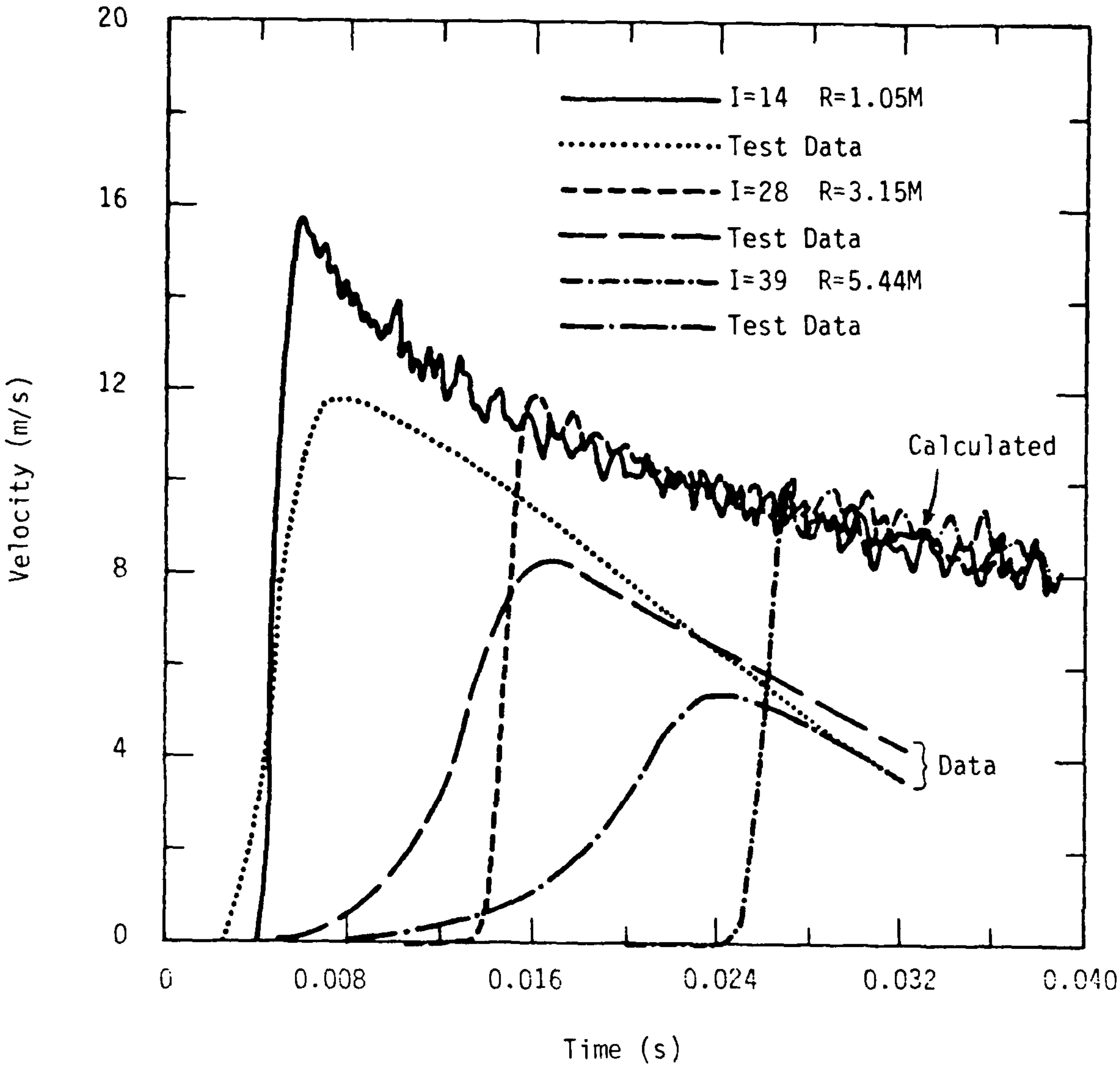

Figure 18. Comparison of Data with Calculation Using Lab-Based ARA Model.

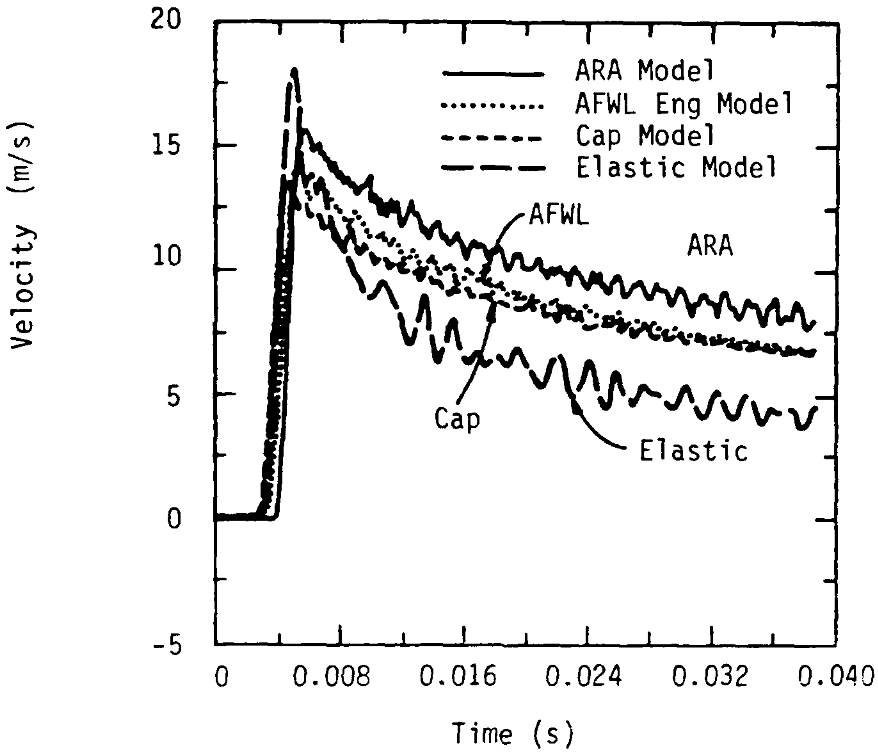

a. Depth = 1.05m

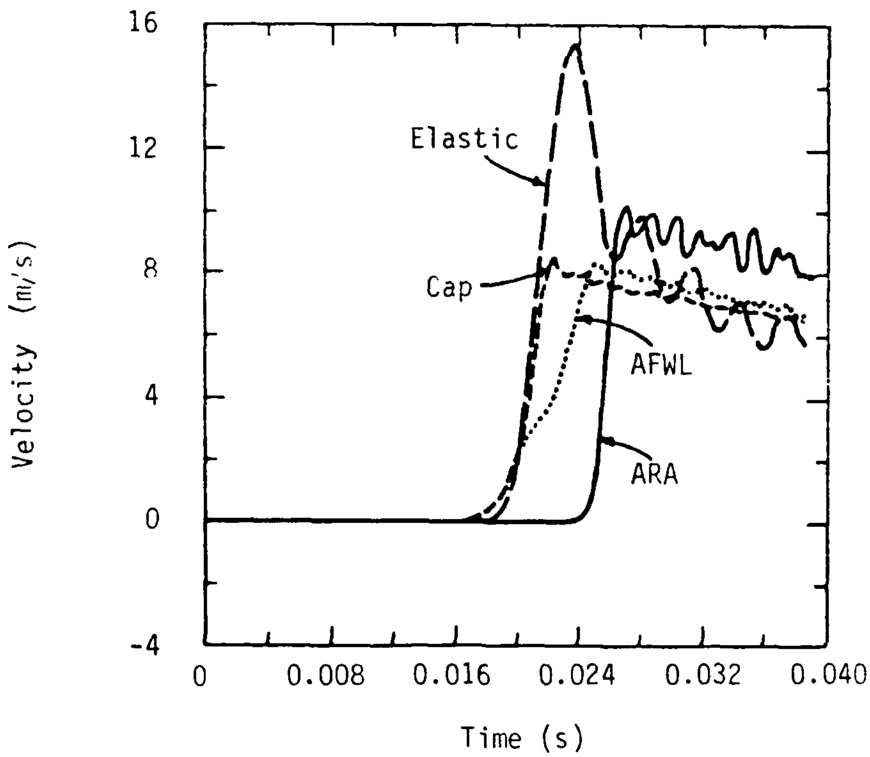

b. Depth = 5.44m

Figure 19. Comparison of 1-D Planar Waveforms Generated Using Various Material Models.

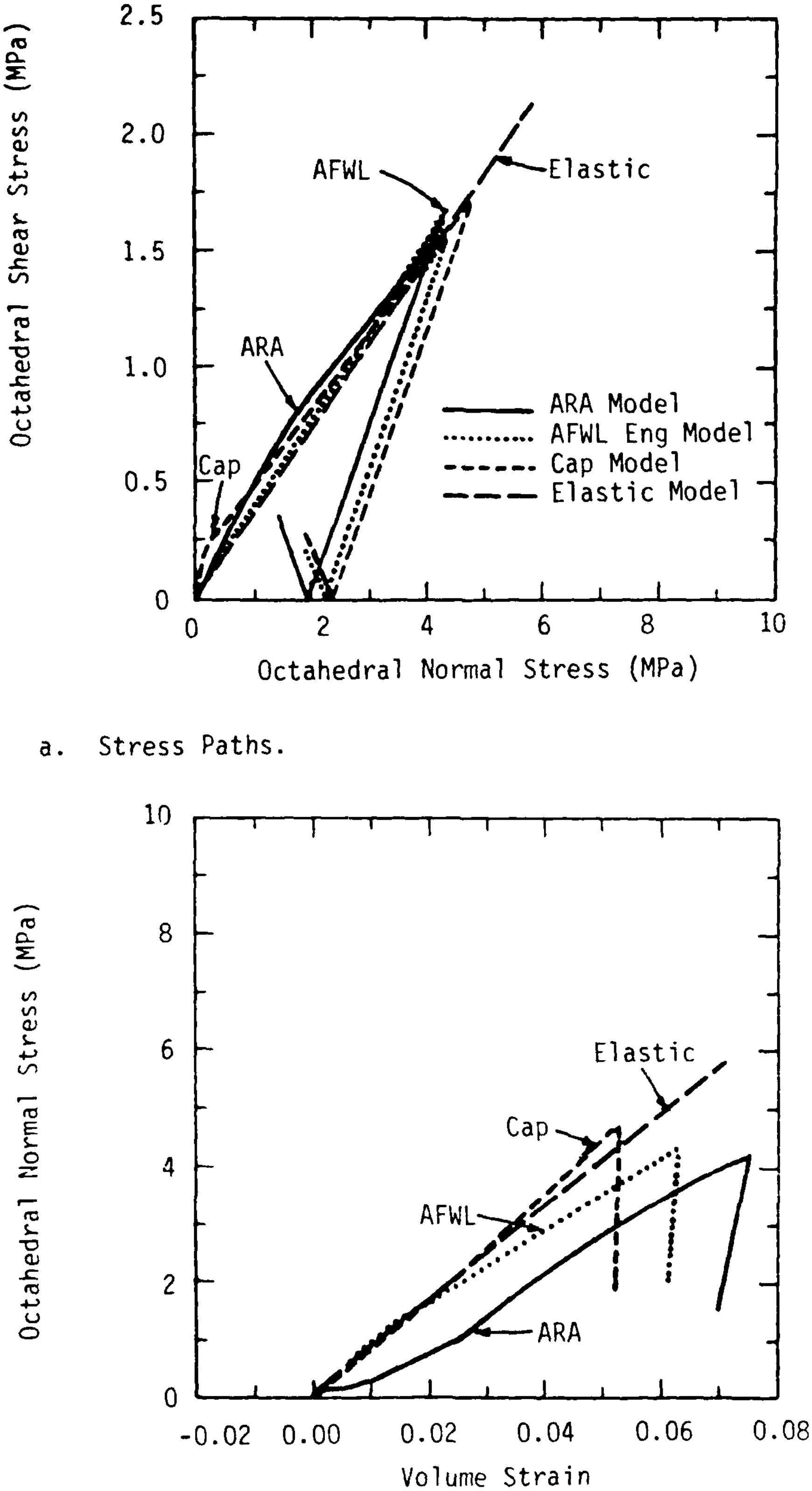

a. Stress Paths.

b. Pressure-Volume Response.

Figure 20. Model Behavior Comparisons for 1-D Planar Wave Propagation at Depth = 1.05m

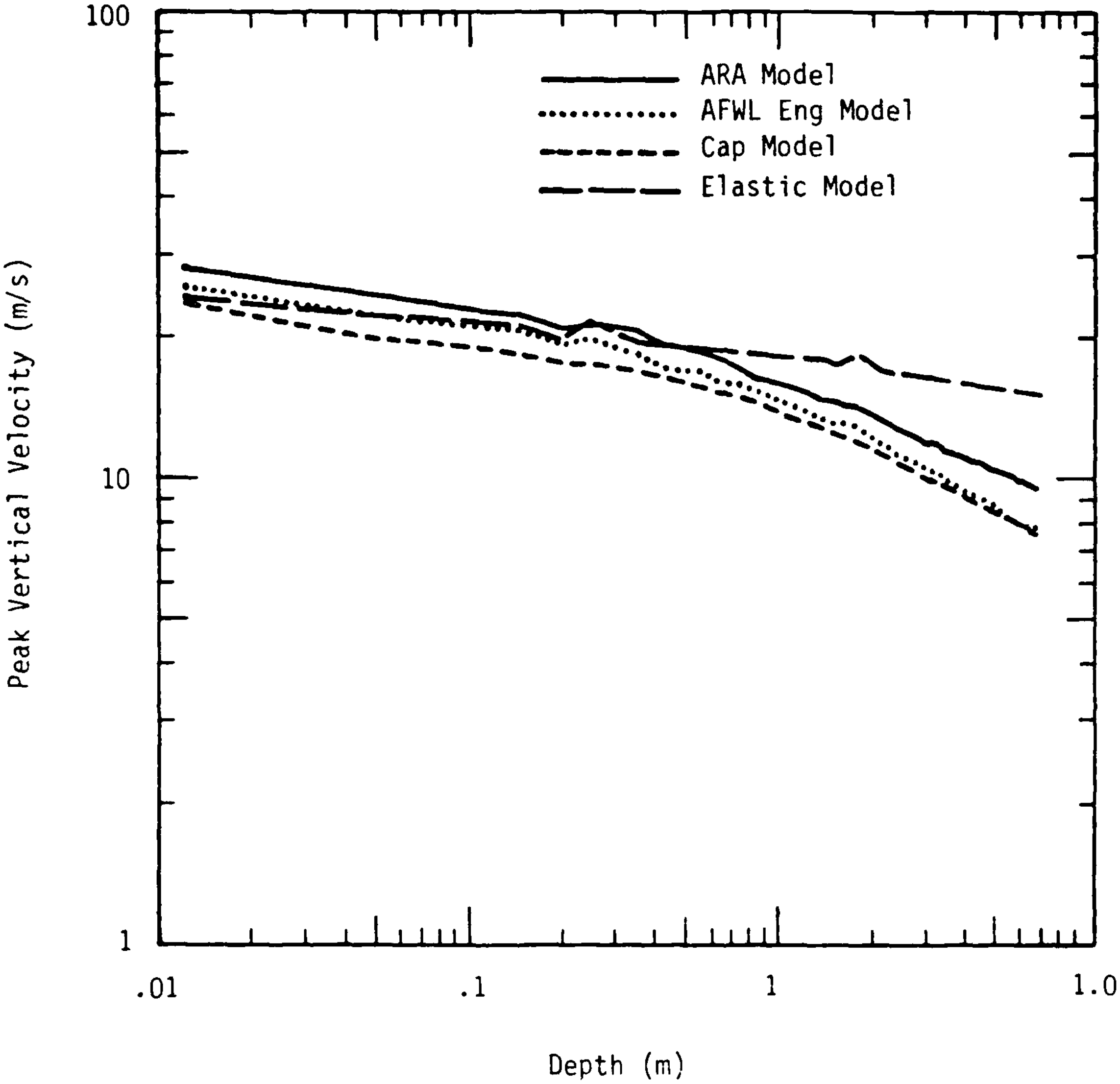

Figure 21. 1-D Planar Peak Velocity Attenuation - Model Comparisons.

to strictly uniaxial strain conditions (two principal strains equal to zero). Spherical wave propagation is the next step, where two principal strains (hoop) are also equal, but not generally zero. The resultant stress paths are more general, and exercise the shear yield surface and tensile failure components of a model much more than does uniaxial strain.

The problem selected for these calculations was the detonation of a small fully-buried sphere of high explosive. This kind of experiment has been conducted many times in conjunction with several DOD programs; e.g., MOLE, ESSEX, and most recently, ISST. The MAT PROP #1 charge was a twenty pound (9.05 Kg) sphere of C-4 explosive, buried twenty meters deep in alluvium at the ISST test site near Yuma, Arizona [Trulio (1983)]. Figure 22 shows this configuration. The test itself was not very successful (data recovery was minimal), but it does provide a case of a small buried charge in alluvium. Figure 23 shows the calculational grid for these calculations. A uniform geology was assumed. An initial isotropic prestress corresponding to a depth of 20 m was applied, but no gravity forces were used in the calculation. The HE sphere was modeled using the JWL equation of state [Lee, et al. (1968)] for nitromethane. The JWL equation of state is an empirical relationship used to predict the behavior of explosives by accounting for large expansion of the detonation products. The equation for pressure (P) is:

$$P = A\left(1 - \frac{\omega}{R_1 V}\right) e^{-R_1 V} + B\left(1 - \frac{\omega}{R_2 V}\right) e^{-R_2 V} + \frac{\omega E}{V} \qquad (64)$$

where V stands for relative volume (V/V_0), E is energy density (per unit volume), and A, B, R_1, R_2, and ω are experimentally derived constants. Table 4 lists the parameters for nitromethane, which were used to approximate C-4. The explosive was not burned (i.e., no detonation front was propagated), so peak cavity stress was lower than would actually occur. However, actual peak cavity stress decays so rapidly with range that it is immediately damped down to a non-burned level in a calculation using these zone sizes (0.1 m). Burning the explosive would therefore have been inconsequential. Figure 24 shows the pressure history generated in the cavity.

The spherical calculations were run to only a very short time, about 2 ms. This is shorter than practical for normal production calculations of this type, but was desirable here for two reasons. First, results from every cycle could

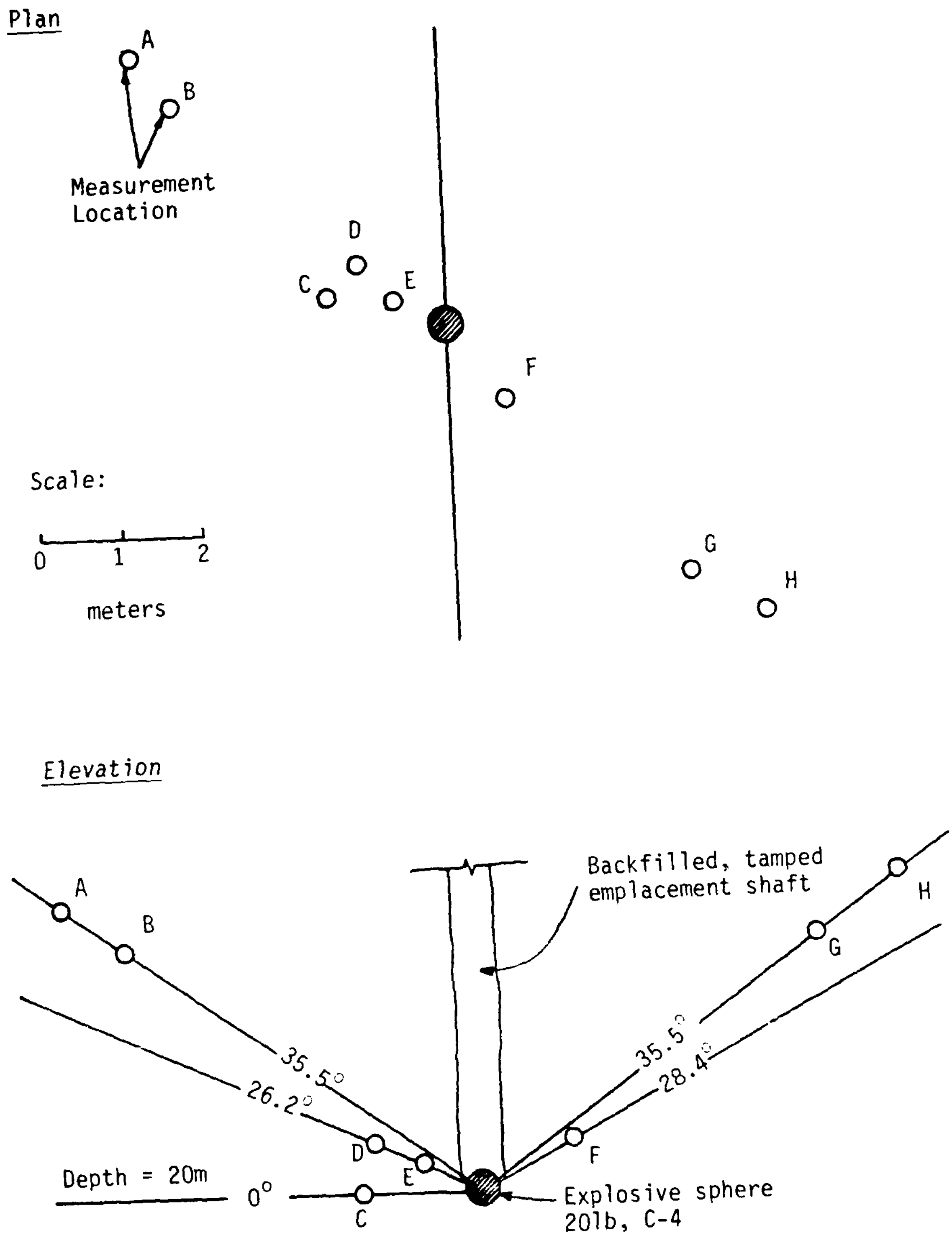

Figure 22. Mat Prop #1 Experiment Configuration.

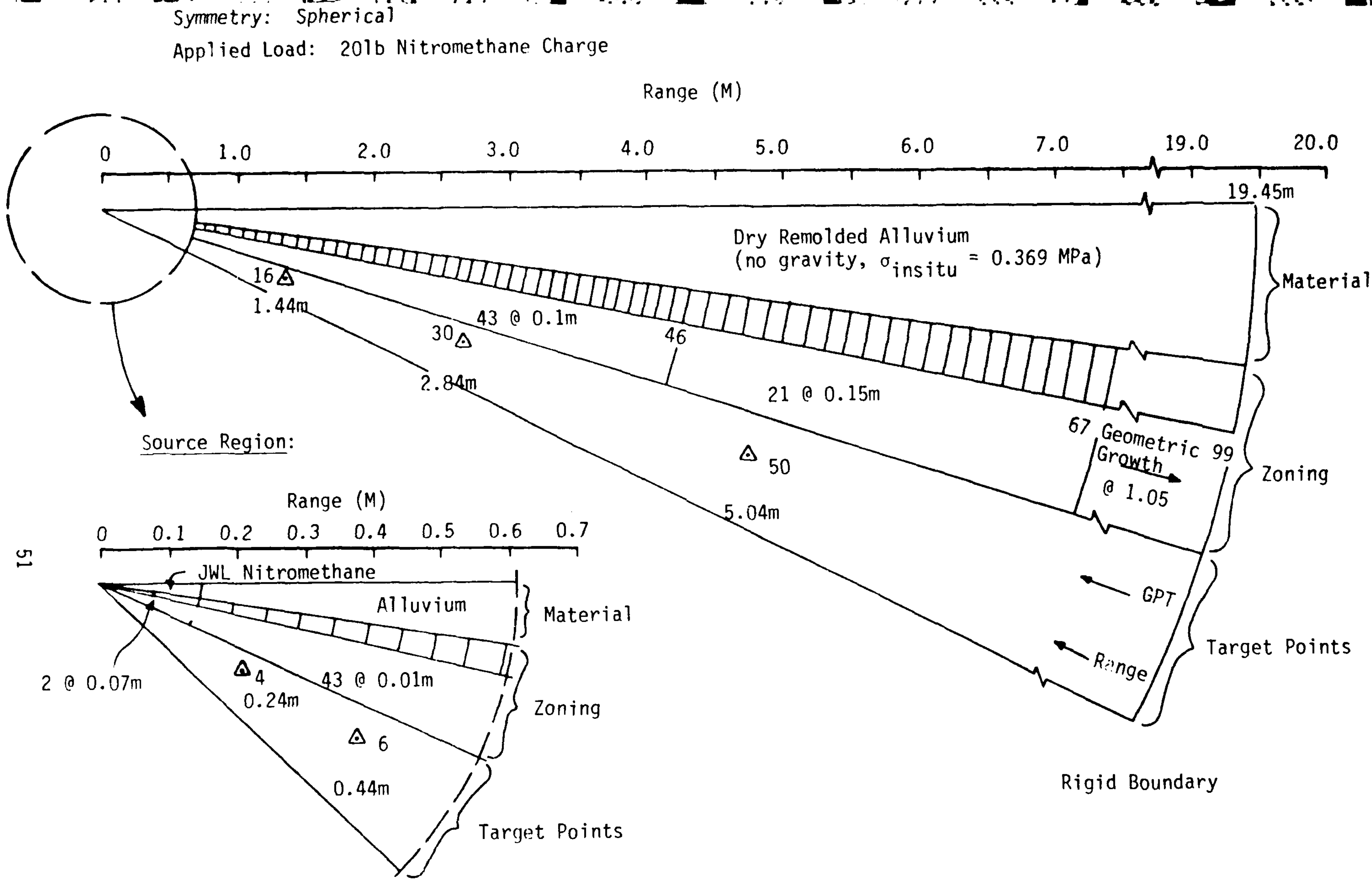

Figure 23. 1-D Spherical Wave Propagation Calculational Configuration.

TABLE 4. JWL EQUATION OF STATE PARAMETERS FOR NITROMETHANE
[Lee, et al. (1968:5)]

Parameter	Symbol	Value	Units
Constants	A	2.0925×10^{11}	J/M^3
	B	5.0895×10^{9}	J/M^3
	R_1	4.4	--
	R_2	1.2	--
	ω	0.30	--
Mass Density	ρ_0	1128.	kg/m^3
Total Available Energy	E_0	5.1×10^{9}	J/M^3

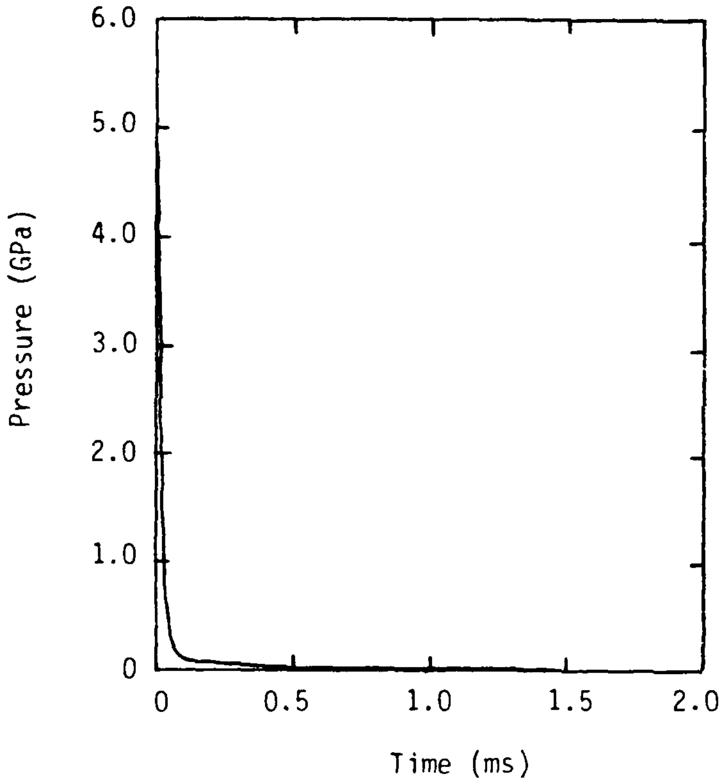

Figure 24. 1-D Spherical Cavity Pressure.

be plotted, which showed exactly how the model was performing without any gaps due to plotting restrictions. Second, the zones immediately adjacent to the source were of most interest because of their severe compression and then rapid hoop expansion. It is often true that for very severe environment calculations, the first few cycles tell the whole story. Running this calculation out to longer duration would also eventually require rezoning, which has not yet been fully developed for the ARA model.

Radial velocity and displacement waveforms generated using the ARA model are shown in Figure 25. Very steep motion gradients close to the source are due in large part to grid size effects. At a loading wavespeed of roughly 400 m/s, 0.1 m zones will act as a 2000 Hz low pass filter on the pressures generated in the cavity. Velocity waveforms are compared with results from several other models in Figure 26. The elastic model is the only model which produces a substantially different waveform, mainly because no shear failure occurs. This is shown in Figure 27, where stress paths at the 0.44 m target point are overlaid for the different models. The highest shear stress is achieved during the initial loading. Subsequent loops in the ARA and AFWL Engineering model stress paths are caused by rejoin after spall. Spall is caused by the rapid hoop expansion, rejoin is caused by the relatively high pressure which remains in the cavity. Figure 28 compares the strain paths calculated using the four models.

4.4.4 Cylindrical (CIST) Calculations. Within the constraints of one-dimensional wave propagation, cylindrical geometry is capable of producing the most general stress paths. This is because the three principal stresses and strains are not equal. Thus, a material model's ability to account for many situations encountered in two-dimensional calculations is tested.

The Cylindrical Insitu Test (CIST) geometry was chosen for these calculations because of the large insitu dynamic data base generated by these experiments. There have been twenty-three CIST's to date, in dry soil, wet soil, and rock geologies. All have had essentially identical charge design: a two foot diameter borehole filled with racked 400-grain PETN detonating cord, and an explosive density of 5 lbs/linear ft of cavity. The nominal peak cavity pressure for this explosive configuration is about 40 MPa. Subsequent decay of cavity pressure varies with depth and the properties of the surrounding geologic

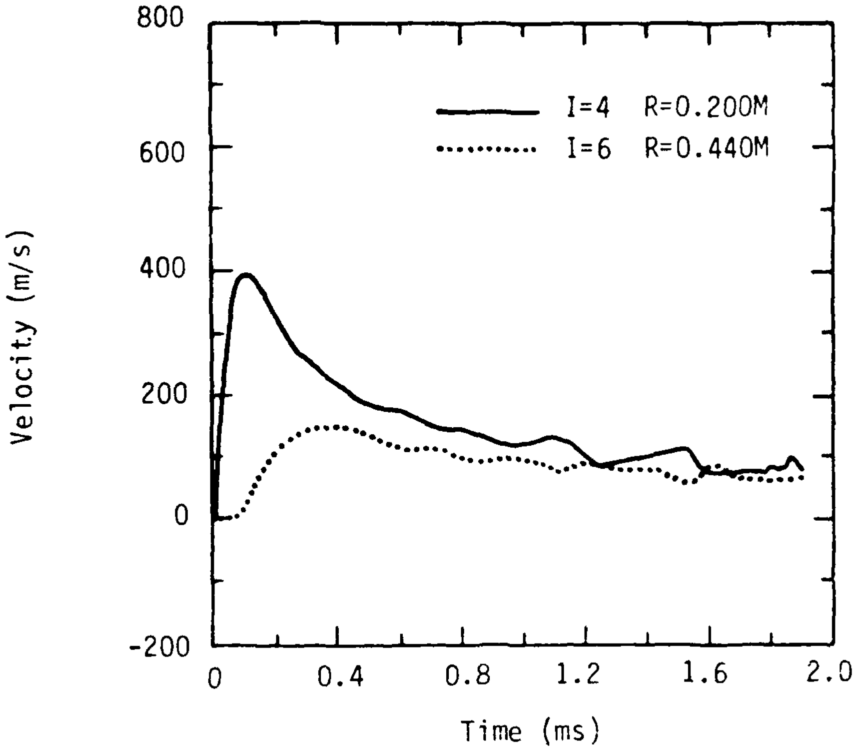

a. Radial Velocity.

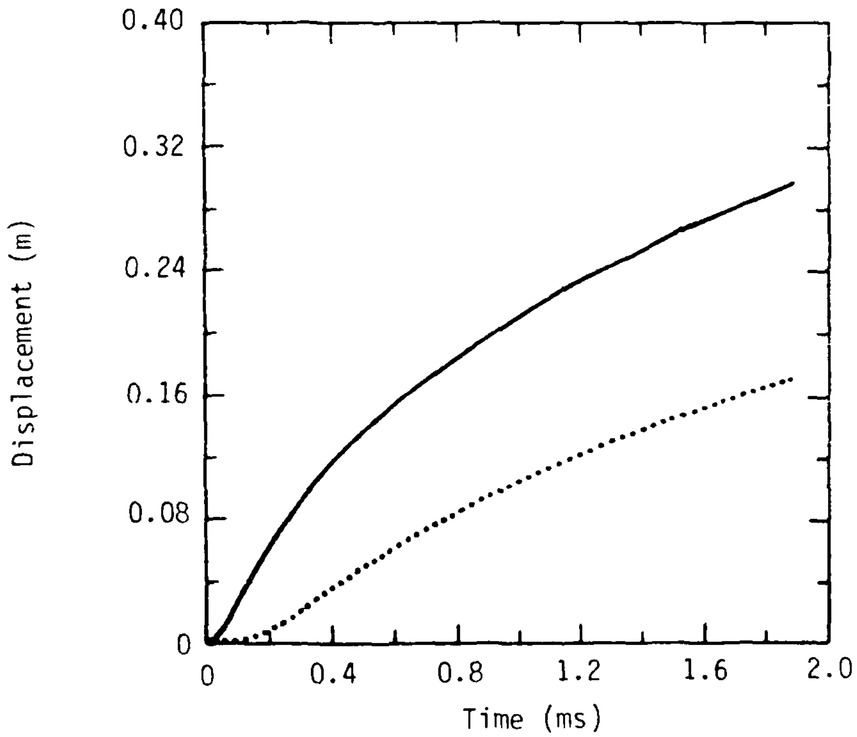

b. Radial Displacement.

Figure 25. ARA Model 1-D Spherical Calculated Motions.

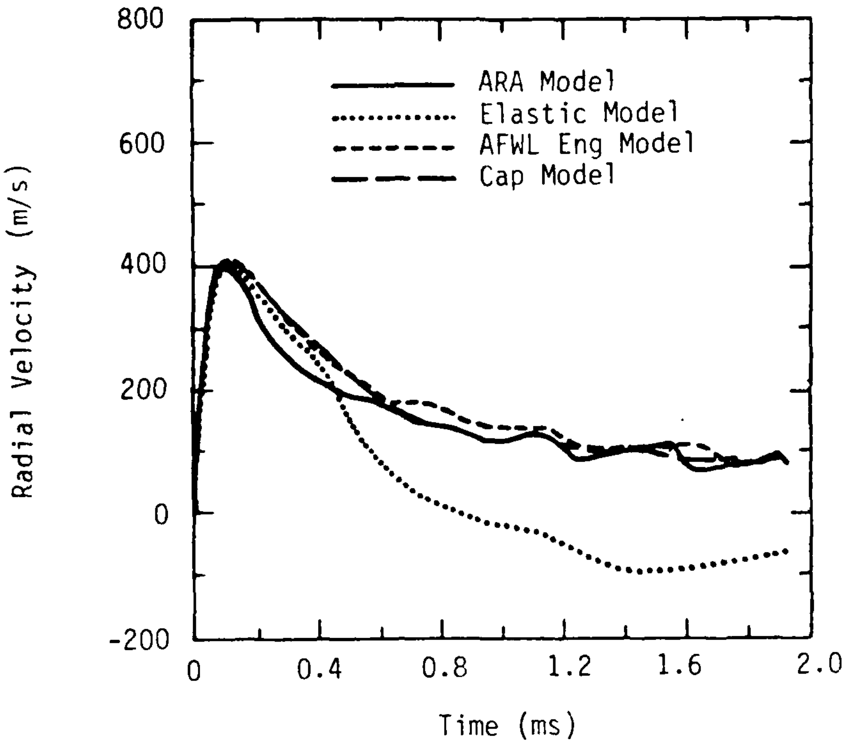

a. Range = 0.24m (Grid Point No. = 4)

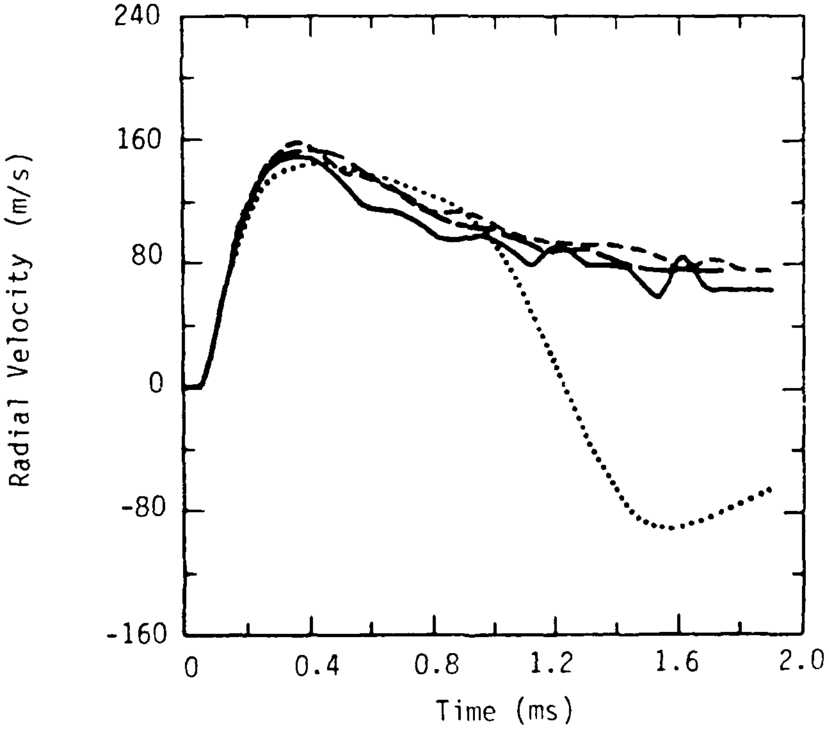

b. Range = 0.44m (Grid Point No. = 6)

Figure 26. Comparison of 1-D Spherical Waveforms Generated Using Various Material Models.

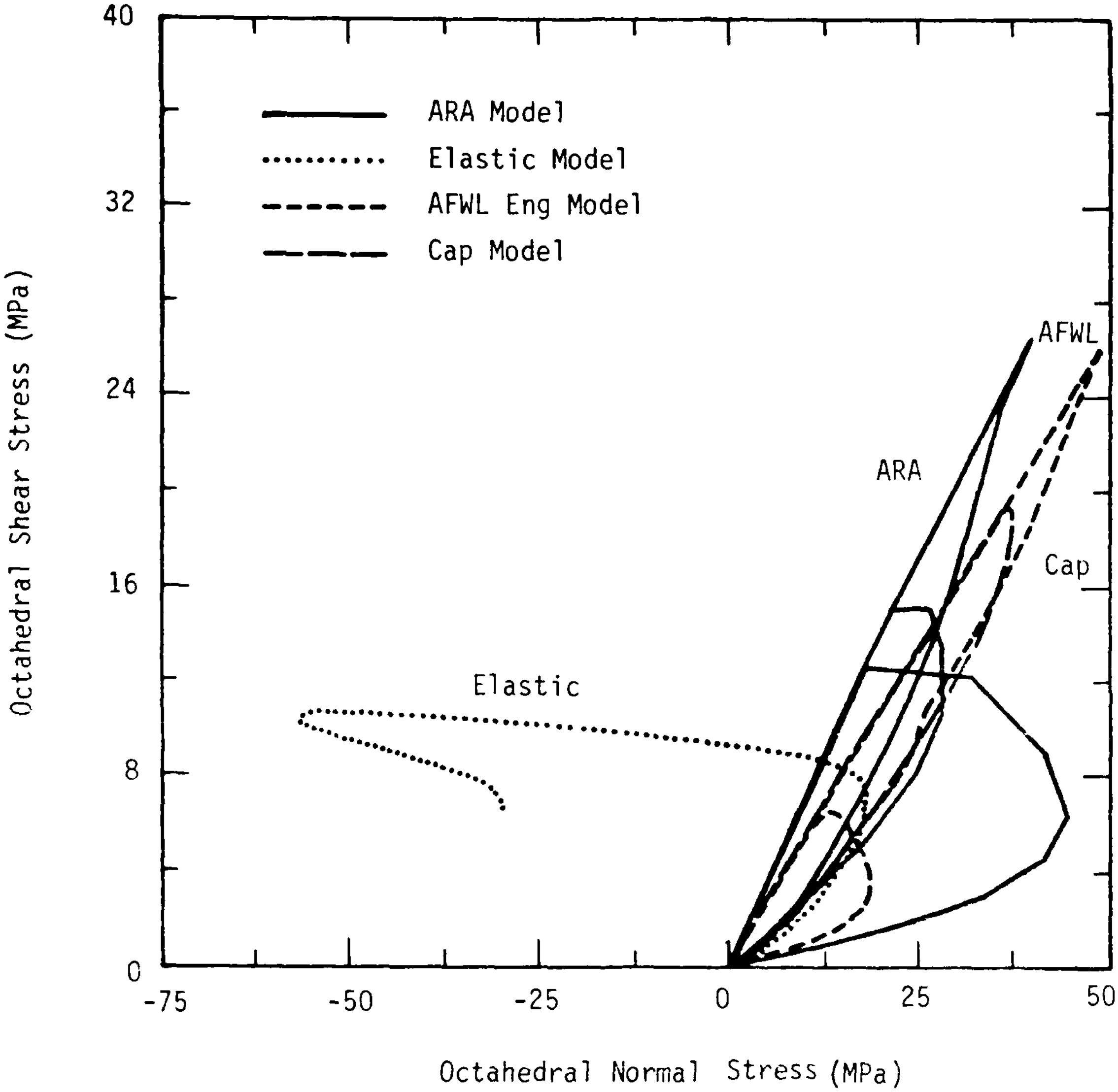

Figure 27. Stress Path Comparison for Various Models in 1-D Spherical Wave Propagation.

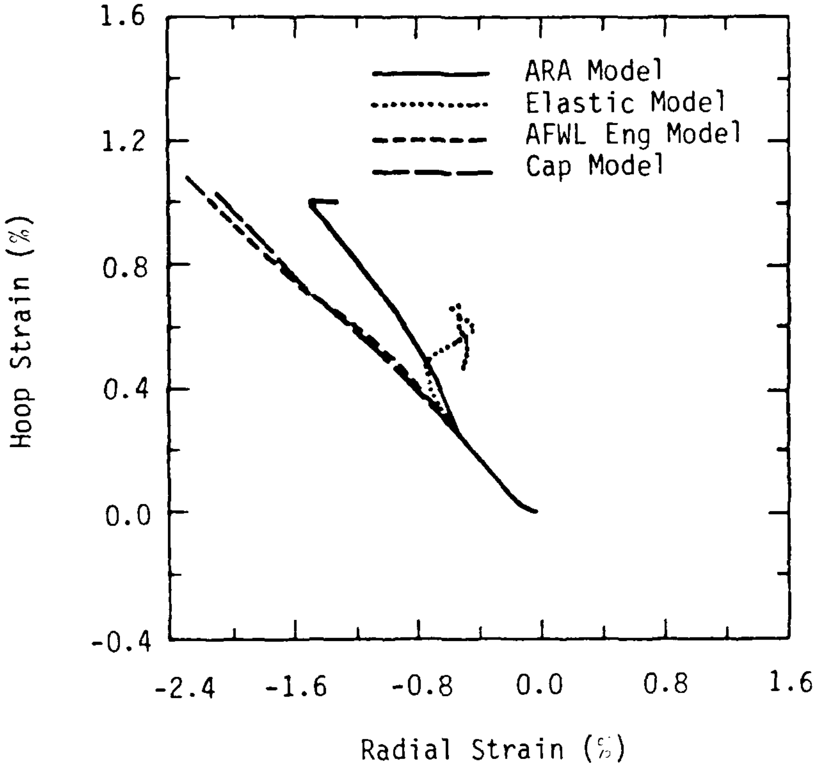

a. Range = 0.24m (Grid Point No. = 4).

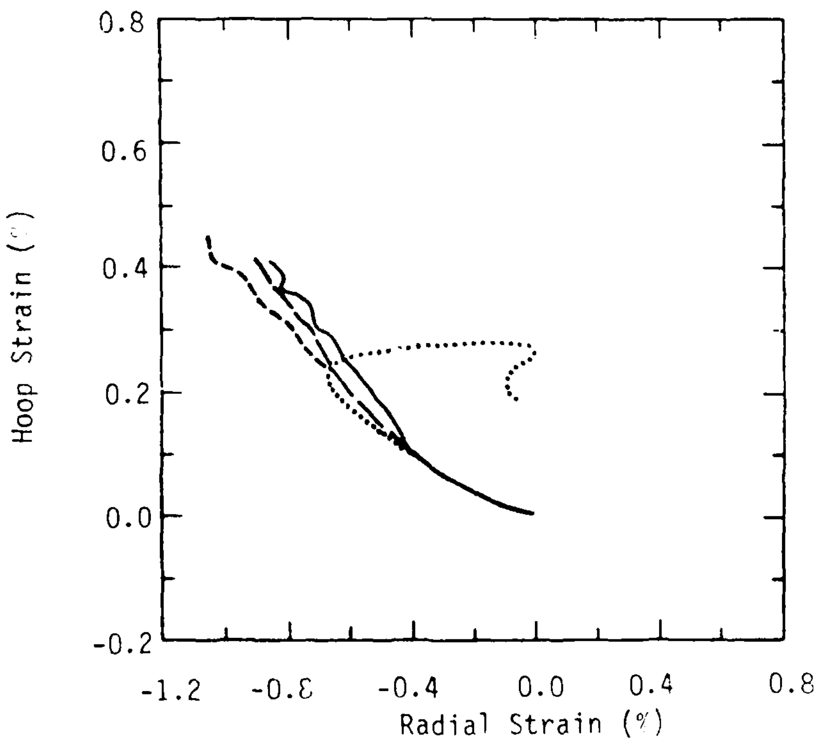

b. Range = (44m (Grid Point No. = 6).

Figure 28. Comparison of Calculated 1-D Spherical Strain Paths Using Various Material Models.

material. CIST 18 was conducted at the HAVE HOST site, at a location close to the two experiments discussed previously. It was actually two tests, CIST 18 s (shallow) and CIST 18 d (deep). The configuration of CIST 18 s&d is shown in Figure 29. More information is given by Amend, Ullrich, and Thomas (1977).

The axisymmetric calculation used to model CIST 18 is shown in Figure 30. One material was used throughout the grid. Gravity was not used, but an isotropic prestress of 0.18 MPa, corresponding to about a 10 m depth, was applied. The target points used include the typical CIST gage radii of 0.91, 1.52, and 2.44 meters.

The appropriate pressure boundary for driving CIST calculations is always uncertain because there have been few successful measurements made in the explosive cavity. CIST 18 was one of the few tests which yielded a reasonable pressure history, so this was used to fit a two-term exponential function. The form of the equation used was:

$$P(t) = 21\ e^{-900t} + 19\ e^{-165t} \qquad (t > 0.000125) \qquad (65)$$

with units of MPa and seconds. This pressure history and its impulse are shown in Figure 31. These calculations were run to a duration of about 40 ms.

Calculated motions using the ARA model are shown in Figure 32. A tendency for low frequency outward flow is noted at all ranges due to shear failure and a very high unload-reload modulus. The higher frequency motions superimposed on this are caused by post-spall rejoin signals generated near the source. These late time spikes are not real, i.e., they are not observed in test data, and are consequences of using a minimum pressure cutoff for a tensile failure criterion. Figure 33a shows the volume compression response calculated at several ranges. The tendency for the model to continue to compress during post-peak cycles of reloading is the most interesting aspect of this behavior. Figure 33b shows strain paths for these same ranges.

Calculated velocity is compared with some representative composite data from CIST 18 s&d in Figure 34. Again, the lab-based model is clearly deficient in predicting insitu motions.

Cylindrical results were generated using the three other models for comparison with the ARA model. The velocity waveforms for the ARA and the AFWL Engineering models are very similar (Figure 35). The cap model seems to do

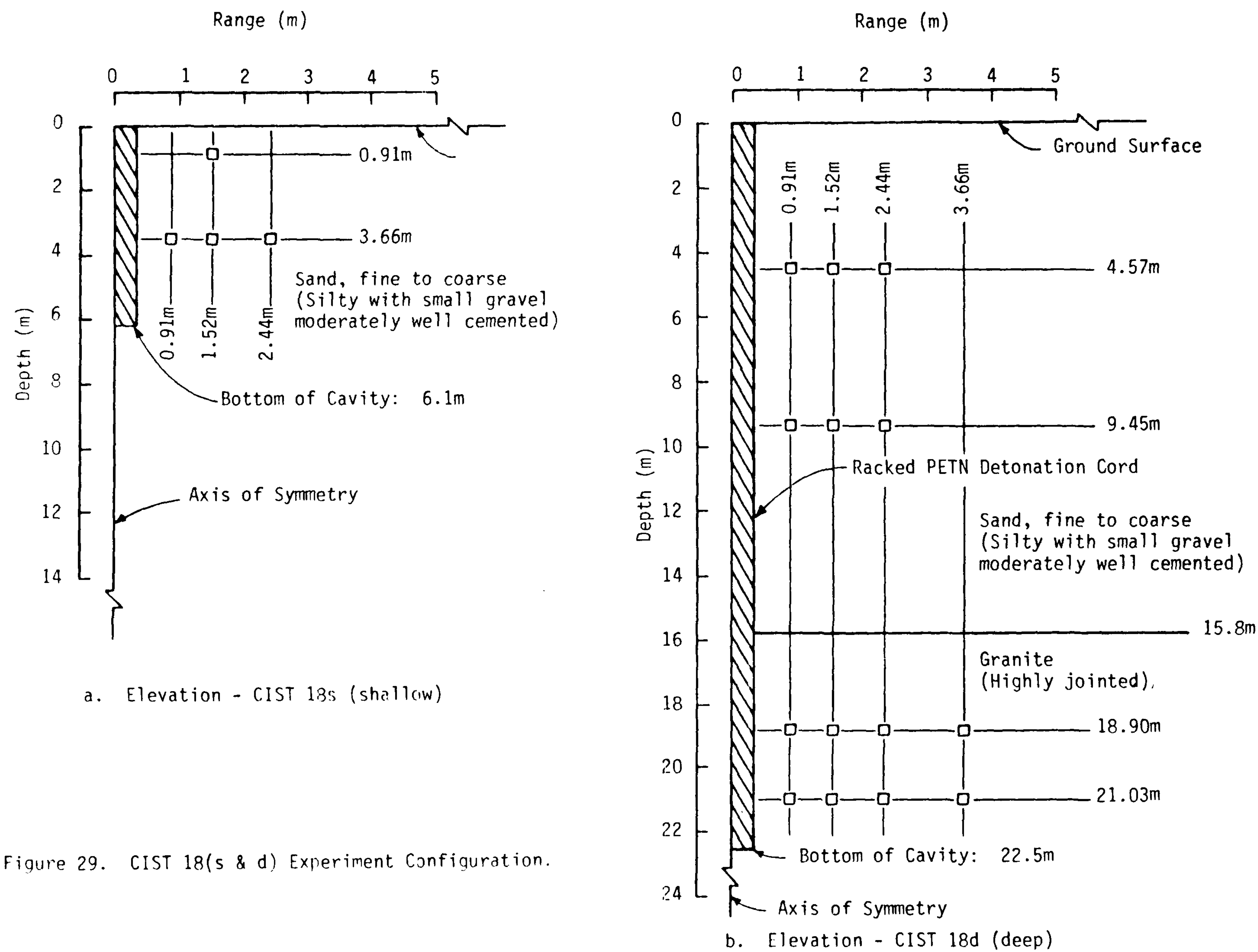

Figure 29. CIST 18(s & d) Experiment Configuration.

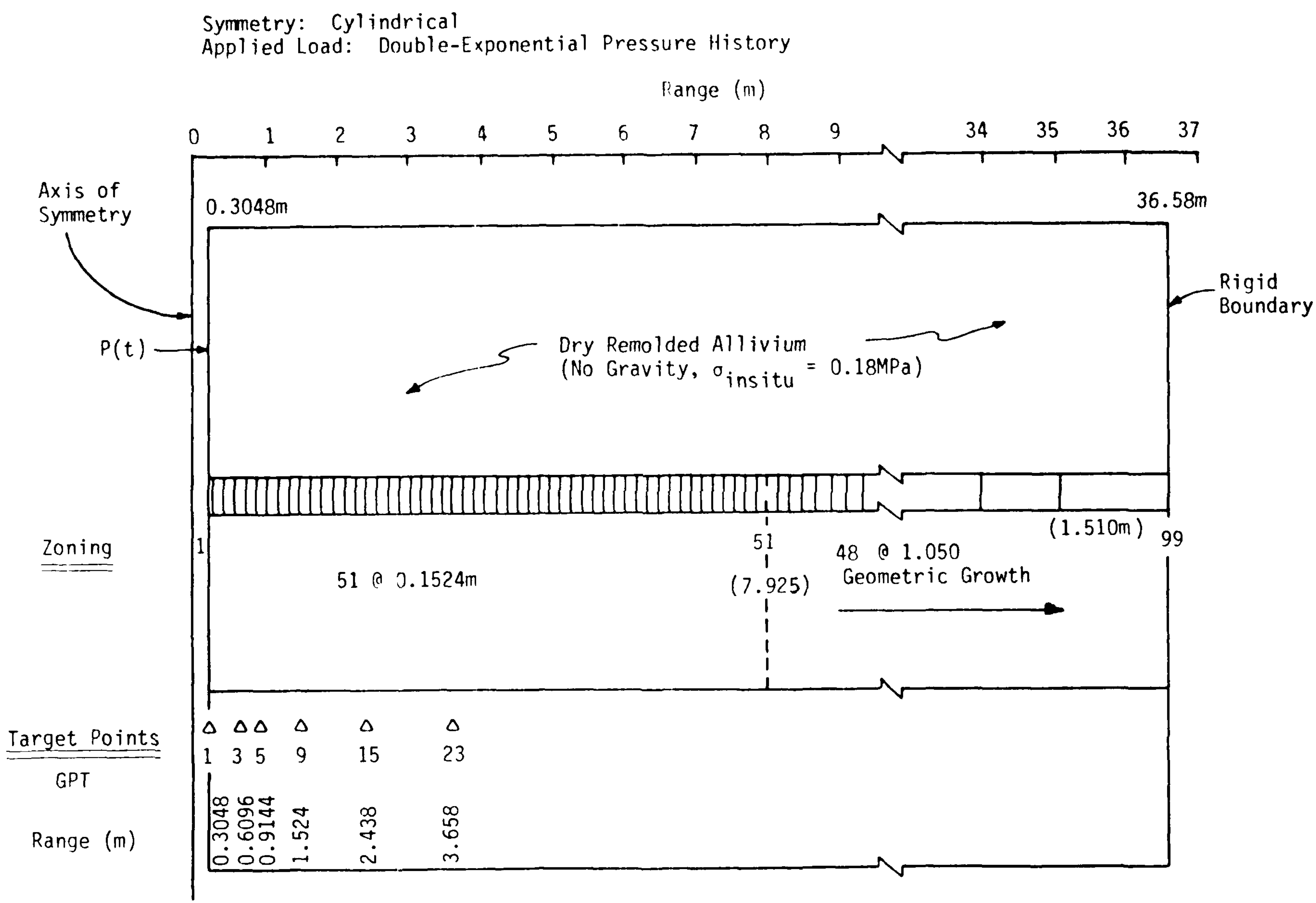

Figure 30. 1-D Cylindrical Wave Propagation Calculational Configuration.

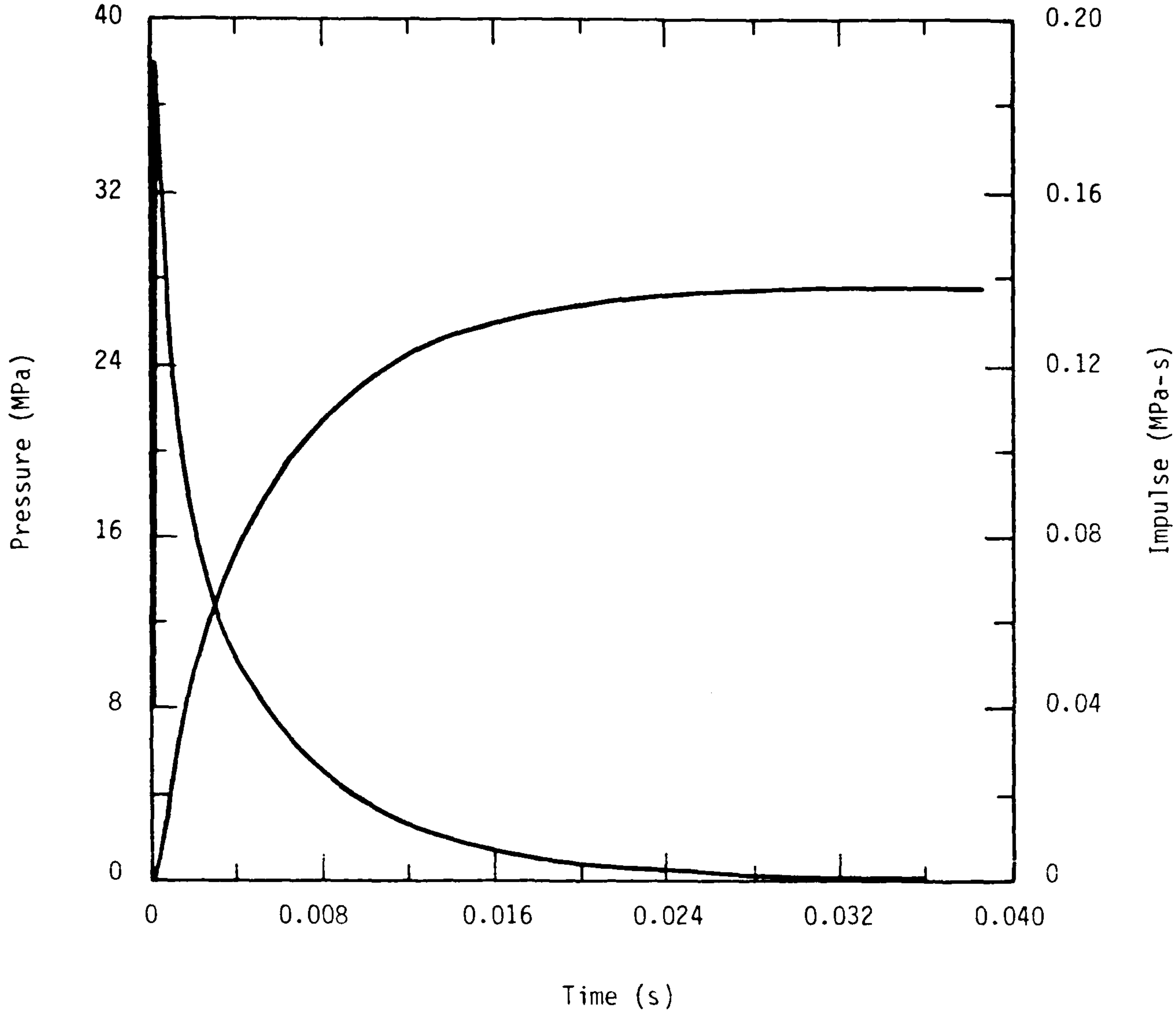

Figure 31. Applied Cavity Pressure and Impulse Histories for the 1-D Cylindrical Problem.

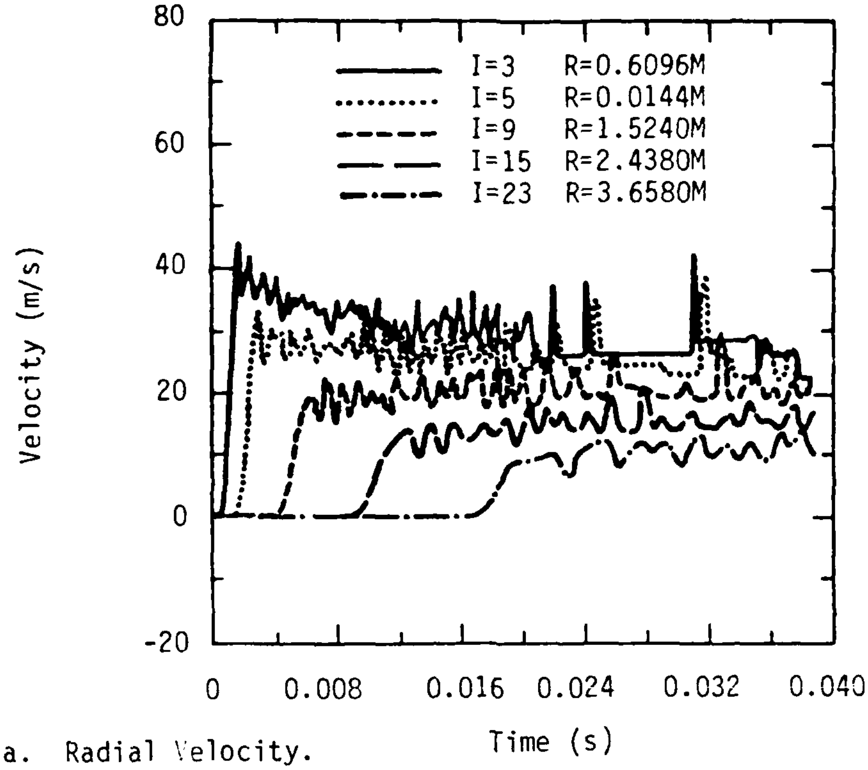

a. Radial Velocity.

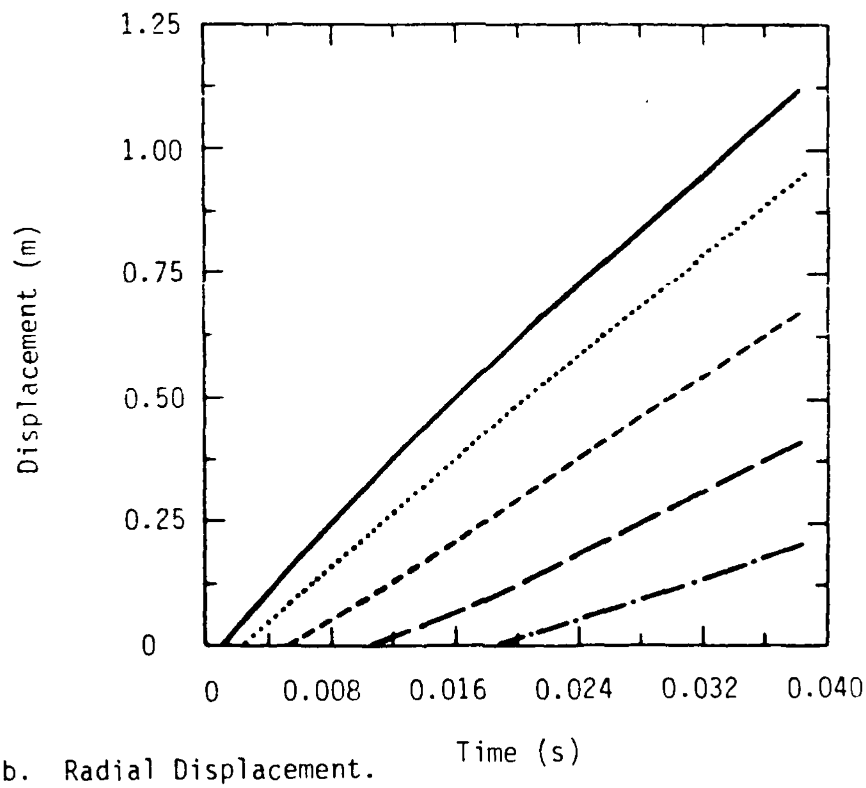

b. Radial Displacement.

Figure 32. ARA Model 1-D Cylindrical Calculated Motions.

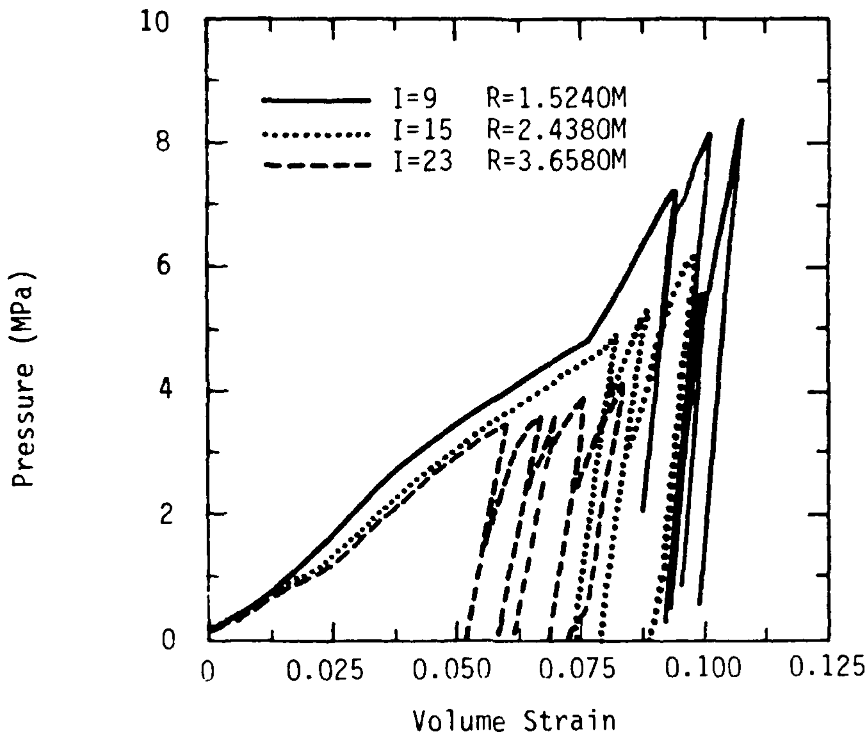

a. Pressure-Volume Response.

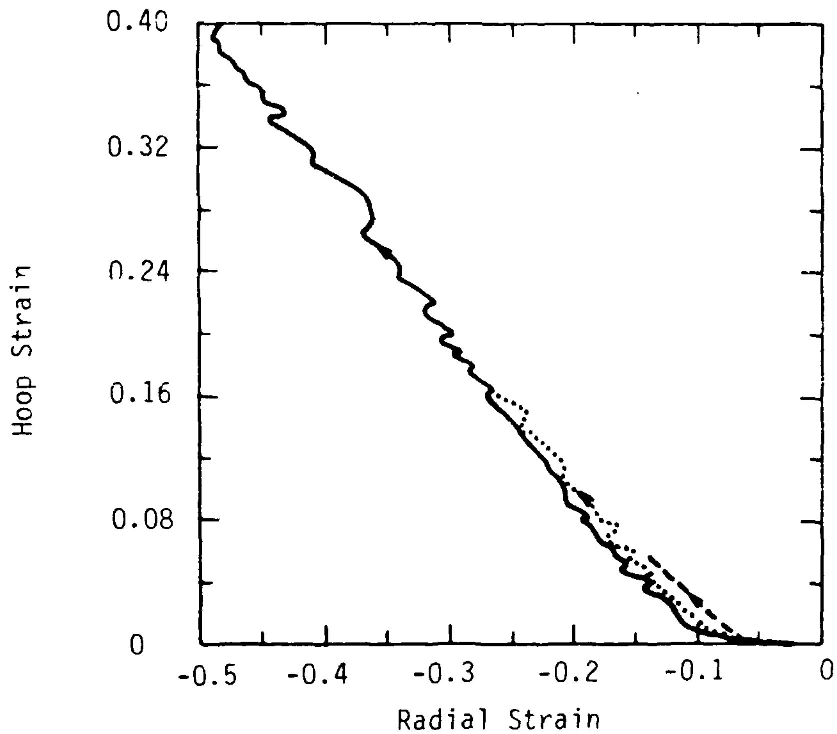

b. Strain Paths.

Figure 33. ARA Model 1-D Cylindrical Calculated Material Response.

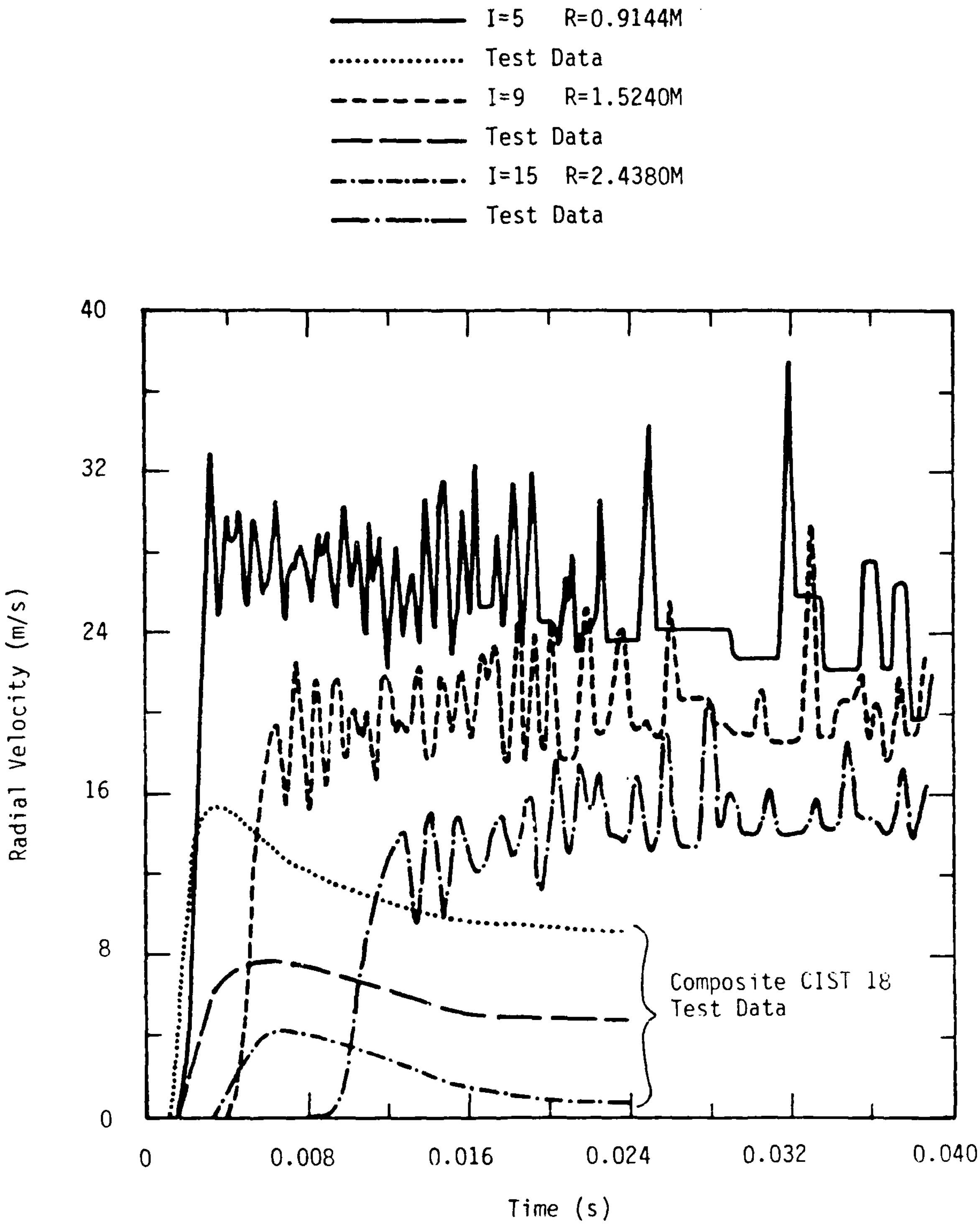

Figure 34. Comparison of 1-D Cylindrical Insitu Data with Calculation Using Lab-Based ARA Model.

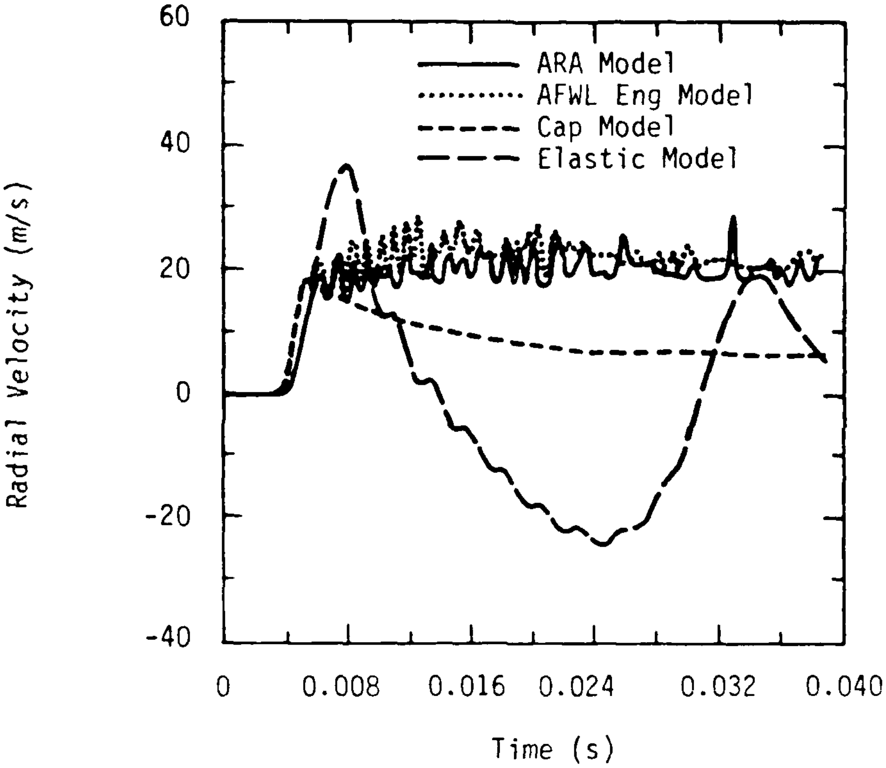

a. Range = 1.52m (Grid Point No. 9).

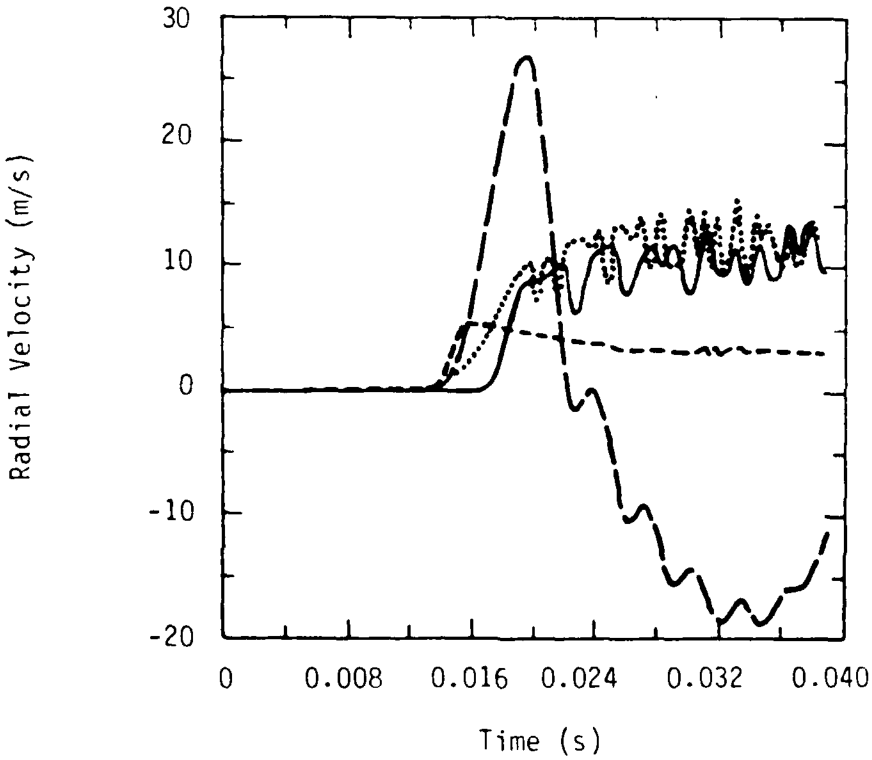

b. Range = 3.66m (Grid Point No. 23).

Figure 35. Comparison of 1-D Cylindrical Waveforms Generated Using Various Material Models.

better and does not tend to flow out as do the others. The reason is its volume response under these conditions, shown in Figure 36. The cap model has a much higher effective unload-reload modulus and does not cycle as much as either the ARA or AFWL Engineering models. Strain paths at two ranges are compared in Figure 37.

4.4.5 Discussion of One-Dimensional Calculations. In an effort aimed primarily at successful model implementation, emphasis is naturally on computational aspects rather than on actual soil behavior. So the first thing to be said about the one-dimensional results is that they show the ARA model is capable of functioning in a dynamic finite difference wave propagation environment. The fact that the ARA model results do not always match observed insitu behavior is not too troublesome at this point. The data comparisons, when shown, provide a goal toward which the model fitting process can procede.

Most of the effort which went into the calculations with the ARA model was spent on eliminating the kinds of numerical errors discussed in Section 3.2. Yield surface violation due to both plastic and elastic overshoot was the most serious problem. The subcycling technique was devised to circumvent reformulation of the expansive plastic work function to avoid the singularity at the isotropic axis, or modification of the solution technique (from incremental stiffness to predictor-corrector). Subcyling may not be the most efficient approach. The next biggest problem turned out to be the tensile failure logic (spall model). With the tendency of the stress point to move quickly down the yield surface, many of the zones (particularly near the source) spent most of the time at the apex of the expansive yield surface. Tracking spall strain and providing for orderly rejoin was therefore critical for overall success. Gravity initialization was the third major outcome of the one-dimensional calculations.

The ARA model was the most time-consuming of the four models compared. Table 5 compares times spent in various parts of the calculations. A grid cycle is the calculation of the response for the entire grid for one time step. Grid cycle times varied for the ARA model and the cap models because a different number of zones may be subcycled for any given cycle. Since subcycling occurs mostly near the isotropic axis for the ARA model, application of anisotropic gravity stress (grid setup) in the 1-D planar case took a great deal of time, but substantially reduced subsequent dynamic calculation time.

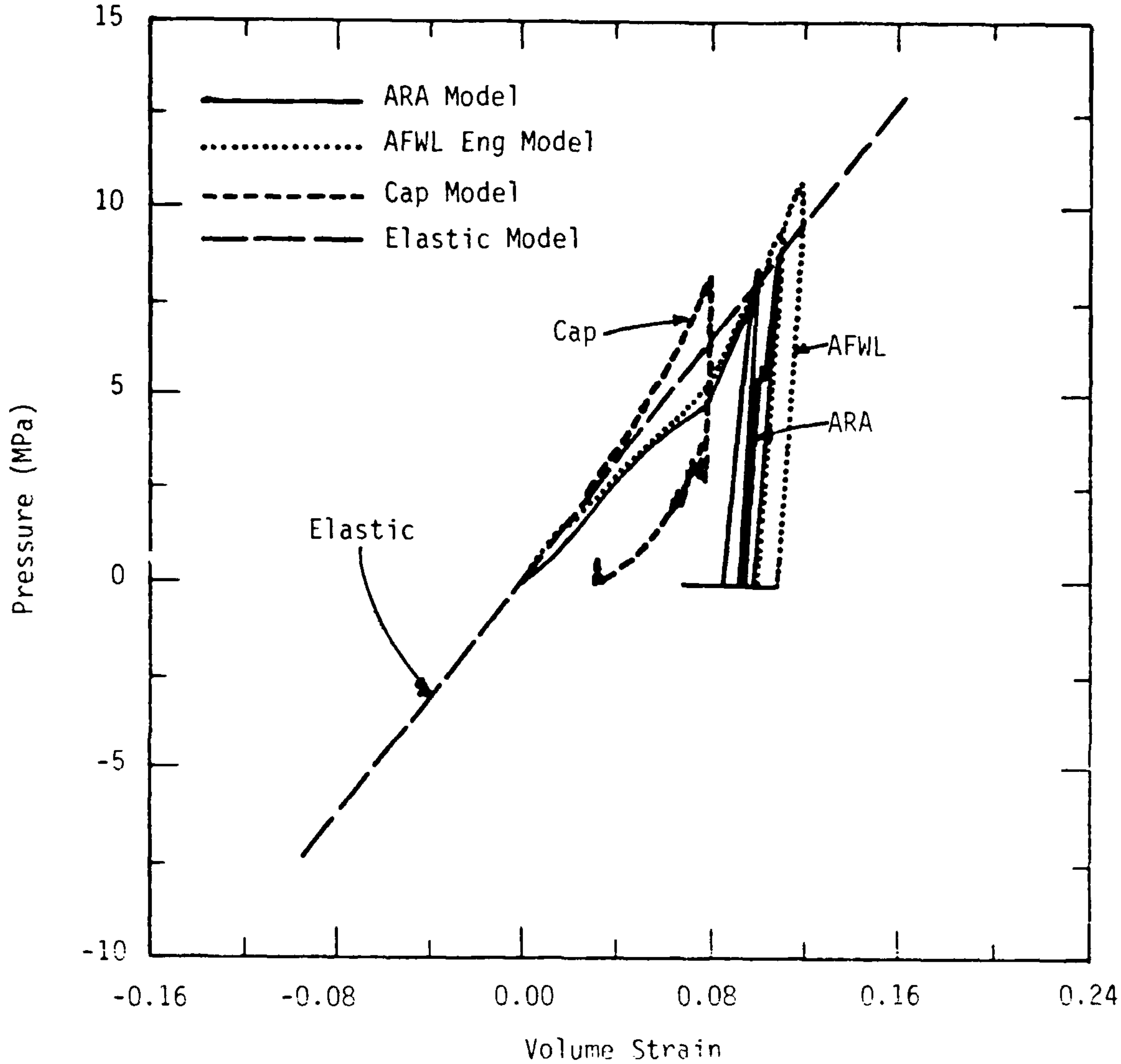

Figure 36. Compressive Behavior Comparison of Various Models in 1-D Cylindrical Wave Propagation.

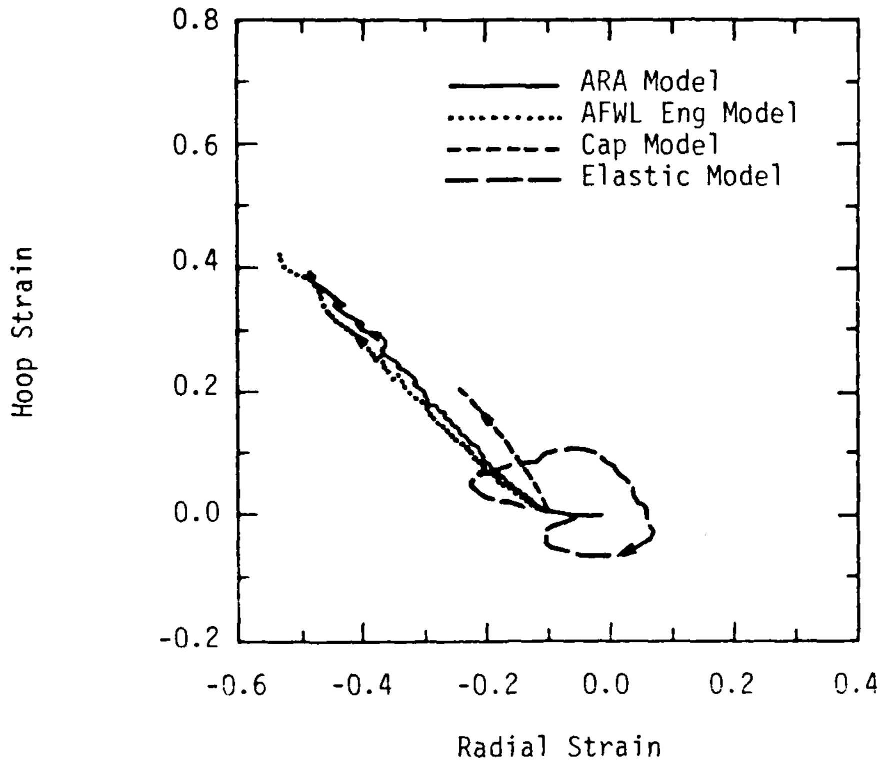

a. Range = 1.52m (Grid Point No. 9).

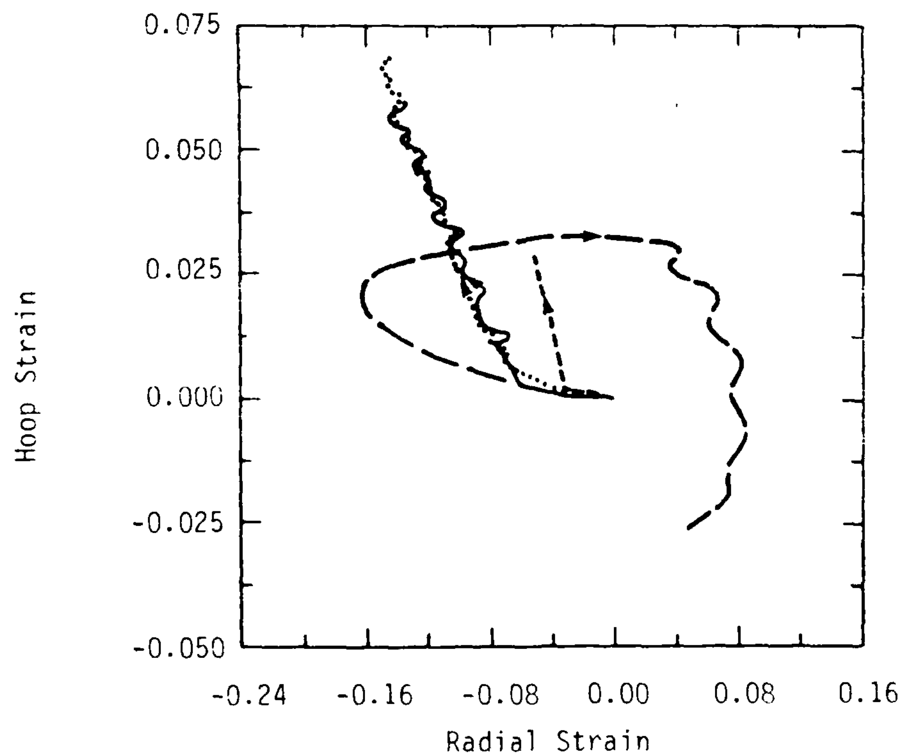

b. Range = 3.66m (Grind Point No. 23).

Figure 37. Comparison of Calculated 1-D Cylindrical Strain Paths Using Various Material Models.

TABLE 5. TIMING COMPARISON FOR ONE-DIMENSIONAL WAVE PROPAGATION

		CPU Seconds			
Calculation	Model	Total	Plotting	Grid Setup	Grid Cycle
Planar (40 ms)	ARA	7114	45	2326	4.22- 4.29
	Cap	1881	45	730	0.45- 1.19
	AFWL Eng.	595	45	5	0.48- 0.50
	Elastic	135	46	4	0.21
Spherical (2 ms)	ARA	1247	21	5.19	2.14-10.29
	Cap	381	24	4.43	0.42- 6.34
	AFWL Eng	151	21	5.13	0.52- 0.54
	Elastic	94	21	4.48	0.25
Cylindrical (40 ms)	ARA	5366	52	3.18	3.38-15.60
	Cap	866	54	2.74	0.11- 2.22
	AFWL Eng	438	55	2.96	0.49
	Elastic	146	54	2.77	0.21

Notes: (1) All calculations had 99 grid points, 98 zones

(2) Computer used was a Digital VAX 11/750, system clock resolution = 0.01 sec.

(3) "Total" CPU time includes the entire calculation.

(4) "Plotting" CPU time is the time taken to generate the time histories and grid plots, and is not influenced by model type.

(5) "Grid setup" CPU time includes dimensioning zones, numbering, etc., as well as initialization of zone stress to account for gravity.

(6) A "grid cycle" is the time required for one calculational cycle through all 99 grid points.

4.5 Two-Dimensional Calculations

4.5.1 Code Description. The code chosen for the two-dimensional wave propagation calculations was STEALTH. STEALTH (Solids and Thermal Hydraulics Codes for EPRI Adapted from Lagrange TOODY and HEMP) is a general purpose commercially available code developed by Hofmann (1978) for the Electric Power Research Institute (EPRI) and is completely documented in [Hofmann (1981)]. The DOD version of STEALTH was used for these calculations and is an adaptation of Version 4.1a. The principal reasons for choosing STEALTH were:

(1) Prior experience with the code for blast and shock problems

(2) Available to the public and fully documented

(3) Code modularity and ease of modification.

4.5.2 SEM-STEALTH/2D Link. One of the common sources of uncertainty which arise when comparing calculations made with different codes but ostensibly the same material model stems from small coding differences between the model versions actually used. This uncertainty can be eliminated by using the same physical coding, drawn from a central library, for each code. This is possible, and, in fact, practical, for many finite difference and finite element codes because the required material model formulation is often code independent. The inputs are a strain increment tensor, the old stress tensor, and state variables and the output is a new stress tensor.

Toward this goal, the Soil Element Model (SEM) may be viewed as a library of constitutive models. Under this effort, the SEM was implemented as such and linked directly with STEALTH 2D on the AFWL CRAY. The way in which this was accomplished is outlined in Figure 38. There were four principal places where STEALTH needed to be modified to incorporate the SEM models:

(1) The main program, where SEM common blocks holding material properties were inserted to insure contiguous memory locations. The actual link-up between the programs occurs during the loader/linker phase where the SEM routines are made available to STEALTH as a binary library.

(2) The material input phase, where the input was reconfigured to use the SEM parameter input subroutine (INPEOS). In this way, the SEM library of model parameters could be read by STEALTH directly. Input model parameters are also echoed using the SEM routine for this (OUTEOS).

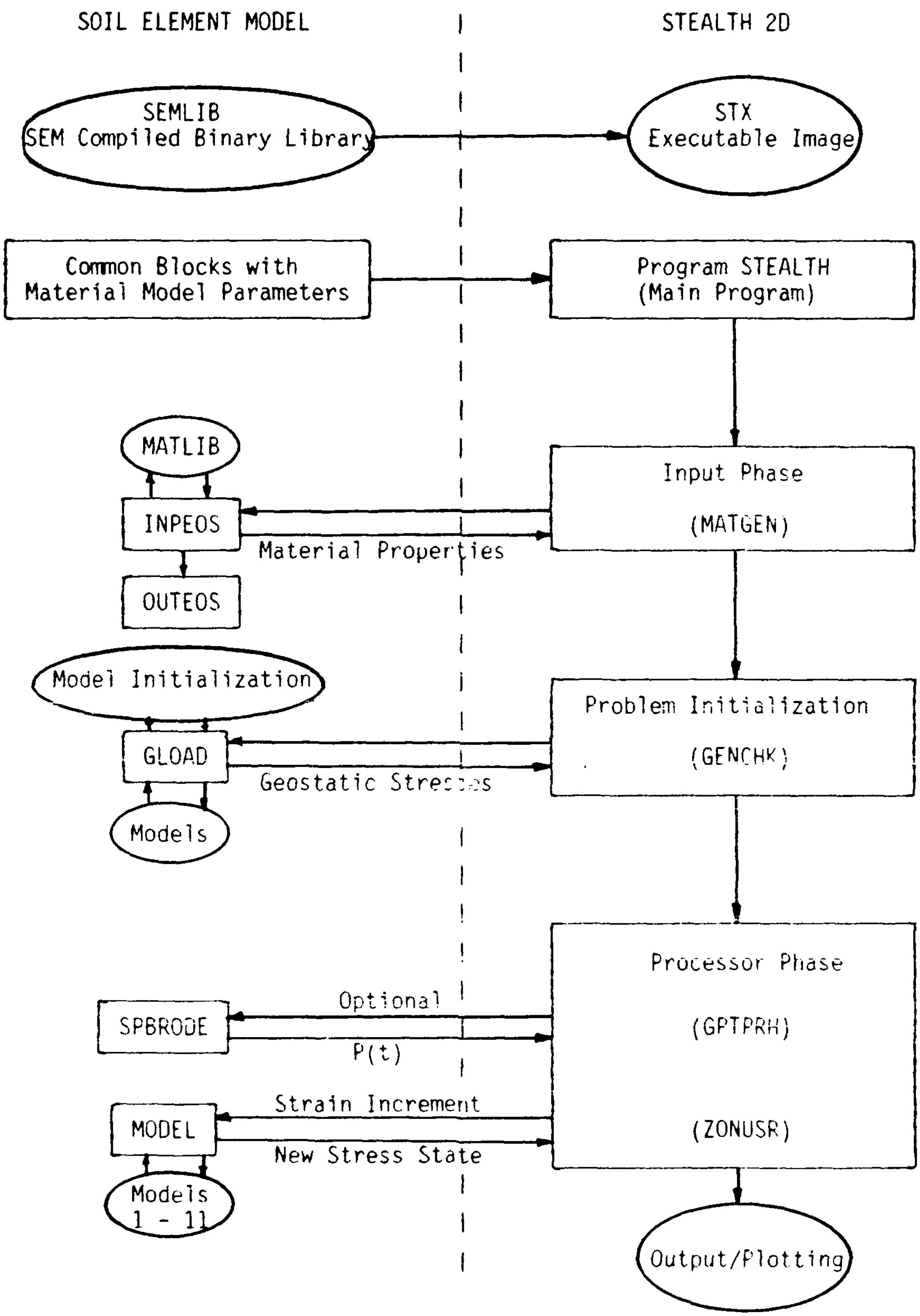

Figure 38. Soil Element Model - STEALTH 2D Interface.

(3) The problem initialization phase, where gravity stresses are set for each zone. Again, a SEM routine was used (GLOAD), which sets gravity stresses depending on the appropriate SEM material model.

(4) The zone processor phase, where STEALTH simply calls the main SEM model subroutine (MODEL) which in turn calls the appropriate model. Some of the SEM boundary load application routines used in SNEAKY, e.g., Speicher-Brode Nuclear Overpressure (SPBRODE), may also be used as an option.

Thus, all the models implemented in the SEM are now implemented in STEALTH 2D. This interface was used for the ARA model two-dimensional continuum code checkout. A full listing of the updates for the SEM-STEALTH modification is provided in Appendix B.

4.5.3 Planar (DIHEST) Calculations. Several options were considered while choosing a problem for the two-dimensional calculations, including: a traveling nuclear airblast over a half-space (HEST), a buried explosive sphere, a surface-flush cylindrical charge (CIST), and a vertically-oriented planar array of buried charges (DIHEST). All would have been adequate choices because they are all used by the Air Force in simulating one aspect or another of nuclear weapon ground shock effects, and all produce two-dimensional wave fields. The DIHEST was chosen for the test case because:

(1) It produces waves which immediately interact with the free surface, an important aspect of many two-dimensional problems.

(2) It has a relatively simple geometry.

(3) Many DIHEST experiments have been performed in dry alluvium and data is available for comparison.

DIHEST events are commonly used to simulate upstream-induced ground shock effects. They have also been used to simulate earthquake-like motions, and the geometry of the problem calculated here was taken from the SIMQUAKE test series [Higgins, et al. (1983)]. Figure 39 shows the SIMQUAKE II experiment. For these calculations, a single DIHEST array was assumed. The calculational geometry is shown in Figure 40. Note that the grid is inverted with the ground surface at the bottom of the figure. This conforms to the STEALTH convention, and is the most consistent way of visualizing the calculational set-up.

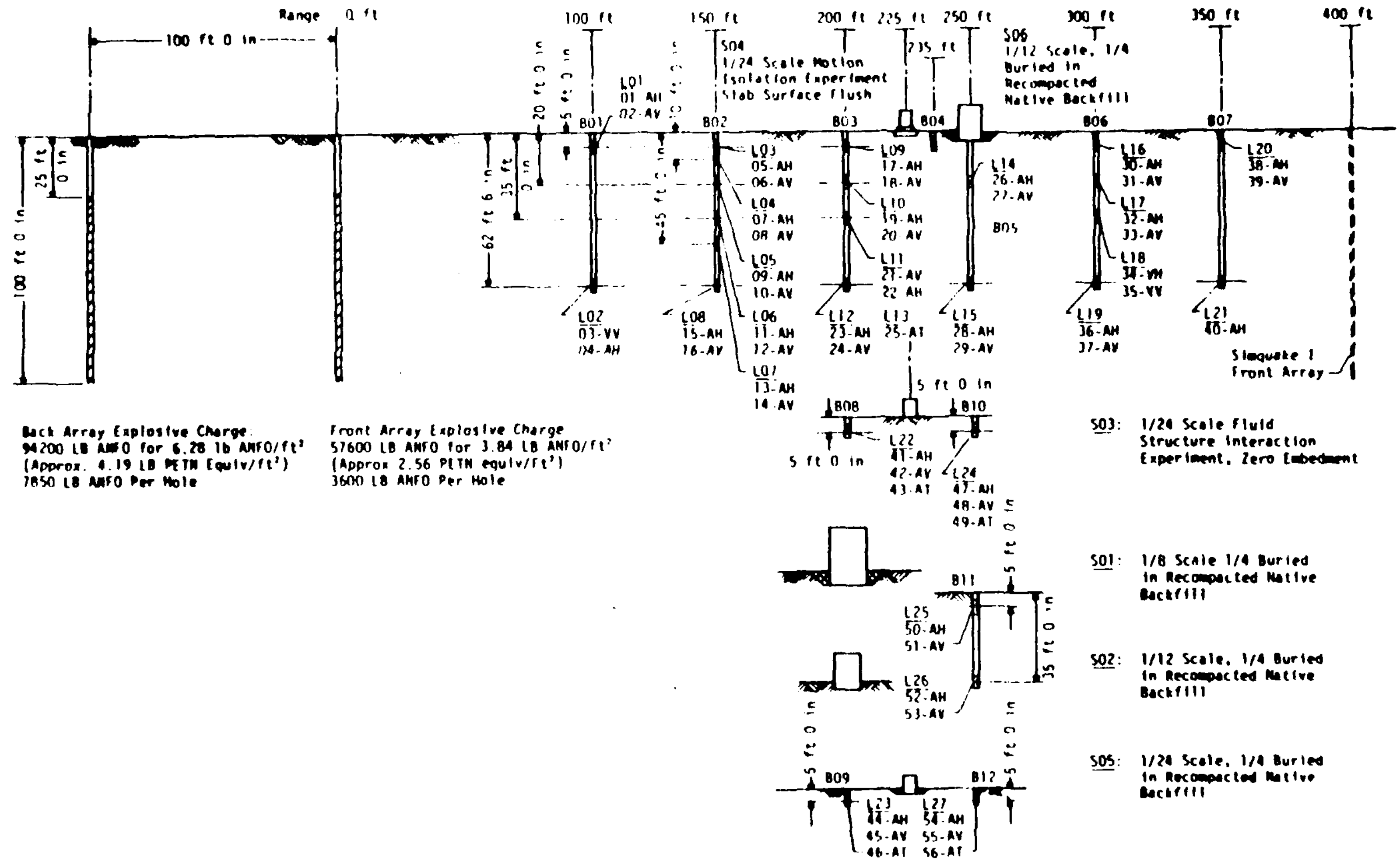

Figure 39. Simquake II Elevation [Higgins, et al (1983:2-4)].

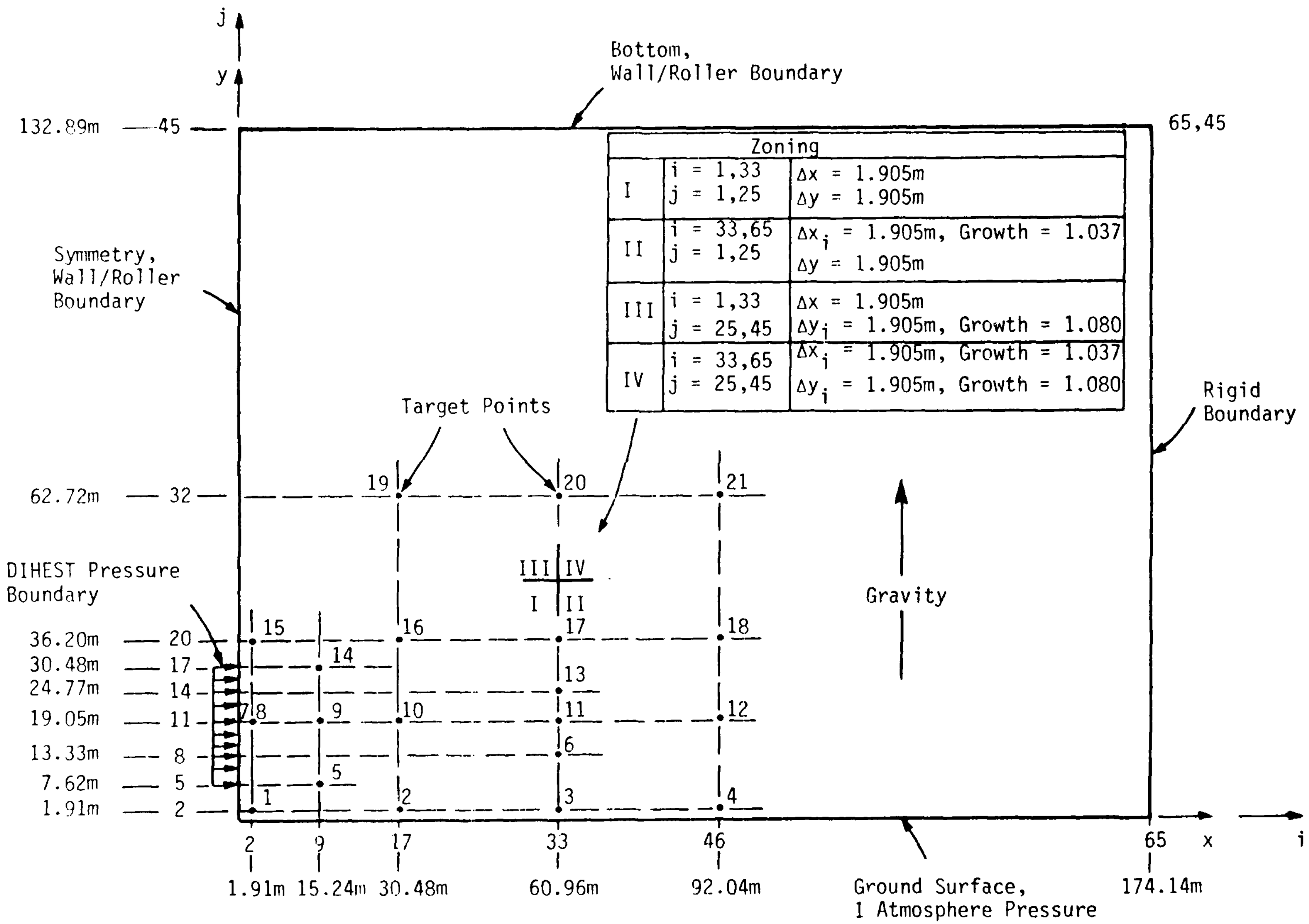

Zoning		
I	i = 1,33 j = 1,25	Δx = 1.905m Δy = 1.905m
II	i = 33,65 j = 1,25	Δx_i = 1.905m, Growth = 1.037 Δy = 1.905m
III	i = 1,33 j = 25,45	Δx = 1.905m Δy_i = 1.905m, Growth = 1.080
IV	i = 33,65 j = 25,45	Δx_i = 1.905m, Growth = 1.037 Δy_i = 1.905m, Growth = 1.080

Figure 40. 2-D DIHEST Calculation Configuration.

The mesh was approximately 175 m wide by 133 m deep, and had 2,925 grid points. The grid was large enough to avoid boundary reflection effects (from the top and right side) into the region of interest within the time of interest. The problem was run to 0.5 second. As in the one-dimensional calculations, only quadratic artificial was employed (in compression) and the coefficient of artificial viscosity (CQV) was set equal to 2.0.

A pressure history which corresponded to a SIMQUAKE-like array was applied to the left side of the grid. The form of the pressure function was that used by Higgins, Johnson and Triandafilidis (1978):

$$P(t) = P_0(1-t/t_0)e^{-a\ t/t_0} \quad (0 \le t \le t_v) \tag{66}$$

where P = pressure (Pa), t = time (sec), P_0 = peak pressure (Pa), t_0 = duration coefficient (sec), a = decay coefficient, and t_v = time of venting (sec).

The peak pressure, P_0, is a function of explosive type and was taken to be 15×10^6 Pa, which was used in SIMQUAKE. The duration coefficient, t_0, is a function of explosive loading density and time to venting, and was set to 0.070 sec. The decay coefficient, a, is also a function of explosive loading density as well as soil type and was assumed to be 11.4 for this problem. The pressure history and associated impulse are shown in Figure 41.

The target point locations were chosen to provide complete coverage of a rectangular area within 100 m laterally and 60 m vertically of the origin. Many target points were chosen to correspond with gage locations in the SIMQUAKE events. Target point locations are indicated in Figure 40 and listed in Table 6 along with the kind of plots made for each. A view of the distorted grid near the source is shown in Figure 42.

4.5.4 Discussion of Two-Dimensional Results. The ARA model was used to calculate free-field response to the DIHEST loading out to 500 ms. The same model parameters used in the one-dimensional calculations were used here, except cohesion was set to zero to enhance the effect of the free surface.

Calculated horizontal and vertical velocities are shown in Figures 43 and 44. Several points may be made upon examination of these figures:

(1) From the times-of-arrival along the array mid-depth gage line, the calculated wavespeed is seen to be 321 m/s. The peak is traveling at 230 m/s.

(2) The peak horizontal velocity along this same gage line attenuates as shown in Figure 45. Near-surface horizontal velocity attenuation is also shown.

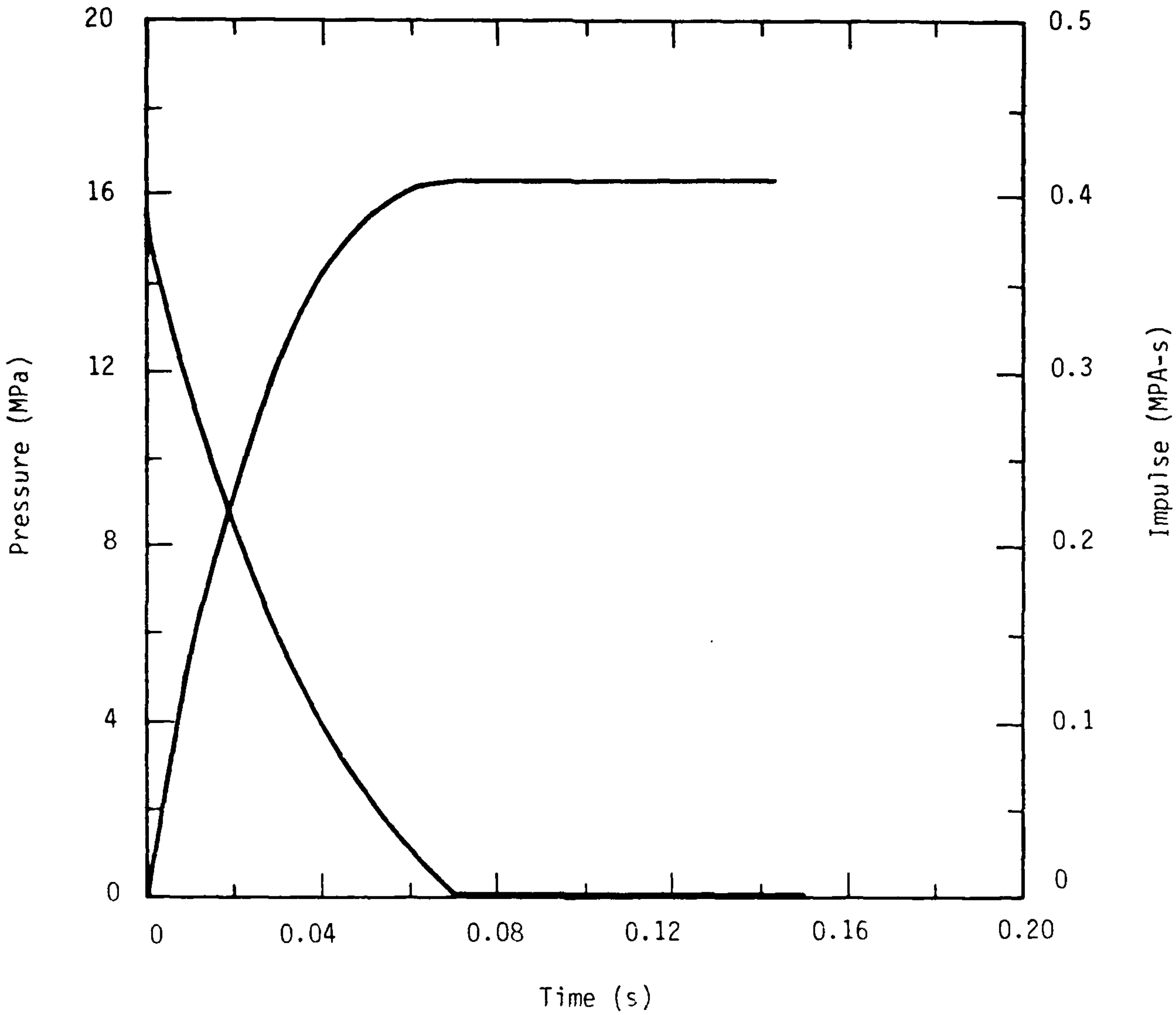

Figure 41. DIHEST Pressure Function.

TABLE 6. TARGET POINTS FOR THE 2-D DIHEST CALCULATION

Target Point Number	Grid Point		Location (M)		Plotted Information						
	i	j	x	y	V_{xy}	σ_{xy}	$P-\epsilon_v$	σ_{path}	ϵ_{path}	E_i	P,I
1	2	2	1.91	1.91	✓	✓	✓	✓	✓		
2	17	2	30.48	1.91	✓	✓	✓	✓	✓	✓	
3	33	2	60.96	1.91	✓						
4	46	2	92.04	1.91	✓	✓	✓	✓	✓		
5	9	5	15.24	7.62	✓						
6	33	8	60.96	13.33	✓						
7	1	11	0.00	19.05							✓
8	2	11	1.91	19.05	✓	✓	✓	✓	✓	✓	
9	9	12	15.24	19.05	✓						
10	17	11	30.48	19.05	✓	✓	✓	✓	✓	✓	
11	33	11	60.96	19.05	✓	✓	✓	✓	✓	✓	
12	46	11	92.04	19.05	✓	✓	✓	✓	✓	✓	
13	33	14	60.96	24.77	✓						
14	9	17	15.24	30.48	✓						
15	2	20	1.91	36.02		✓					
16	17	20	30.48	36.20	✓	✓	✓	✓	✓	✓	
17	33	20	60.96	36.20	✓						
18	46	20	92.04	36.20	✓						
19	17	32	30.48	62.72	✓						
20	33	32	69.06	62.72	✓						
21	46	32	92.04	62.72	✓	✓	✓	✓	✓	✓	

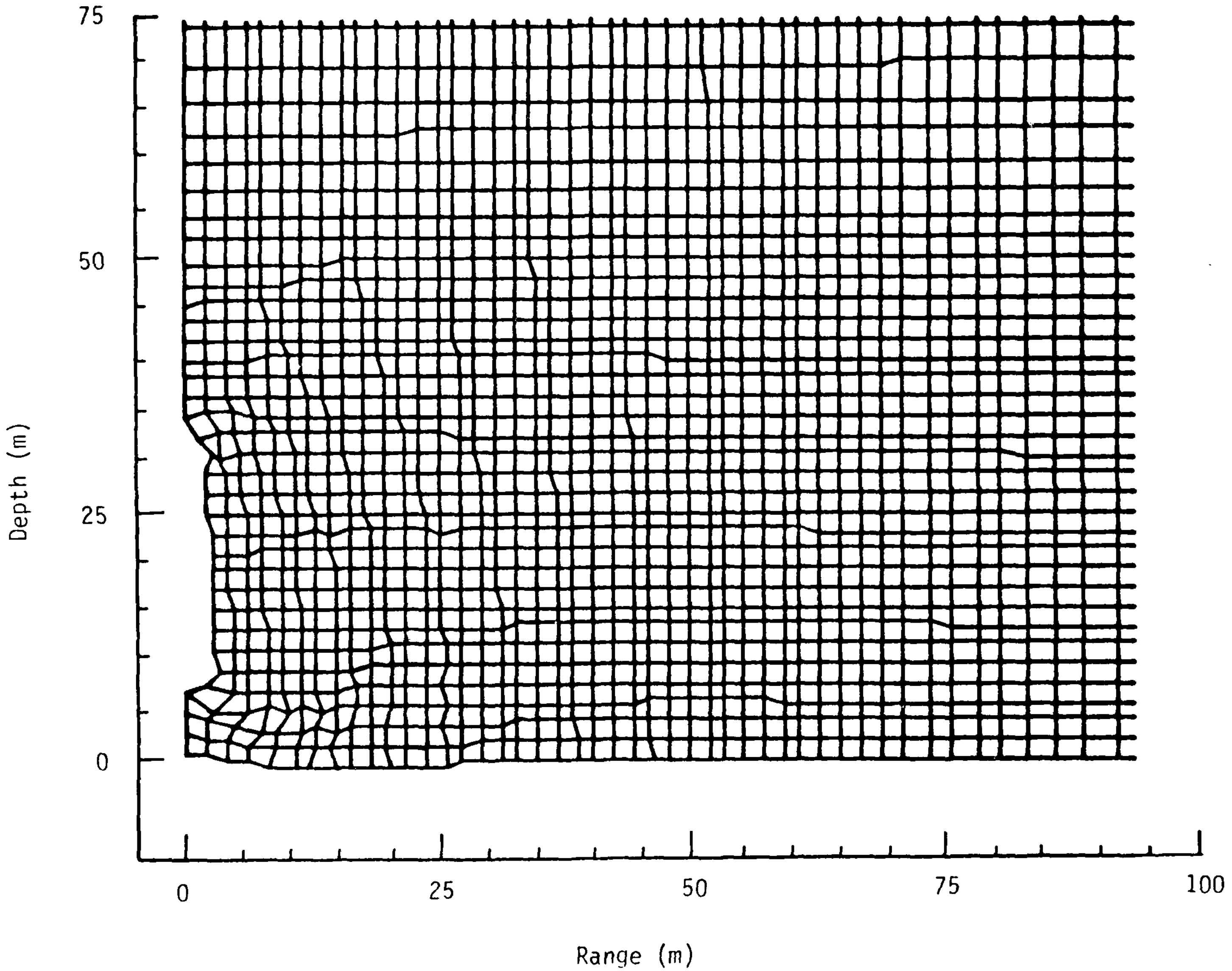

Figure 42. Distorted 2-D Mesh (Partial View) at 500 ms.

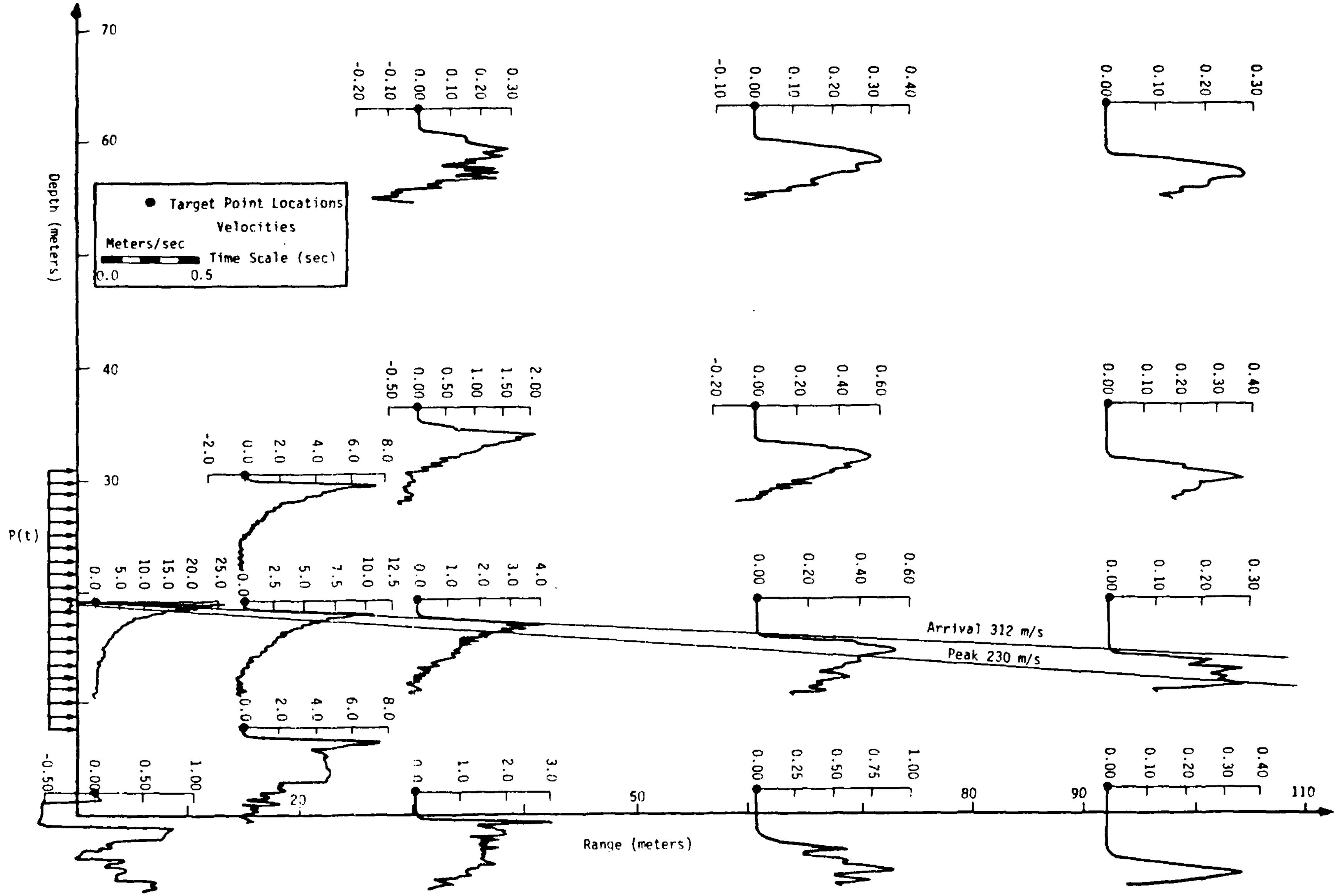

Figure 43. Calculated DIHEST Horizontal Velocity Histories Using the ARA Model.

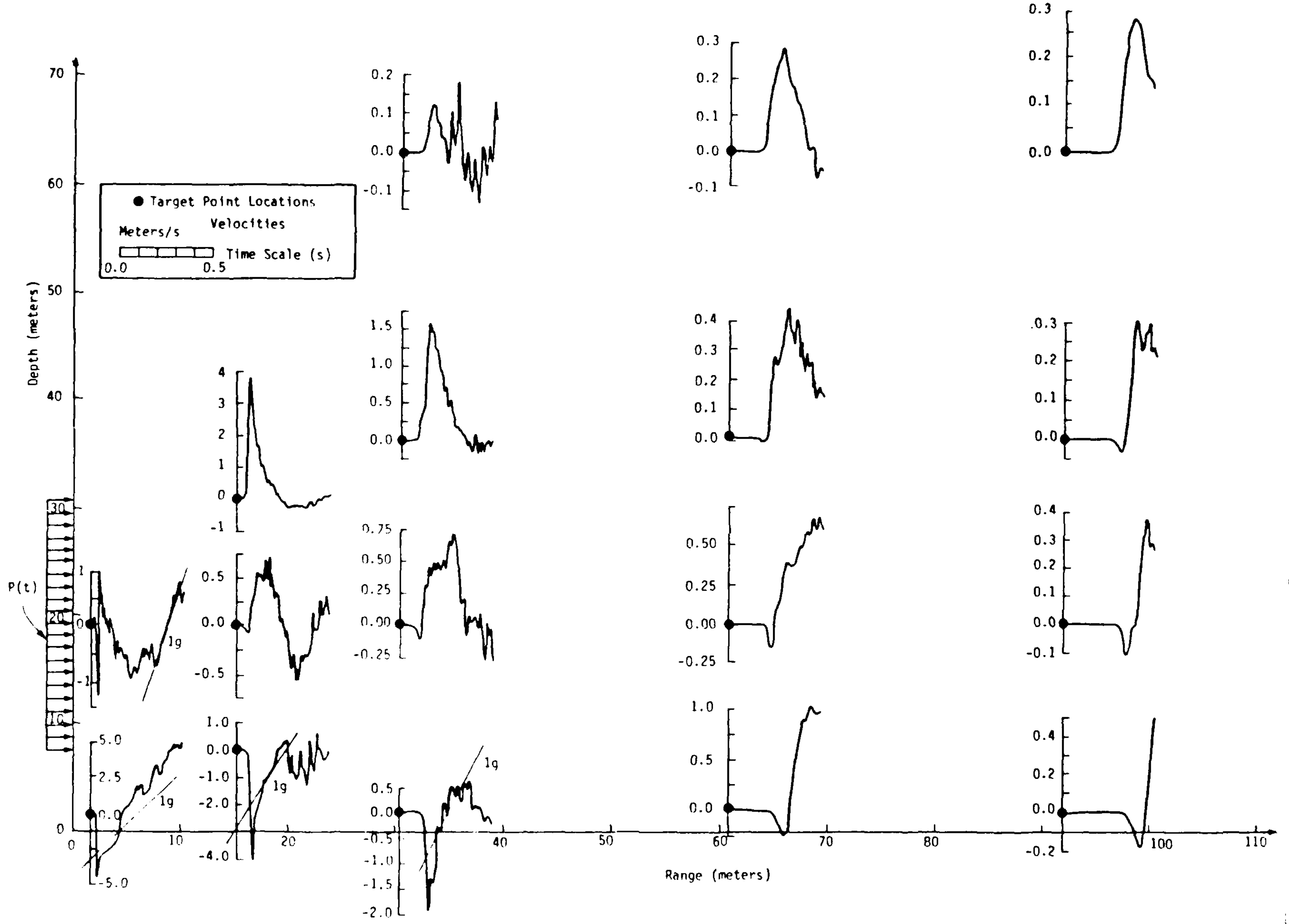

Figure 44. Calculated DIHEST Vertical Velocities Using the ARA Model.

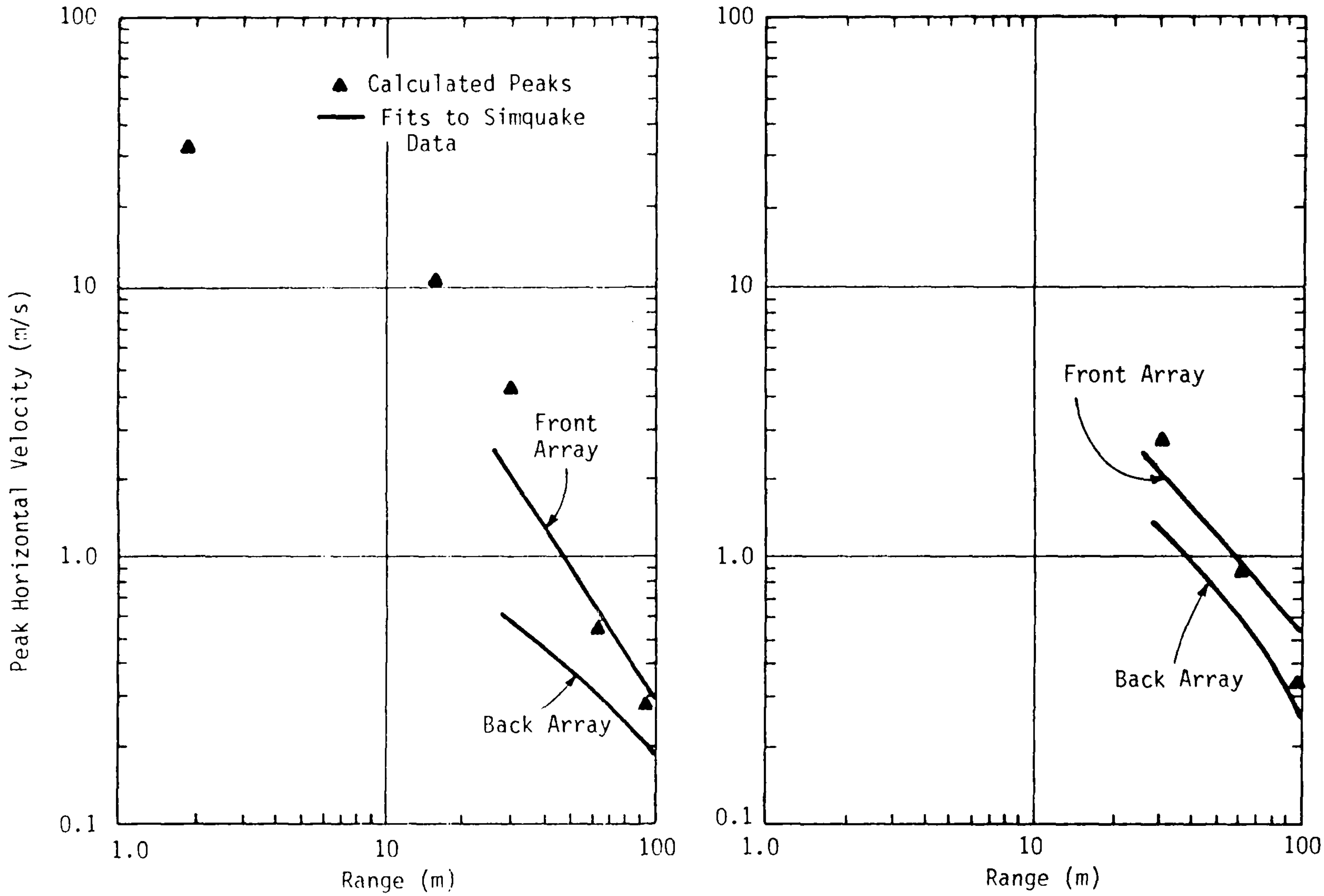

a. Array Mid-Depth (19.05m).

b. Near Surface (1.91m).

Figure 45. Peak Horizontal Velocity Attenuation at Array Mid-Depth and Near-Surface.

(3) The duration of the calculation does not permit full development of a negative horizontal velocity phase.

(4) Horizontal velocities at ranges greater than 50 m tend to be greater near the surface than at array mid-depth.

(5) The spall duration can be observed in the close-in, near-surface vertical velocity traces and in some zones near the edges of the source.

In order to better understand ARA model behavior under general two-dimensional stress and strain paths, calculated octahedral stress paths and pressure-volume response were tracked at several locations. These are shown in Figures 46 and 47, respectively. The following observations can be made from these results:

(1) Loading (even directly in front of the source) rapidly diverges from uniaxial strain conditions, and the stress point quickly encounters the expansive yield surface.

(2) Due to geostatic stresses, loading from the side causes an initial drop in shear stress (as demonstrated in Section 4.2). Very near the surface, this initial drop is not observed because loading is oriented more toward vertical.

(3) The variability in stress paths is due to the many different kinds of waves emanating from the source, reflections off the free surface, and numerical oscillations associated with the grid.

(4) The variability in volume compressibility response is due to the same factors mentioned above because different stress paths cause variable activation of the two yield surfaces in this model. Much of the differences with range can be attributed to the changing peak stress level.

(5) Spall and rejoin behavior is very important near the surface at close-in ranges, as well as near the edges of the source.

The array mid-depth target point at 61 m range is a good example of the complex loading history experienced in this kind of event. Figure 48 reviews the stress path and pressure-volume response for this location. Corresponding points on the two curves have been noted and the complete history may be followed beginning at point 1. Note the difference in effective bulk modulus depending on the direction of the stress path and currently activated yield surface(s).

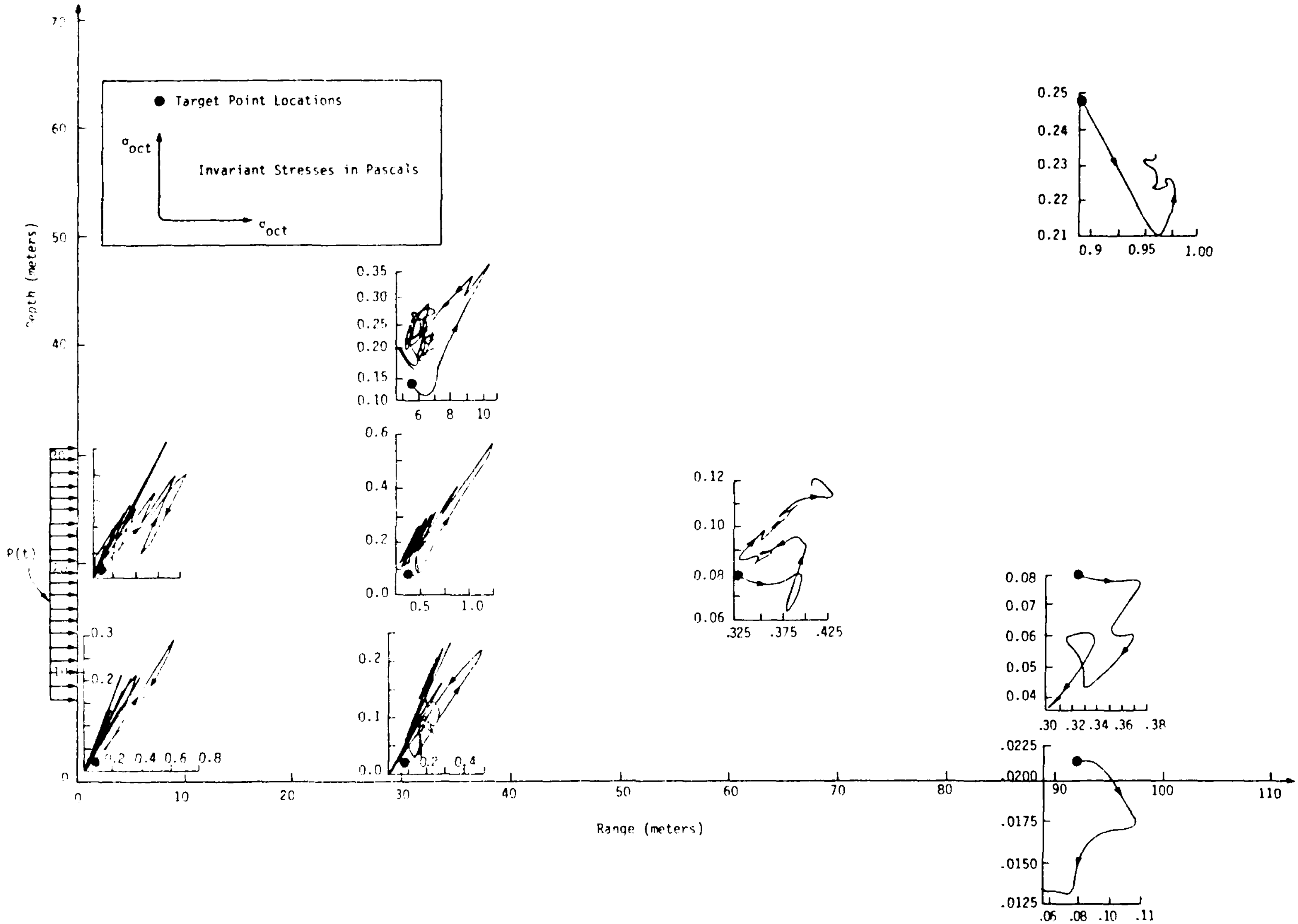

Figure 46. Calculated Two Dimensional Stress Paths Using the ARA Model.

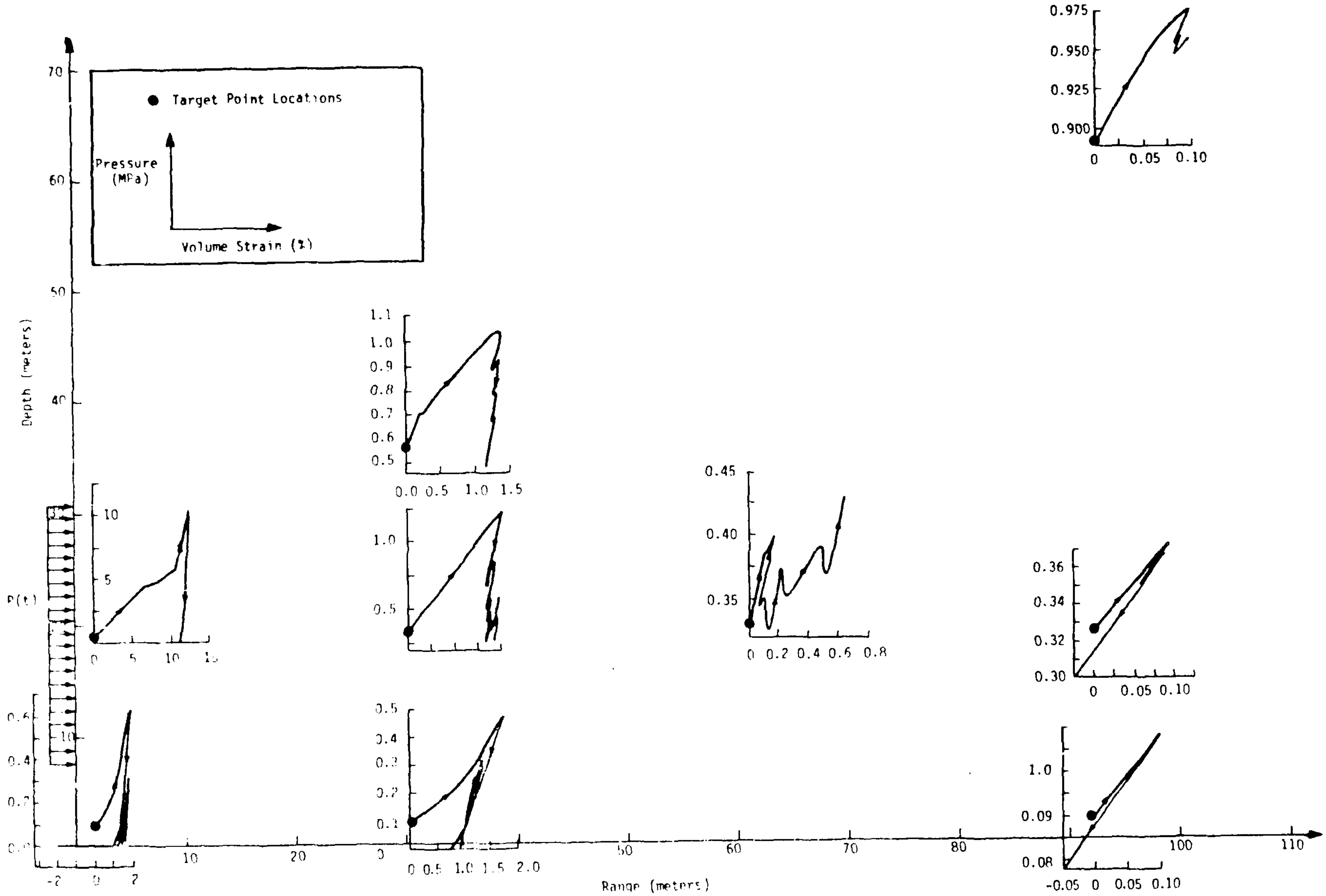

Figure 47. Calculated Pressure-Volume Response Under DIHEST Loading Using the ARA Model.

AD-A170 072 COMPUTATIONAL ASPECTS OF THE ARA THREE INVARIANT CONSTITUTIVE MODEL(U) APPLIED RESEARCH ASSOCIATES INC ALBUQUERQUE NM W C DASS ET AL. 29 MAY 86 5934 2/2

UNCLASSIFIED AFOSR-TR-86-0463 F49620-84-C-0066 F/G 8/13 NL

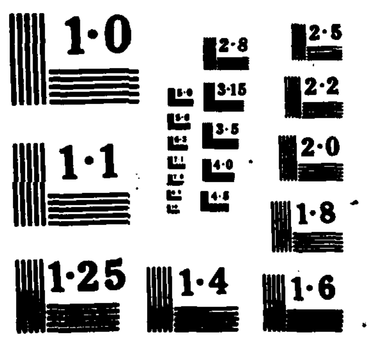
1·0
2·8
2·5
3·15
2·2
3·5
2·0
1·1
4·0
4·5
1·8
1·25
1·4
1·6

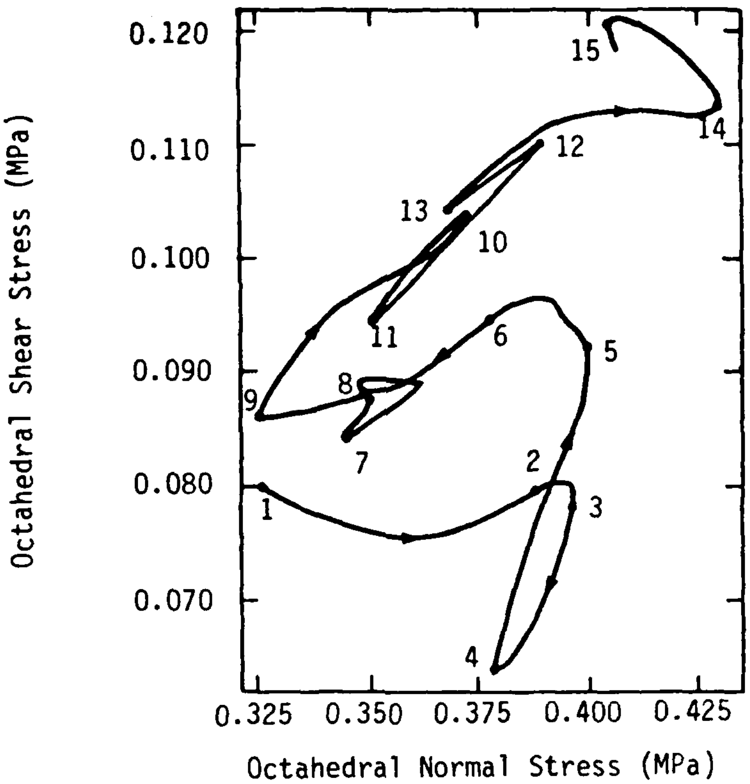

a. Stress Path.

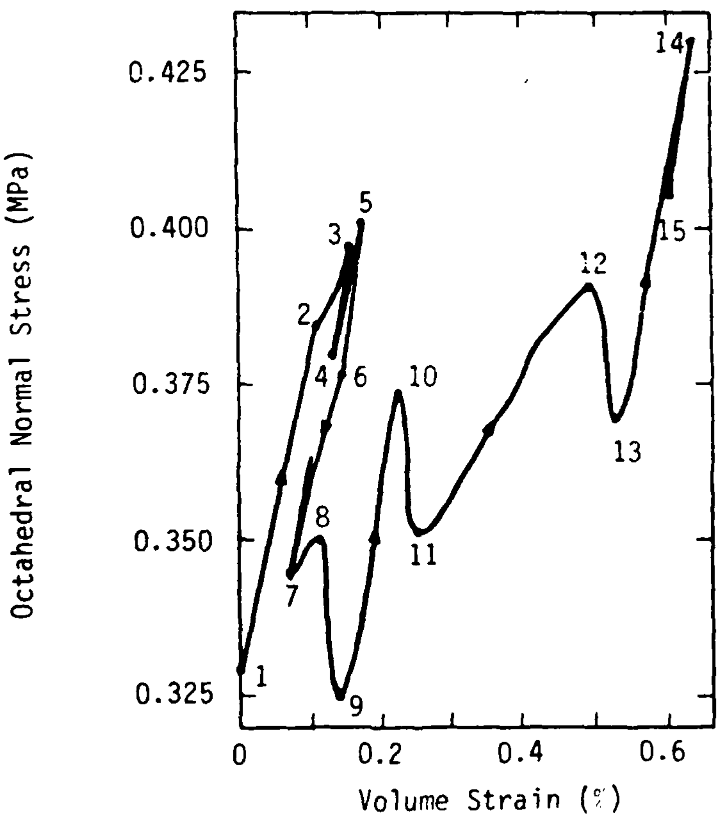

b. Pressure-Volume Response.

Figure 48. Stress and Strain History at Range = 61m, Depth = 19m.

The calculation using the ARA model can be compared to SIMQUAKE data, although it should be recalled that the model parameters have not been fit with insitu behavior in mind. The inability of the lab-based model to predict insitu behavior was clearly demonstrated in the one-dimensional calculations. The behavior there was generally too soft (high velocities) and too slow (late arrivals, peaks). Also recall that SIMQUAKE was conducted at McCormick Ranch, which is also a dry alluvial site, but McCormick Ranch sand has somewhat different properties than does CARES-DAY alluvium.

Figure 49 shows comparisons between the calculation and SIMQUAKE II data at the 61 m range. The overall trends appear correct, however, the timing and magnitudes are not.

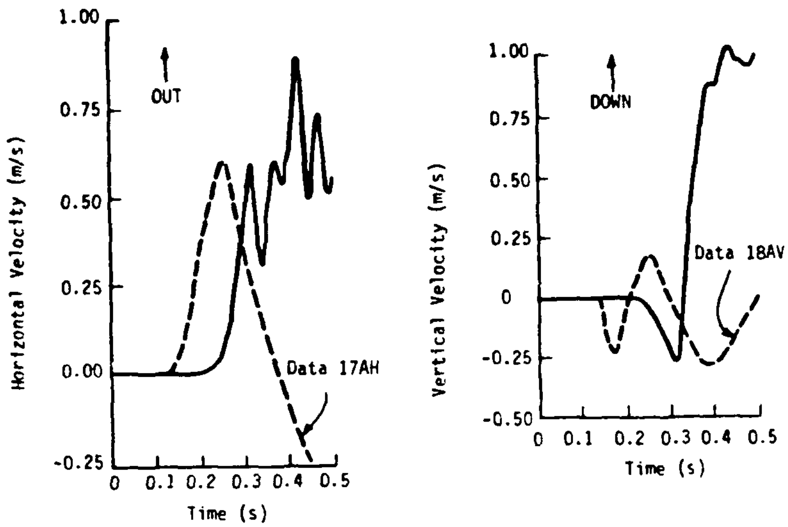

a. Near Surface (Depth = 1.5 - 2.0m)

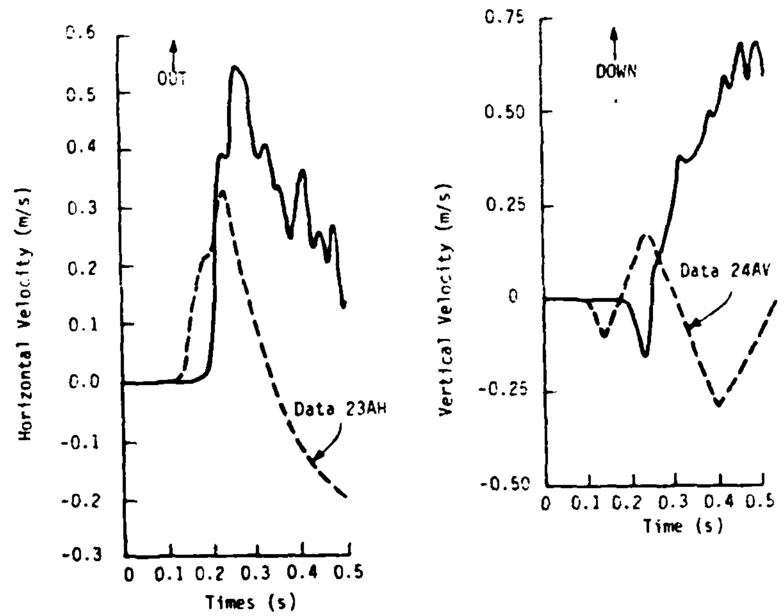

b. Mid-Array Depth (Depth = 19m).

Figure 49. Comparison of Velocity Waveforms Calculated Using the ARA Model with Simquake II Data at the 61m Range.

5.0 CONCLUSIONS AND SUMMARY

5.1 ARA Model Assessment

The primary goal of this effort has been achieved: the ARA model developed and previously tested under laboratory stress and strain paths has been successfully implemented and tested in dynamic finite difference calculations. Many aspects of the model, including numerical errors, cohesion, work-softening, and tensile failure issues have been adjusted and/or improved.

The most important aspect of the ARA three invariant model is that it accounts for many observed features of soil behavior in the framework of a rigorous plasticity-based formulation. In this respect, it is fundamentally different from most models currently in use for ground shock calculations. Intuitively, one would expect a model which can accurately predict the laboratory response of soil under a complete suite of stress and strain paths will better predict insitu blast loading response. The calculations performed for this study, however, do not entirely support intuition. In many cases, the ARA model did not produce substantially improved wave propagation response. Two questions must then be addressed: (1) Why not?, and (2) Can this observation be extrapolated to calculations of ground shock in general?

One of the aspects of soil behavior under blast loading that becomes immediately apparent upon studying calculated stress paths is that a given element of soil spends only a small fraction of its entire stress history in initial loading. Typically, the soil is loaded, unloads in pressure, and quickly approaches yielding in shear. Much of the post peak response is dominated by the unload-reload behavior of the model. Any secondary loading is heavily influenced by this, as well. In many cases, the soil will also fail in tension, and this makes post-spall behavior critical. Thus, a fairly general hypothesis can be proposed: any new model which concentrates on initial loading and plasticity effects related to initial loading, but reverts to simple elastic behavior upon unloading or reloading will tend to produce dynamic waveforms very similar to that which can already be produced with simpler models. The one and two dimensional calculations presented here provide some evidence to support this. More detailed study and analysis, including models with improved unload-reload behavior, are required to substantiate the hypothesis.

Additionally, the treatment of tensile failure, where the material in a zone can become distended or cracked, is very important for many blast loading geometries. Directional tensile failure is particularly tricky to incorporate in a model formulated like the ARA model, because it is not clear how the yield and plastic potentials would be affected. So, much of the similarity between waveforms produced by the ARA and other models can potentially be explained by fundamentally similar treatment of unload-reload and tension behavior.

Given the similarity of results, one of the main computational deficiencies of the ARA model is its expense. A typical wave propagation calculation takes an order of magnitude longer to run than an elastic calculation, seven to eight times longer than an AFWL Engineering model calculation, and three to six times longer than a cap model calculation. The biggest slowdown occurs when strain subcycling is required to satisfy the consistency condition on the expansive yield surface. This occurs upon initial departure of the stress point from the hydrostatic axis, which usually begins during geostatic loading. Although the ARA model logic itself is certainly more complicated than that of the other models, this does not really result in a significant time penalty. Improvements in the subcycling technique or in the formulation of the expansive work relationship (to eliminate the singularity at zero expansive work) would be most beneficial to overall efficiency of the model.

Probably the most important aspect of the ARA model calculations is the coupling of shear and volumetric response through dilatation. This is most observable in the regions of highest shear such as those adjacent to an explosive source. However, there are still some issues which relate to this kind of behavior which remain to be resolved. For example, the ARA model has a separate plastic potential related to the expansive yield surface which allows for direct control of dilatation. But how is this plastic potential affected by unloading and subsequent reloading? The ARA model is capable of dilation while unloading in pressure while remaining on the expansive yield surface. To determine whether this is physically realistic would require some laboratory testing. The tendency in the ARA model for the stress point to move very rapidly down the failure surface toward the apex seems to significantly influence calculated behavior. In fact, this is likely the biggest reason for the differences observed between the ARA and cap model calculated results. This phenomenon and the parameters responsible for it need to be better understood.

Many questions regarding the suitability of the ARA model for general use in ground shock and soil-structure interaction problems cannot be answered solely on the basis of the calculations completed under this effort. Therefore, it is appropriate to record here recommendations for continued improvement of the ARA model.

5.2 Recommendations for Continued Study

The following is a prioritized list of tasks which would help to move the ARA model into the mainstream of ground shock computing and improve its predictive capabilities:

(1) Improve the subcycling procedures for correcting yield surface overshoot due to both extrapolation of $\partial f_p'/\partial W_p$ over a timestep and elastic punch-through. The goal is improved efficiency, competitive with currently available models such as the cap model.

(2) Re-examine the work-softening aspect of the ARA model to determine if it can be successfully incorporated in two-dimensional calculations without violating uniqueness.

(3) Reformulate the compressive yield function (f_c') into a dimensionless form. This will eliminate the very large numbers encountered with some sets of stress units (such as Pascals) and allow the model to be used on smaller computers in these units.

(4) Fit the ARA model parameters to stress-strain data which is most representative of insitu behavior for the specific site of each field test and rerun the dynamic calculations. Evaluate the ARA model in its ability to predict blast-loading events.

(5) Formulate a rezoning strategy which accounts for a redistribution of the state parameters in the ARA model. Rezoning is a nasty fact of life and is used often in severe-environment calculations. It involves the smearing and lumping-together of greatly compressed or distorted zones to allow the calculation to proceed at a reasonable timestep. The several state variables used by the ARA model must be consistently transported from old zones to new zones. Note that this is not a problem unique to the ARA model and must be dealt with when using any constitutive model with history-dependent parameters.

(6) Implement the unloading-reloading hysteresis coding which has been formulated based on a Masing-like relationship for bulk moduli. Test out the formulation for stability in a finite difference calculation. If this approach fails to produce improved unload-reloading cyclic behavior, consider incorporating kinematic hardening relationships into the model.

(7) Perform sensitivity studies to evaluate the effect of various model parameters on calculated waveform features. This is a critical and necessary step in the acceptance of the ARA model as a viable ground shock model.

(8) Couple the ARA model with a good tensile failure model which allows directional cracking. This appears to be necessary for many kinds of loading. For example, in an axisymetric explosion geometry, it is desirable to allow the material to separate in the hoop direction while still transmitting stress in the radial direction.

(9) More fully test out the high pressure-temperature equation of state developed in this effort in appropriate calculations, perhaps culminating in a two-dimensional nuclear source energy-deposition calculation.

(10) Upon completion (or at least resolution) of items 1-9, use the ARA model to calculate a more complicated blast loading problem of current interest to the Air Force. Two suggestions at this point in time would be a combined HEST-DIHEST simulation or an NSS event. However, there may be more appropriate choices when the time comes to seriously apply the ARA model.

(11) Because the ARA model can accurately model shear-volume response coupling, it is a good candidate for the grain matrix in a coupled fluid-mechanical calculation. Incorporating this model into a dynamic fluid-mechanical code should be considered.

6.0 REFERENCES

Air Force Weapons Laboratory, 1980: "Analysis of SIMCAL 1, 2, and 3," AFWL-TR-80-42, Kirtland Air Force Base, New Mexico.

Akers, S.A., 1985: "Axisymmetric Strain Path Tests on CARES-DRY Clayey Sand," U.S. Army Engineer Waterways Experiment Station, Vicksburg, Mississippi.

Amend, J.H., G.W. Ullrich, and J.M. Thomas, 1977: "HAVE HOST Cylindrical Insitu Test (CIST) Data Analysis and Material Model Report," AFWL-TR-77-81, Kirtland Air Force Base, New Mexico.

Brode, H.L., and S.J. Speicher, 1984: "Air Blast from Nuclear Burst - Analytic Approximations," PSR Report 1419-1, Pacific-Sierra Research Corporation, Los Angeles, California.

Cargile, J.D., 1984: "Geotechnical Investigation for the CARES-DRY Site: Laboratory Test Results," U.S. Army Engineer Waterways Experiment Station, Vicksburg, Mississippi.

Dass, W.C., J.L. Bratton, and C.J. Higgins, 1981: "Fundamental Properties of Soils for Complex Dynamic Loadings," AFOSR-TR-82-0101, Applied Research Associates, Inc., Albuquerque, New Mexico.

Dass, W.C., D.H. Merkle, and J.L. Bratton, 1983: "Fundamental Properties of Soils for Complex Dynamic Loadings: Dynamic Constitutive Modeling of Sandy Soils," AFOSR-TR-83-0653, Applied Research Associates, Inc., Albuquerque, New Mexico.

Hart, R.D., 1981: "A Fully Coupled Thermo-Mechanical-Fluid Flow Model for Nonlinear Geologic Systems," Ph.D. Thesis, University of Minnesota, Minneapolis, Minnesota.

Higgins, C.J., K.B. Simmons, S.F. Pickett, G.E. Howard, and P. Ebanez, 1983: "SIMQUAKE II: A Multiple-Detonation Explosive Test to Simulate the Effects of Earthquake-Like Ground Motions on Nuclear Power Plant Models," EPRI NP-2916, Electric Power Research Institute, Palo Alto, California.

Higgins, C.J., R.L. Johnson, and G.E. Triandafilidis, 1978: "The Simulation of Earthquake-Like Ground Motions with High Explosives," Final Report No. CE-45(78), University of New Mexico, Albuquerque, New Mexico.

Hofmann, R., 1978: "STEALTH, A Lagrange Explicit Finite-Difference Code for Solids, Structural, and Thermohydraulic Analysis," EPRI NP-176-1, Electric Power Research Institute, Palo Alto, California.

Jackson, A.E., Jr., 1984: "Preliminary Material Property Estimates for ISST," Letter Report prepared for Ballistic Missile Office by Geomechanics Division, Structures Laboratory, U.S. Army Engineer Waterways Experiment Station, Vicksburg, Mississippi.

Lade, P.V., and R.B. Nelson, 1981: "Incrementalization Procedure for Elasto-Plastic Constitutive Model with Multiple, Simultaneous Yield Surfaces," Implementation of Computer Procedures and Stress-Strain Laws in Geotechnical Engineering, C. S. Desai and S. K. Saxena (Eds.), Vol. II, Acorn Press, Durham, North Carolina, pp. 503-518.

Lee, E.L., H.C. Hornig, and J.W. Cury, 1968: "Adiabatic Expansion of High Explosive Detonation Products," UCRL-50422, Lawrence Radiation Laboratory, University of California, Livermore, California.

Merkle, D.H., and W.C. Dass, 1983: "Fundamental Properties of Soils for Complex Dynamic Loadings: Dynamic Constitutive Model Fundamentals," AFOSR-TR-84-0166, Applied Research Associates, Inc., Albuquerque, New Mexico.

Merkle, D.H., and W.C. Dass, 1985: "Fundamental Properties of Soils for Complex Dynamic Loadings: Development of a Three Invariant Constitutive Model," AFOSR-TR-85-1232, Final Report on AFOSR Contract No. F49620-80-C-0088, Applied Research Associates, Inc., Albuquerque, New Mexico.

Schuster, S., and J. Isenberg 1972: "Equations of State for Geologic Materials," DNA 2925Z, Agbabian Associates, Los Angeles, California.

Schuster, S., J. Macalas, V. Koik, and E. Stokes, 1984: "CRALE User's Manual (Revision 1)," AFWL-TR-83-48, California Research and Technology, Inc., Chatsworth, California.

Trulio, J., 1983: "CARES Event MP #1: Preliminary Analysis of Data," ATR-83-55-2, Applied Theory, Inc., Los Angeles, California.

APPENDIX A

LISTING OF THE ARA MODEL

```
      SUBROUTINE ARA3(SIGO,DEPO,ZIE)
C-----------------------------------------------------------------------
C
C     APPLIED RESEARCH ASSOCIATES THREE-INVARIANT SOIL MODEL
C
C     VERSION 1...PROGRAMMED BY D.MERKLE, W.DASS, AND J.PARTCH, FEBRUARY 1984
C                 FOR DOCUMENTATION OF MODEL THEORY, SEE:
C                 Merkle,D.H. and W.C.Dass,"FUNDAMENTAL PROPERTIES OF SOILS
C                 FOR COMPLEX DYNAMIC LOADINGS: Development of a Three
C                 Invariant Constitutive Model",AFOSR-TR-85-XXXX, Applied
C                 Research Associates,Inc., Albuquerque, NM, April 1985.
C     VERSION 2...HIGH PRESSURE-TEMPERATURE EQUATION OF STATE (HPEOS)
C                 ADDED AUGUST 1985 BY W.DASS AND D.MERKLE
C     VERSION 3...INACTIVE DEVELOPMENT CODING AND DIAGNOSTIC WRITE STATEMENTS
C                 DELETED BY W.DASS, OCTOBER 1985
C
C     DATA IN.....(1) SIGO = INITIAL STRESS TENSOR (6X1), + IN TENSION
C                 (2) DEPO = STRAIN INCREMENT TENSOR (6X1), + IN TENSION
C                 (3) ZIE  = INTERNAL ENERGY (DENSITY*VOLUME)
C     DATA OUT....(1) SIGO = FINAL STRESS TENSOR (6X1), + IN TENSION
C
C     INTERNAL SIGN CONVENTIONS...STRESS = + IN COMPRESSION
C                                          - IN TENSION
C                                 STRAIN = + IN COMPRESSION
C                                          - IN TENSION
C
C     MODEL TYPES...MTYPE=-1...FAILED IN TENSION
C                          0...ELASTIC
C                          1...COMPRESSIVE (COLLAPSE) YIELDING ONLY
C                          2...EXPANSIVE YIELDING ONLY
C                          3...COMBINED COLLAPSE + EXPANSIVE YIELDING
C-----------------------------------------------------------------------
C
      COMMON /NUMBER/  ITEST,IUNDR,ISKIP,JPRINT,JPLOT,IPLT(30),KOUNT,
     1                 IEXEC,IPROB,NPROB,ISAVE(10),JSAVE,NPARAM(11),
     2                 NSVAR(11),NINP(11),PATM(8),NFIN1,NFIN2,NFIN3,
     3                 NFIN4,NFIN5,NFOT1,NFOT2,NFOT3,NFOT4,NFOT5,NFPLT
      COMMON /PROP10/  AKUR,AN,APOI,ACRV,AACC(4),AAPC(4),ABRK(3),
     1                 AR,AEY,AMY,AETA1,APBAR,AL,AALPH,ABETA,
     2                 ATG,ARG,AB3,APEX,AHSWTCH,AHA,AHN,AHLAM,AHGAM,
     3                 AHBET,ACONFP,ASCOT,ACC,APC,AWPPK,AQ,AA,AB,
     4                 AETA20,AWC,AWP,FP2PTYP,AWSCFT,AHE,AEMELT,ACTE,
     5                 AJ2,AETAR,AHY
      COMMON /ALLMOD/  IEOS,IUNITS,ATMO,CONV,RHOREF,MTYPE,GR,GRP,
     1                 BSP(3),VSTN(3),BMODN,GMODN,STATE(10)
      COMMON /CONSTANT/WONTHD,TOOTHD,SQRT2,SQRT3,SQRT6,SQRT23,
     1                 TWOPI,BIGPOS,BIGNEG
      COMMON /PROP10A/ ARAET(6),ARAEC(6),ARAEP(6),ARAEE(6)
      COMMON /SNEAK/   NCCYC,NCYCLE,TLIMIT,IGP,NGP,NSSYM,NMBL,IFL,NMBR,
     1                 IFR,PEND,NTPS,ITP(10),IXQTH(4,10),IYQTH(4,10),
     2                 IQPR(10),ISTYP,SPINC,TGRID(16),NSKIP,JPLT,CQV,
     3                 CLV,ROS,XACGR,NMP,NMAT,ITPS,IFFT,PI,TIE,TKE,TEG,
     4                 AVTP(3),SMLNUM,BIGNUM,MODPRT
C
      DIMENSION SIGO(6),SIGI(6),DEPO(6),DEPI(6),SIG(6),DEP(6),SDEV(6),
     *          SCOF(6),EOCT(6),DEOCT(6),DFCPDS(6),DGCDS(6),A1(6),A2(6),
     *          B1(6),B2(6),ACE(6,6),ACEP(6,6),DSIG(6),DFPPDS(6),
```

```
     *              DGPDS(6),FBAR(6,2),DSQ(2,2),ABAR(2,6),ALBAR(2,6),
     *              ALBARI(2,6),BBAR(2,6),GBAR(6,2),DLAM(2),ACEG(6),
     *              TCEP(6,2),DFEP(2),AMCOL(6),STATSAV(8)
      REAL J2,J3
C
C     DENCONV AND ENGCONV ARE CONVERSION FACTORS TO CONVERT DENSITY TO GM/CM
C     AND ENERGY DENSITY(ENERGY PER UNIT MASS) TO TERG/GM IN THE HPEOS.
C
      DIMENSION DENCONV(8),ENGCONV(8)
      DATA(DENCONV(I),I=1,8)/1.0E-3,1.0    ,0.0,0.0,0.0,1.E-9,0.0,1.0/
      DATA(ENGCONV(I),I=1,8)/1.0E8 ,1.0E12,0.0,0.0,0.0,1.0E8,0.0,1.0/
C
C     DMN IS A MINIMUM DENSITY (G/CC) FOR THE HPEOS
C
      DATA DMN /0.01/
C
      DATA TOLC /5.0E-6/, EMUNUM1 /1.0E-08/, ZERO/0.0/, ISTOP/0/
      DATA(AMCOL(I),I=1,6)/1.0,1.0,1.0,0.0,0.0,0.0/
C
C     STATEMENT FUNCTIONS
C
      C(SOCT)=SOCT+APEX
      FCP(SOCT,TOCT)=3.*AR*C(SOCT)**2+3.*TOCT**2
      FC2P(AWC)=ATMO**2*(AWC/(ACC*ATMO))**(1/APC)
      TOL STRESS =AMAX1(STRESS,ATMO/100.)
      FP(SOCT,TOCT,COS3W)=(TOCT/ATMO)*(1.-AEY*COS3W)*
     *                    (ATMO/TOL(C(SOCT))+AMY)
      TOCTF(SOCT,FACP)=C(SOCT)*(FACP/(1.-AEY*COS3W))/
     *                    (1.+ C(SOCT)  ATMO)*AMY
      FCTP(AWP)=AMAX1(0.0,EFAC)*
     *           (AA*(EXP(-AE*AWP/ATMO)-EXP(-AQ*AWP/ATMO)))
      TOLAWP(AWP)=AMAX1(AWP,1.E-15)
      DFP2PDW(AWP)=
     +    AA/ATMO*(AQ*EXP(-AQ*AWP/ATMO)-AE*EXP(-AE*AWP/ATMO))
      F1(J2,J3,SOCT)=WONTHD*(SQRT23*J2**0.5-3*AEY*J3/(SQRT2*J2))
     *                 /C(SOCT)**2
      F2(J2,J3,SOCT)=(1/SQRT(6.*J2)+3*AEY*J3/(SQRT2*J2**2))
     *                 * (1/C(SOCT)+AMY/ATMO)
      F3(J2,SOCT)=3*AEY/(SQRT2*J2)*(1/C(SOCT)+AMY/ATMO)
      G1(AETA2,SOCT)=(AETA2/(3*ATMO))*(1+AMY*C(SOCT)/ATMO)**2
      G2(J2,J3)=(1/SQRT(6.*J2)+3*AEY*J3/(SQRT2*J2**2))/ATMO
      G3(J2)=3*AEY/(SQRT2*J2*ATMO)
C
C     SIGN CHANGE
C
      CALL MSCALR(SIG0,6,1,-1.0,SIGI)
      CALL MSCALR(SIGI(4),3,1,SQRT2,SIGI(4))
      CALL MSCALR(DEP0,6,1,-1.0,DEPI)
      CALL MSCALR(SIGI,6,1,1.0,SIG)
C
C     INITIALIZATIONS
C
      MTYPE=0
      DWC=0.0
      DWP=0.0
      ISUB=0
      NSUB=0
```

```
      OVSHOOT=0.0
   10 DO 11 I=1,NSVAR(10)
   11 STATSAV(I)=STATE(I)
C
C     RESTORE STATE VARIABLES
C
   20 ASOCT=STATE(1)
      AWC=STATE(2)
      AWP=STATE(3)
      AJ2=STATE(4)
      ASPALL=STATE(5)
      ACONFP=STATE(6)
      AEV=STATE(7)
      ASPENG=STATE(8)
      APVAP=STATE(9)
C
C     SAVE INITIAL STRESS POINT AND YIELD SURFACE LOCATIONS
C
   30 SOCTSAV=SOCT
      TOCTSAV=TOCT
      FCPSAV=FCP(SOCT,TOCT)
      FC2PSAV=FC2P(AWC)
      FPPSAV=FPP(SOCT,TOCT,COS3W)
      FP2PSAV=FP2P(AWP)
C
C     MODIFY INCOMING STRESS STATE:
C     (1) SUBTRACT OUT VAPOR PRESSURE
C
   35 DO 37 I=1,6
   37 SIGI(I)=SIGI(I)-APVAP*AMCOL(I)
      CALL MSCALR(SIGI,6,1.D0,SIG)
C
C     INITIALIZE ENERGY RELATED VARIABLES
C
      ETA=1./(1.-AEV)
      DENS=RHOREF*ETA
      ENGN=ZIE/RHOREF
      DENG=ENGN-ASPENG
      ASPENG=ENGN
      RE=ENGN/AEMELT
      EFAC=1.0-RE
      IF(AHE.NE.1.0)EFAC=1.0
      DELMUEN=ACTE*DENG*AHE
      IF(EFAC.LT.0.0)DELMUEN=0.0
C
C     CALCULATE MECHANICAL(DEVM) AND ENERGY(DEVE) VOLUME STRAIN INCREMENTS
C
      DEVM=DEPI(1)+DEPI(2)+DEPI(3)
      DEVE=DELMUEN/ETA**2
C
C     INCREMENT TOTAL VOLUME STRAIN
C
      DEV=DEVM+DEVE
      AEV=AEV+DEV
C
C     ADD ENERGY-RELATED STRAIN INCREMENT TO ORIGINAL STRAIN INCREMENT TENSOR
C
```

```
      DEPI(1)=DEPI(1)+DEVE*WONTHD
      DEPI(2)=DEPI(2)+DEVE*WONTHD
      DEPI(3)=DEPI(3)+DEVE*WONTHD
C
C     SET INITIAL STRAIN INCREMENT
C
      CALL MSCALR(DEPI,6,1,1.0,DEP)
C
 0001 IF(ISTOP.EQ.1)GO TO 9300
C
C     CHECK FOR SPALLED CONDITION
C       ASPALL TRACKS THE EXPANSION VOLUME STRAIN WHEN THE MATERIAL EXCEEDS THE
C       SPALL LIMIT (APEX) AND BECOMES EXTENDED. WHEN ASPALL IS ZERO (OR
C       POSITIVE), MATERIAL IS COMPRESSING. WHEN ASPALL IS NEGATIVE, MATERIAL
C       IS SPALLED. ON REJOIN, USE ONLY PORTION OF STRAIN INCREMENT.
C
   40 IF(ISUB.NE.0)GO TO 50
    4 ASPSAV=ASPALL
   42 IF(ASPALL.GE.0.0)GO TO 50
      DEVI=(DEPI(1)+DEPI(2)+DEPI(3))
      ASPALL=ASPALL+DEVI
      IF(ASPALL.LE.0.0)GO TO 6003
      ERATIO=ASPALL/DEVI
      DO 45 I=1,3
   44 DEPI(I)=ERATIO*DEPI(I)
   45 DEP(I)=DEPI(I)
      ASPALL=0.0
C
   50 IF(AJ2.EQ.1.0) GO TO 700
C
C     STRAIN INCREMENT WITH FP2P=0.0 (AJ2=0.0)
C
  100 CALL ARAINV(SIG,SDEV,SCOF,J2,J3,SOCT,TOCT,COS3W)
      CALL ARASTAT(SIG,ACE)
  110 AFCP=FCP(SOCT,TOCT)
      AFC2P=FC2P(AWC)
      IF((AFC2P-AFCP).GT.TOL2)GO TO 300
C
  200 CALL MADD(SIG,6,1,AMCOL,2.0,(2.*(AR-1.)*SOCT),DFCPDS)
      CALL MSCALR(DFCPDS,6,1,1.0,DGCDS)
      DFC2PDW=ATMO/(ACC*APC)*(AFC2P/ATMO**2)**(1.-APC)
      HC=2*AFCP
      DSQ(1,1) = DFC2PDW*HC
      CALL MTMULT(DFCPDS,6,1,ACE,6,6,1.0,A1)
      CALL MMULT(A1,1,6,DGCDS,6,1,1.0,RL11)
      RL11=RL11+DSQ(1,1)
      RL1=1.0/RL11
      CALL MSCALR(A1,1,6,RL1,B1)
      CALL MMULT(B1,1,6,DEP,6,1,1.0,DLAMC)
      DWC=HC*DLAMC
      IF(DWC.GT.0.0) GO TO 400
C
  300 CALL MMULT(ACE,6,6,DEP,6,1,1.0,DSIG)
      MTYPE=0
      GO TO 500
C
  400 AWC=AWC+DWC
```

```
      CALL MADD(ARAEC,6,1,DGCDS,1.0,DLAMC,ARAEC)
      CALL MMULT(ACE,6,6,DGCDS,6,1,1.0,ACEG)
      CALL MMULT(ACEG,6,1,B1,1,6,1.0,ACEP)
      CALL MADD(ACE,6,6,ACEP,1.0,-1.0,ACEP)
      CALL MMULT(ACEP,6,6,DEP,6,1,1.0,DSIG)
      MTYPE=1
C
  500 CALL MADD(SIG,6,1,DSIG,1.,1.,SIG)
      CALL ARAINV(SIG,SDEV,SCOF,J2,J3,SOCT,TOCT,COS3W)
      IF(J2.LE ATMO/1.E10) GO TO 2000
C
C                 FIRST ACTIVATION OF EXPANSIVE MODE
C
  600 AJ2=1.0
      BFPP=FPP(SOCT,TOCT,COS3W)
      BFP2P=BFPP
  650 TRIAL=BFP2P/(AA*(AQ-AB))
      ITER=0
  655 ITER=ITER+1
      IF(ITER.GT.100)STOP656
  660 ANEW=-1.0/AQ*ALOG(EXP(-AB*TRIAL)-BFP2P/AA)
      IF(ABS(ANEW-TRIAL).LT.SMLNUM)GO TO 670
      TRIAL=ANEW
      GO TO 655
  670 DWP=ANEW*ATMO
  675 AWP=AWP+DWP
      MTYPE=MTYPE+2
      GO TO 2000
C
C                 GENERAL CASE  (AJ2=1.0)
C
  700 CALL ARAINV(SIG,SDEV,SCOF,J2,J3,SOCT,TOCT,COS3W)
      CALL ARASTAT(SIG,ACE)
C
C     IF MATERIAL HAS FULLY MELTED, USE ELASTIC MODULII
C
  705 IF(EFAC.LE.0.0)GO TO 1300
C
C     COMPARE CURRENT STRESS POINT POSITION WITH LOCATION OF EXPANSIVE AND
C     COMPRESSIVE SURFACES TO DETERMINE POSSIBLE MODES OF YIELDING
C
  710 AFCP=FCP(SOCT,TOCT)
      AFC2P=FC2P(AWC)
      AFPP=FPP(SOCT,TOCT,COS3W)
      AFP2P=FP2P(AWP)
      IF(AWP.GT.AWPPK)AFP2P=AFP2P*AWSOFT+FP2P(AWPPK)*(1.0-AWSOFT)
      AETA2 = AETA20+ASG*AFP2P
  720 IF((AFC2P-AFCP).GT.TOL2) GO TO 900
C
  800 IF((AFP2P-AFPP).GT.TOL2) GO TO 1100
      GO TO 1000
C
  900 IF((AFP2P-AFPP).GT.TOL2) GO TO 1300
      GO TO 1200
C
C     STRESS POINT IS AT THE CORNER OF THE COMPRESSIVE AND EXPANSIVE SURFACES
C
```

```
 1000 CALL MADD(SIG,6,1,AMCOL,2.0,(2.*(AR-1.)*SOCT),DFCPDS)
      CALL MSCALR(DFCPDS,6,1,1.0,DGCDS)
      DFC2PDW=ATMO/(ACC*APC)*(AFC2P/ATMO**2)**(1.-APC)
      HC=2*AFCP
      RF1=F1(J2,J3,SOCT)
      RF2=F2(J2,J3,SOCT)
      RF3=F3(J2,SOCT)
      RG1=G1(AETA2,SOCT)
      RG2=G2(J2,J3)
      RG3=G3(J2)
      CALL ARAFUNC(J2,RF1,RF2,RF3,SDEV,SCOF,DFPPDS)
      CALL ARAFUNC(J2,RG1,RG2,RG3,SDEV,SCOF,DGPDS)
      DFP2P=DFP2PDW(AWP)
      IF(AWP.GT.AWPPK)DFP2P=DFP2P*AWSOFT
      HP=-RG1*3.*SOCT+2*RG2*J2-3*RG3*J3
      DO 1001 I=1,6
        FBAR(I,1)=DFCPDS(I)
        FBAR(I,2)=DFPPDS(I)
        GBAR(I,1)=DGCDS(I)
 1001   GBAR(I,2)=DGPDS(I)
      DSQ(1,1)=DFC2PDW*HC
      DSQ(1,2)=0.0
      DSQ(2,1)=0.0
      DSQ(2,2)=DFP2P*HP
      CALL MTMULT(FBAR,6,2,ACE,6,6,1.0,ABAR)
      CALL MMULT(ABAR,2,6,GBAR,6,2,1.0,ALBAR)
      CALL MADD(ALBAR,2,2,DSQ,1.,1.,ALBAR)
      ALCAP=ALBAR(1,1)*ALBAR(2,2)-ALBAR(1,2)*ALBAR(2,1)
C
C     MODE DETERMINATION (CORNER ONLY) ---POLAR METHOD
C
 1010 IF(ALBAR(1,1).LE.0..OR.ALBAR(2,2).LE.0..OR.ALCAP.LE.0.)GO TO 1011
      GO TO 1019
 1011 CONTINUE
C/////STOP CALCULATION - NONUNIQUE MODE SELECTION DETECTED
      ISTOP=1
      GO TO 0001
 1019 CALL MMULT(ABAR,2,6,DEP,6,1,1.0,DFEP)
 1020 CALL POLAR1(ALBAR(1,1),ALBAR(2,1),AL1,RHO)
      CALL POLAR1(ALBAR(1,2),ALBAR(2,2),AL2,PSI)
      CALL POLAR1(DFEP(1),DFEP(2),DFE,OMEG)
 1029 IF(OMEG.GT.RHO .AND. OMEG.LT.PSI)GO TO 1030
      IF(OMEG.GT.-(TWOPI/4.) .AND. OMEG.LE.RHO)GO TO 1040
      IF(OMEG.GE.PSI .AND. OMEG.LT.(TWOPI/2.))GO TO 1050
      GO TO 1300
C/////ECP MODE ACTIVE
 1030 DLAMC=DFE*AL2/ALCAP*SIN(PSI-OMEG)
      DLAMP=DFE*AL1/ALCAP*SIN(OMEG-RHO)
      DWC=DLAMC*HC
      DWP=DLAMP*HP
      ALFAC=1.0/ALCAP
      ALBARI(1,1)=ALBAR(2,2)
      ALBARI(1,2)=-ALBAR(1,2)
      ALBARI(2,1)=-ALBAR(2,1)
      ALBARI(2,2)=ALBAR(1,1)
      CALL MSCALR(ALBARI,2,2,ALFAC,ALBARI)
      CALL MMULT(ALBARI,2,2,ABAR,2,6,1.0,BBAR)
```

```
      GO TO 1800
C/////EC MODE ACTIVE
 1040 DLAMC=DFEP(1)/ALBAR(1,1)
      DWC=DLAMC*HC
      CALL MTMULT(DFCPDS,6,1,ACE,6,6,1.0,A1)
      ALFAC=1.0/ALBAR(1,1)
      CALL MSCALR(A1,1,6,ALFAC,B1)
      GO TO 1600
C/////EP MODE ACTIVE
 1050 DLAMP=DFEP(2)/ALBAR(2,2)
      DWP=DLAMP*HP
      CALL MTMULT(DFPPDS,6,1,ACE,6,6,1.0,A2)
      ALFAC=1.0/ALBAR(2,2)
      CALL MSCALR(A2,1,6,ALFAC,B2)
      GO TO 1700
C
C      STRESS POINT ON COLLAPSE YIELD SURFACE
C
 1100 CALL MADD(SIG,6,1,AMCOL,1.0,(2.*(AR-1.)*SOCT),DFCPDS)
      CALL MSCALR(DFCPDS,6,1,1.0,DGCDS)
      DFCDPDW=ATMC/(ACC*APC)*(AFCDP/ATMC**2)**(1.-APC)
     -1)*2.*AFCP
      DSQ(1,1)=DFCDPDW*HC
      CALL MTMULT(DFCPDS,6,1,ACE,6,6,1.0,A1)
      CALL MMULT(A1,1,6,DGCDS,6,1,1.0,AL11)
      AL11=AL11+DSQ(1,1)
      ALFAC=1.0/AL11
      CALL MSCALR(A1,1,6,ALFAC,B1)
      CALL MMULT(B1,1,6,DEP,6,1,1.0,DLAMC)
      DWC=DLAMC*HC
      IF(DWC.GT.0.0) GO TO 1600
      GO TO 1800
C
C      STRESS POINT ON EXPANSIVE YIELD SURFACE
C
 1200 RF1=F1(J2,J3,SOCT)
      RF2=F2(J2,J3,SOCT)
      RF3=F3(J2,SOCT)
      RG1=G1(AETA2,SOCT)
      RG2=G2(J2,J3)
      RG3=G3(J2)
      CALL ARAFUNC(J2,RF1,RF2,RF3,SDEV,SCOF,DFPPDS)
      CALL ARAFUNC(J2,RG1,RG2,RG3,SDEV,SCOF,DGPDS)
      DFP2P=DFP2PDW(AWP)
      IF(AWP.GT.AWPPK)DFP2P=DFP2P*AWSOFT
      HP=-RG1*3.*SOCT +2*RG2*J2 -3*RG3*J3
      DSQ(2,2)=DFP2P*HP
      CALL MTMULT(DFPPDS,6,1,ACE,6,6,1.0,A2)
      CALL MMULT(A2,1,6,DGPDS,6,1,1.0,AL22)
      AL22=AL22+DSQ(2,2)
      ALFAC=1.0/AL22
      CALL MSCALR(A2,1,6,ALFAC,B2)
      CALL MMULT(B2,1,6,DEP,6,1,1.0,DLAMP)
      DWP=DLAMP*HP
      IF(DWP.GT.0.0) GO TO 1700
C
C       ELASTIC STRESS INCREMENT
```

```
      C
       1300 CALL MMULT(ACE,6,6,DEP,6,1,1.,DSIG)
       1304 CALL MADD(SIG,6,1,DSIG,1.,1.,SIG)
            MTYPE=0
       1305 CALL ARAINV(SIG,SDEV,SCOF,J2,J3,SOCT,TOCT,COS3W)
      C
      C     IF ELASTIC TRIAL EXCEEDS THE EXPANSIVE YIELD SURFACE NEAR THE
      C     APEX, CORRECT STRESS POINT BACK AT CONSTANT SOCT
      C
       1306 IF(DWP.LT.0.0 .OR. DWC.LT.0.0)GO TO 1319
            IF(EFAC.LE.0.0)GO TO 1319
            NK=0
            EFCP=FCP(SOCT,TOCT)
            EFC2P=FC2P(AWC)
            EFPP=FPP(SOCT,TOCT,COS3W)
            EFP2P=FP2P(AWP)
            IF(AWP.GT.AWPPK)EFP2P=EFP2P*AWSOFT+FP2P(AWPPK)*(1.0-AWSOFT)
       1307 IF((EFC2P-EFCP).GT.TOL2)GO TO 1308
            NK=1
       1308 IF((EFP2P-EFPP).GT.TOL2)GO TO 1309
            IF(NK.EQ.0)NK=2
            IF(NK.EQ.1)NK=3
       1309 CONTINUE
            IF(NK.EQ.0)GO TO 1319
            IF((((SIG(1)+SIG(2)+SIG(3))/3.0)+APEX).GT.ATMO/10)GO TO 1315
       1310 RATIO=TOCTFF(SOCT,AFP2P)/TOCT
            DO 1312 I=1,3
            SDEV(I)=SDEV(I)*RATIO
       1312 SIG(I)=SDEV(I)+SOCT
       1314 CALL ARAINV(SIG,SDEV,SCOF,J2,J3,SOCT,TOCT,COS3W)
            GO TO 1319
      C
      C     IF STRESS POINT EXCEEDS EITHER YIELD SURFACE BEYOND THE APEX,
      C     SUBCYCLE BASED ON THE RATIO F'/F". PRE-EXISTING OVERSHOOT
      C     CANNOT BE CORRECTED AND IS SUBTRACTED OUT.
      C
       1315 IF(NSUB.EQ.0)GO TO 1316
            GO TO 3011
       1316 OVSHOOT=AMAX1((EFPP/EFP2P-FPPSAV/FP2PSAV),
           *                (EFCP/EFC2P-FCPSAV/FC2PSAV))
            IF(OVSHOOT.GT.640)GO TO 3105
       1317 NSUB=MAX0(2,(IFIX(50.*OVSHOOT)-49))
            GO TO 3107
       1319 CONTINUE
      C
      C     COLLAPSE YIELDING ONLY STRESS INCREMENT
      C
       1600 AWC=AWC+DWC
            CALL MADD(ARAEC,6,1,DGCDS,1.0,DLAMC,ARAEC)
            CALL MMULT(ACE,6,6,DGCDS,6,1,1.0,ACEG)
            CALL MMULT(ACEG,6,1,B1,1,6,1.0,ACEP)
            CALL MADD(ACE,6,6,ACEP,1.0,-1.0,ACEP)
            CALL MMULT(ACEP,6,6,DEP,6,1,1.0,DSIG)
            CALL MADD(SIG,6,1,DSIG,1.,1.,SIG)
            MTYPE=1
            GO TO 2000
      C
```

```
C       EXPANSIVE YIELDING ONLY STRESS INCREMENT
C
 1700 AWP=AWP+DWP
      CALL MADD(ARAEP,6,1,DGPDS,1.0,DLAMP,ARAEP)
      CALL MMULT(ACE,6,6,DGPDS,6,1,1.0,ACEG)
      CALL MMULT(ACEG,6,1,B2,1,6,1.0,ACEP)
      CALL MADD(ACE,6,6,ACEP,1.0,-1.0,ACEP)
      CALL MMULT(ACEP,6,6,DEP,6,1,1.0,DSIG)
      CALL MADD(SIG,6,1,DSIG,1.,1.,SIG)
      MTYPE=2
      GO TO 2000
C
C       COMBINED COLLAPSE AND EXPANSIVE YIELDING STRESS INCREMENT
C
 1900 AWC=AWC+DWC
      AWP=AWP+DWP
      CALL MADD(ARAEC,6,1,DGCDS,1.0,DLAMC,ARAEC)
      CALL MADD(ARAEP,6,1,DGPDS,1.0,DLAMP,ARAEP)
      CALL MMULT(ACE,6,6,DBAR,6,2,1.0,TCEP)
      CALL MMULT(TCEP,6,2,BBAR,2,6,1.0,ACEP)
      CALL MADD(ACE,6,6,ACEP,1.0,-1.0,ACEP)
      CALL MMULT(ACEP,6,6,DEP,6,1,1.0,DSIG)
      CALL MADD(SIG,6,1,DSIG,1.,1.,SIG)
      MTYPE=3
      GO TO 2000
C
C       DETERMINE END-OF-INCREMENT (OR SUBINCREMENT) STRESS STATE
C
 2000 CALL ARAINV(SIG,SDEV,[illegible],SOCT,TOCT,COS3W)
C
C       CHECK FOR FP CONSISTENCY - SUBCYCLE IF NOT ADEQUATELY SATISFIED
C
 3000 IF(MTYPE.LT.2 .AND. NSUB.EQ.0)GO TO 5000
 3010 IF(NSUB.EQ.0)GO TO 3100
 3011 ISUB=ISUB+1
      IF(ISUB.GT.NSUB)GO TO 5000
C       CHECK SPALL FOR EACH SUB-INCREMENT
      IF(SOCT.GE.-(APEX))GO TO 3015
      GO TO 6001
 3015 GO TO 700
C/////DETERMINE NO. OF SUBCYCLES BASED ON RATE OF CHANGE OF DFP2PDW
 3100 BFPP=FPP(SOCT,TOCT,COS3W)
      BFP2P=FP2P(AWP)
      IF(AWP.GT.AWPPK)BFP2P=BFP2P*AWSOFT+FP2P(AWPPK)*(1.0-AWSOFT)
      FPDIFF=BFP2P-BFPP
      IF(FPDIFF.GE.-(TOL2))GO TO 5000
      AWPSAV=STATSAV(3)
      DW1=DFP2PDW(AWPSAV)
      DW2=DFP2PDW(AWP)
      IF(DW2.GT.SMLNUM)GO TO 3104
      IF(DW1.GT.SMLNUM)NSUB=1000
      IF(DW1.LT.SMLNUM)NSUB=2
      GO TO 3109
 3104 OVSHOOT=DW1/DW2
      IF(OVSHOOT.LT.640.)GO TO 3106
 3105 NSUB=1000
      GO TO 3109
```

```
      3106 NSUB=IFIX(50.*OVSHOOT)-49
      3107 NSUB=MIN0(NSUB,1000)
      3108 IF(NSUB.LE.1)GO TO 5000
      3109 RSUB=1./NSUB
           CALL MSCALR(DEPI,6,1,RSUB,DEP)
           CALL MSCALR(SIGI,6,1,1.0,SIG)
      3300 DO 3310 I=1,NSVAR(10)
      3310 STATE(I)=STATSAV(I)
           ISUB=1
           ASOCT=STATE(1)
           AWC=STATE(2)
           AWP=STATE(3)
           AJ2=STATE(4)
           ASPALL=STATE(5)
           ACONFP=STATE(6)
           APVAP=STATE(9)
           GO TO 3001
C
C          TENSILE FAILURE - SET STRESSES AND TRACK SPALL STRAIN
C
      6000 IF(ITEST.EQ.2)GO TO 7000
      6002 IF(SDOT.GT.-(APEX))GO TO 7000
      6001 CONTINUE
      6003 DO 6005 I=1,3
      6004 SIG(I)=-APEX
      6005 SIG(I+3)=0.0
           IF(NSUB.GT.0)GO TO 6006
           ASPALL=ASPSAV+(DEPI(1)+DEPI(2)+DEPI(3))
           GO TO 6007
      6006 ASPALL=ASPSAV+AMIN1(0.0,((NSUB-ISUB+1)*(DEP(1)+DEP(2)+DEP(3))))
      6007 MTYPE=-1
C
C          ENERGY DEPENDENT PRESSURE CONTRIBUTION
C            THE GAM RELATIONSHIP IS EMPIRICAL WITH UNIT-DEPENDENT CONSTANTS.
C            UNITS ARE GMS, TERGS, MBAR (C-G-MS).  DENSITY AND ENERGY ARE
C            CONVERTED TO GM/CC AND TERGS/GM PRIOR TO ENTERING THIS EQUATION
C            GAM ITSELF IS DIMENSIONLESS.
C
      7000 IF(AHE.NE.1.0)GO TO 7900
      7250 DPSOLE=0.0
           DPVAPR=0.0
           DPVAPE=0.0
           IF(EFAC.GE.0.0)GO TO 7300
           EEX=EXP(EFAC)
           ESTAR=(ENGN-AEMELT)*(1.-EEX)
           DD=AMAX1(DMN,DENS*DENCONV(IUNITS))
           EE=AMAX1(ESTAR,AEMELT)/(DD*ENGCONV(IUNITS))
           GAM=(0.35*ALOG10(EE)-0.464)**2 + 0.40 + 0.12*ALOG10(DD)
           APVAP=GAM*DENS*ESTAR
      7300 CONTINUE
C
C          MODIFY STRESS TENSOR TO REFLECT HP EOS:
C          (1) ADD VAPOR PRESSURE TO STRESS TENSOR
C          (2) REDUCE DEVIATOR STRESSES DUE TO PARTIAL OR FULL MELTING
C              AND RECALCULATE STRESS TENSOR
C
      7400 DO 7420 I=1,6
```

```
      SDEV(I)=SDEV(I)*AMAX1(EFAC,0.0)
 7420 SIG(I)=SDEV(I)+(SOCT+APVAP)*AMCOL(I)
      BMODN=(SOCT+APVAP-SOCTSAV)/DEV
C
 7900 CONTINUE
C
 9000 CONTINUE
C
C     SUM STRAIN COMPONENTS
C
 9100 CALL MADD(ARAET,6,1,DEP,1.0,1.0,ARAET)
      CALL MADD(ARAET,6,1,ARAEC,1.0,-1.0,ARAEE)
      CALL MADD(ARAEE,6,1,ARAEP,1.0,-1.0,ARAEE)
 9300 CONTINUE
C
C     SAVE MAXIMUM CURRENT MODULII FOR COURANT CONDITION
C     TIMESTEP CALCULATION
C
 9600 IF(MTYPE.EQ.2)GO TO 9650
      CMODN=AMAX1(ACEP(1,1),ACEP(2,2))
      CMODN=AMAX1(CMODN,ACEP(3,3))
      GO TO 9680
 9650 CMODN=ACE(1,1)
 9680 BMODN=AMAX1(ATMO,(CMODN*(1-APOI)/(3*(1-APOI))))
      GMODN=AMAX1(ATMO,(CMODN*(1-2*APOI)/(2*(1-APOI))))
 9690 CONTINUE
C
C     SIGN CHANGE
C
 9700 CALL MSCALR(SIG(4),3,1,1.0,SQRT2,SIG(4))
 9701 CALL MSCALR(SIG,6,1,-1.0,SIGO)
 9702 CALL MSCALR(DEPI,6,1,-1.0,DEPI)
C
C     SAVE STATE VARIABLES
C
 9800 STATE(1)=ASOCT
      STATE(2)=AWC
      STATE(3)=AWP
      STATE(4)=AJ2
      STATE(5)=ASPALL
      STATE(6)=ACONFP
      STATE(7)=AEV
      STATE(8)=ASPENG
      STATE(9)=APVAP
C
 9999 RETURN
      END
```

APPENDIX B

LISTING OF SEM-STEALTH 2D INTERFACE UPDATES

```
*version semlink
   updates used by applied research assoc., albuquerque, nm
*l none*
*n none*
*/
*/         this file contains the atlas update cards
*/         for stealth2d version 4-1d, as specified:
*/
*/         bigxxx - grid size adjustments to common blocks
*/         addxxx - add variables to stealth common blocks
*/         semxxx - stealth 2d link with soil element model
*/            semlnk - programmatic interface
*/            seminp - mods to material input cards for sem input
*/            semstn - engineering strain increments
*/            semmod - zonusr routine for calling sem models
*/            semovb - overburden initialization using sem models
*/         gamxxx - substitution of gamma-law gas for jwl eos
*/         bswxxx - boundary control switches - problem dependent
*/         prpxxx - pressure loading function in 'myfno'
*/         lysxxx - lysmer non-reflecting boundary
*/         actxxx - activity check based on volumetric strain rate
*/         matxxx - matinp changes for resart material model changes
*/         sbcxxx - error flags for subcycling control
*/         sldxxx - corrections to slideline search algorithms
*/
*/         file created : 13 december 1984
*/         last changes : 30 july 1985
*/
*/         use oldps and binary for  stealth version 4-1d
*/
*/         stealth version 4-1d is located on the following cfs path:
*/             /0000536/twod/stealth/cc/seismic2.xx
*/
*/         contact bill dass for info on this file (919)876-0018
*/
*/
*/
*/ ***********************************************************
*/ **                                                      ***
*/ **              file: bigxxx                            ***
*/ **                                                      ***
*/ ***********************************************************
*/
*/
*/         adjustment of maximum grid size
*/
*d maxi/1
65
*/ 51
*d maxj/1
45
*/ 4
*/
*/
*/ ***********************************************************
*/ **                                                      ***
*/ **              file: addxxx                            ***
*/ **                                                      ***
*/ ***********************************************************
*/
```

```
*/    update stealth zonary/var to include more extra variables
*/    and to track original zone dimensions
*/
*i zonary2/16
     * ex7(&maxi&,4), ex8(&maxi&,4), ex9(&maxi&,4),
     * xd0(&maxi&,4), yd0(&maxi&,4),
*i zonvar/13
     * ex7o,ex7n,ex8o,ex8n,ex9o,ex9n,xd0o,xd0n,yd0o,yd0n,
*i gptnew2/117
c     ex7(ic,jb)=0.0
c     ex8(ic,jb)=0.0
      ex9(ic,jb)=0.0
*i zonold2/78
      ex7o=ex7(ic,jc)
      ex8o=ex8(ic,jc)
      ex9o=ex9(ic,jc)
      xd0o=xd0(ic,jc)
      yd0o=yd0(ic,jc)
*i zonnew2/98
      ex7n=ex7o
      ex8n=ex8o
      ex9n=ex9o
      ex7(ic,jb)=ex7n
      ex8(ic,jb)=ex8n
      ex9(ic,jb)=ex9n
      xd0(ic,jb)=xd0o
      yd0(ic,jb)=yd0o
*/
*/    update matary to re-include heat variables
*/
*i matary/21
      common/matary/
     *    macon(10),
     *    acon0(10),acon1(10),acon2(10),acon3(10),acon4(10),
     *    acon5(10),acon6(10),acon7(10),acon8(10),acon9(10),
     *    mashc(10),
     *    ashc0(10),ashc1(10),ashc2(10),ashc3(10),ashc4(10),
     *    ashc5(10),ashc6(10),ashc7(10),ashc8(10),ashc9(10),
     *    maexr(10)
*i matvar/27/
     *    mexr,
*/
*/ ************************************************************
*/ **                                                        ***
*/ **              file: semlnk                              ***
*/ **                                                        ***
*/ ************************************************************
*/
*/
*/    ***** afwl stealth version 4-1d link with soil element model
*/
*/        soil element model common blocks
*/
*string constant
      common /constant/wonthd,toothd,sqrt2,sqrt3,sqrt6,sqrt23,
     1                 twopi,bigpos,bigneg
*string number
      common /number/  itest,iundr,iskip,jprint,jplot,iplt(30),kount,
     1                 iexec,iprob,nprob,isave(10),jsave,nparam(11),
     2                 nsvar(11),patm(8),nfin1,nfin2,nfin3,nfin4,nfin5,
```

```
     3                                     nfot1,nfot2,nfot3,nfot4,nfot5
*string energy
      common /energy/  engd
*string tens
      common /stress/  sigx,sigy,sigz,sigxy,sigyz,sigxz,p,ep,s(3)
      common /strain/  epsx,epsy,epsz,epsxy,epsyz,epsxz,e(3)
*string strinc
      common /strinc/  depsx,depsy,depsz,depsxy,depsyz,depsxz
*string allmod
      common /allmod/  ieos,iunits,atmo,conv,rhoref,mtype,gr,grp,
     1                 bsp(3),vstn(3),bmodn,gmodn,state(10)
*string prop0
      common /prop0/   mloc(11),prop(1)
*string prop1
      common /prop1/   bulk3,shear3
*string prop2
      common /prop2/   bulk1,bulk2,c1,shear1,shear2,cs1
*string prop3
      common /prop3/   bulk,shear,ca,cb,cc,cam,tcut1,fcut1,rule,esp
*string prop4
      common /prop4/   rub,ru,gamc,tauc,tauy,gmax,gamo,bulk4
*string prop5
      common /prop5/   aki,ak1,ak2,akim,ak1m,ak2m,agi,ag1,ag2,ag3,ag4,
     1                 ac,am,bb,ccc,ari,ar1,ar2,aw,ad,akh,akhm,el
*string prop6
      common /prop6/   rnls,rnus,bkl(8),ebl(8),pol(8),bku(8),
     1                 pbu(8),pou(8),st1,y1,s1,vm1,fstype,st2,y2,
     2                 s2,vm2,sptype,pxcut,pycut,pzcut,rihe,emelt,cte,
     3                 pbl(8),ebu(8),evmax,evgrav,espall,epl(3)
*string prop7
      common /prop7/   ekur,en,pois,c,pc,eta1,curvm,r,ss,t,alpha,
     1                 beta,pw,elw,q,wppk,a,b,sigma3,wc,wp
*string prop8
      common /prop8/   hk,hkur,hn,hc,hrf,hphi,hkb,hkbur,hg,hf,hd,
     1                 hsigma3,hei,heur,hfsdiff,hnui,heamax,hevmax
*string prop9
      common /prop9/   exa,exw,ejr1,exb,ejr2,vdet,rlvcj,
     1                 tact,dact,exe,exv
*string prop10
      common /prop10/  akur,an,apoi,acrv,aacc(4),aapc(4),abrk(3),
     1                 ar,aey,amy,aeta1,apbar,al,aalph,abeta,
     2                 atg,arg,asg,apex,ahswtch,aha,ahn,ahlam,ahgam,
     3                 ahbet,aconfp,asoct,acc,apc,awppk,aq,aa,ab,
     4                 aeta20,awc,awp,fp2ptyp,awsoft,aj2,aetar,ahy
*string prop11a
      common /prop11/  pcon(175),wgmax,emuz,umax,umin,gpsz,volc,eng
*/
*/    update stealth program card to include sem i/o units
*d stealth/1-6
      program stealth(stlinp,tape5=stlinp,stlout,tape6=stlout,
     *                fiche,tape20=fiche,stdlib,tape31=stdlib,
     *                usrlib,tape32=usrlib,matlib,tape37=matlib,
     *                tape7,tape8,tape9,tape10,tape11,tape12,
     *                tape13,tape14,tape15,tape16,tape17)
c
*i stealth/73
c
c     insert sem common into stealth as contiguous block
c
&number&
```

```
&constant&
&prop0&
&prop1&
&prop2&
&prop3&
&prop4&
&prop5&
&prop6&
&prop7&
&prop8&
&prop9&
&prop10&
&prop11a&
c
c
c     initialize soil element model constants and unit numbers
c
      wonthd=1./3.
      toothd=2./3.
      sqrt2=sqrt(2.)
      sqrt3=sqrt(3.)
      sqrt6=sqrt(6.)
      sqrt23=sqrt(toothd)
      twopi=8.*atan(1.)
      bigpos=1.0e90
      bigneg=-1.0e90
c
      nfin1 = 5
      nfot1 = 6
      nfin2 = 37
      nfin3 = 38
      nfin4 = 39
      nfin5 = 40
      nfot2 = 6
      nfot3 = 39
      nfot4 = 41
      nfot5 = 42
      iexec = 1
      itest = 10
c
*/ **************************************************************
*/ **                                                         ***
*/ **             file: seminp                                ***
*/ **                                                         ***
*/ **************************************************************
*/
*/
*/             input changes for sem material models
*/
*i matset/15
c
&zonary2&
&number&
&allmod&
&prop0&
c
*d matset/19
     *          namcap(80),nameng(80),namsem(80,11)
*d matset/51-62
c     set up names for sem models  mmdl=-1 thru -11
```

```
      data (namsem(i,1),i=1,80)/
     *    1he, 1hl, 1ha, 1hs, 1ht, 1hi, 1hc, 73*1h /
      data (namsem(i,2),i=1,80)/
     *    1hv, 1hi, 1hs, 1hc, 1ho, 75*1h /
      data (namsem(i,3),i=1,80)/
     *    1he, 1hl, 1hp, 1hl, 1ha, 75*1h /
      data (namsem(i,4),i=1,80)/
     *    1hp, 1hy, 1hk, 1he, 76*1h /
      data (namsem(i,5),i=1,80)/
     *    1hc, 1ha, 1hp, 77*1h /
      data (namsem(i,6),i=1,80)/
     *    1ha, 1hf, 1hw, 1hl, 76*1h /
      data (namsem(i,7),i=1,80)/
     *    1hl, 1ha, 1hd, 1he, 76*1h /
      data (namsem(i,8),i=1,80)/
     *    1hh, 1hy, 1hp, 1he, 1hr, 75*1h /
      data (namsem(i,9),i=1,80)/
     *    1hj, 1hw, 1hl, 77*1h /
      data (namsem(i,10),i=1,80)/
     *    1ha, 1hr, 1ha, 1hl, 76*1h /
      data (namsem(i,11),i=1,80)/
     *    1hw, 1ha, 1hg, 1hn, 1he, 1hr, 74*1h /
*d matset/143-210
c
 2000 imdl =iabs(mmdl)
      ieos=imdl
      maeos(1)=9
      mayld(1)=9
      mashr(1)=9
      mmmat(1)=-1
      mmat=mmmat(1)
 2100 do 2105 ln=1,80
 2105 nammdl(ln,1) = namsem(ln,ieos)
c
*d matset/224
 3100 call inpeos
      read(nfin1,3105)(nammat(ll,lmat),ll=1,80)
 3105 format(80a1)
c
c     store reference density and initial geostatic pressure
c
      ardn(lmat)=rhoref
      acoh(lmat,1)=grp
c
c     store model parameters (80max) in matary
c
 3200 do 3205 ii=1,nparam(ieos)
      rskip=(ii-1)/10
      iiskip=ifix(rskip)
      if(iiskip.ge.4)iiskip=iiskip+1
      locary=10*(ii-1+iiskip)+lmat
 3205 aeos0(locary)=prop(mloc(ieos)+ii)
c
*/
*/ ***********************************************************
*/ **                                                      ***
*/ **              file: semstn                            ***
*/ **                                                      ***
*/ ***********************************************************
*i zonstn2/66
```

```
&strinc&
*i zonstn2/108
c
c     calculate engineering x-y strain increments for sem models
c
      facx=0.5*dlth/xd0o
      facy=0.5*dlth/yd0o
      depsx=facx*((xvlhbr-xvlhtl)+(xvlhtr-xvlhbl))
      depsy=facy*((yvlhtl-yvlhbr)+(yvlhtr-yvlhbl))
      depsxy=facx*((yvlhbr-yvlhtl)+(yvlhtr-yvlhbl)) +
     *       facy*((xvlhtl-xvlhbr)+(xvlhtr-xvlhbl))
      depsyz=0.0
      depsxz=0.0
*i zonstn2/139
c     translational plane strain
      depsz=0.0
*i zonstn2/143
c     axial
      depsz=vsrh*dlth-depsx-depsy
c
*/ *************************************************************
*/ **                                                        ***
*/ **              file: semmod                              ***
*/ **                                                        ***
*/ *************************************************************
*i zonusr/15
c
c     make call to sem model in zonusr
c
&matary&
&timvar&
&number&
&tens&
&strinc&
&energy&
&allmod&
&prop0&
c
c     array locations for extra (state) variables ex1-9 in zonvar
      dimension exg(18)
      equivalence (exg(1),ex1o)
c
*d zonusr/22-41
c
      ieos=lmdl
      rhoref=rdn
c
c     set material properties in /prop/ from /matary/
c
  200 do 210 ii=1,nparam(ieos)
      rskip=(ii-1)/10
      iiskip=ifix(rskip)
      if(iiskip.ge.4)iiskip=iiskip+1
      locary=10*(ii-1+iiskip)+mpno
  210 prop(mloc(ieos)+ii)=aeos0(locary)
c
c     initialize material model state variables
c
  220 do 225 ii=1,nsvar(ieos)
      jj=ii*2-1
```

```
c          check for maxsbc exceeding allowable limit
  260 if(maxsbc.lt.30) go to 270
      write(nfmsg,1261) maxsbc
      write(nfprt,1261) maxsbc
 1261 format
     *      (10x,10h**********
     *      /10x,10h e r r o r
     *      /10x,27hmax subcycle limit exceeded
     *      /10x,8hmaxsbc= ,i10)
      nserr  = 4
      nsext  = 4
      go to 990
  270 dltn   = dltsbc
*/
*/
*/ ****************************************************************
*/ **                                                           ***
*/ **                file: sldxxx                               ***
*/ **                                                           ***
*/ ****************************************************************
*/
*/
*/
*/          slider modifications      83/03/16/14:05
*/
*/          debug of minimum search routine
*/
*d fndpta2/42
      if(lpta.ge.1.and.lpta.le.nlopp) go to 50
c
c          do minimum distance search of entire opposite grid
      dstsml = 0.5 * bignum
      do 25 ll=1,nlopp
      dsttry = (xpnf - xpnarg(ll,iopp)) ** 2
     *       + (ypnf - ypnarg(ll,iopp)) ** 2
      if(dsttry.gt.dstsml) go to 25
      dstsml = dsttry
      lanow  = ll
   25 continue
      go to 400
   50 continue
*i supget2/45
c
c          set left and right points to current point
      xpnl   = xpnf
      ypnl   = ypnf
      xpnr   = xpnf
      ypnr   = ypnf
*/
```

```
c
      go to 30
c
c     normal loop
c
   27 continue
c
*/
*/ *************************************************************
*/ **                                                        ***
*/ **                 file: matxxx                           ***
*/ **                                                        ***
*/ *************************************************************
*/
*/
*/
*/       atlas input for
*/
*/           modifications to matinp to
*/           allow changing of material models during restart.
*/
*/       file last changed 83/06/05/13:58:36
*/
*d matinp/98-99
      mmmdl(1)= mmdl
      if(mmdl.eq.0) go to 40
*/
*/
*/ ****************************************************************
*/ **                                                           ***
*/ **              file: sbcxxx                                 ***
*/ **                                                           ***
*/ ****************************************************************
*/
*/
*/
*/     update for minimum subcycle time step and
*/                maximum subcycles checks and stops
*/
*/     file last changed 83/03/15/20:20
*/
*d sbctim2/79
  200 if(dltn.ge.dltsbc) go to 270
*d sbctim2/83
c
c          check for subcycle time step less than minimum time step
  250 if(dltsbc.ge.dltmin) go to 260
      write(nfmsg,1251) dltmin, dltsbc
      write(nfprt,1251) dltmin, dltsbc
 1251 format
     *      (10x,10h**********
     *      /10x,10h e r r o r
     *      /10x,23hsubcycle time step less
     *      /10x,14hthan allowable
     *      /10x,8hdltmin= ,1pe12.5
     *      /10x,8hdltsbc= ,1pe12.5)
      nserr  = 4
      nsext  = 4
      go to 990
c
```

```
          rlv(ic,jb) = rlv(ic,jc)
          vsr(ic,jb) = vsr(ic,jc)
          com(ic,jb) = com(ic,jc)
          dns(ic,jb) = dns(ic,jc)
          zms(ic,jb) = zms(ic,jc)
          zie(ic,jb) = zie(ic,jc)
          zde(ic,jb) = zde(ic,jc)
          zse(ic,jb) = zse(ic,jc)
          zke(ic,jb) = zke(ic,jc)
          prh(ic,jb) = prh(ic,jc)
          avs(ic,jb) = avs(ic,jc)
          sss(ic,jb) = sss(ic,jc)
          trv(ic,jb) = trv(ic,jc)
          txx(ic,jb) = txx(ic,jc)
          tyy(ic,jb) = tyy(ic,jc)
          tzz(ic,jb) = tzz(ic,jc)
          txy(ic,jb) = txy(ic,jc)
          sxx(ic,jb) = sxx(ic,jc)
          syy(ic,jb) = syy(ic,jc)
          szz(ic,jb) = szz(ic,jc)
          pxx(ic,jb) = pxx(ic,jc)
          pyy(ic,jb) = pyy(ic,jc)
          pzz(ic,jb) = pzz(ic,jc)
          pxy(ic,jb) = pxy(ic,jc)
          epi(ic,jb) = epi(ic,jc)
          eps(ic,jb) = eps(ic,jc)
          yld(ic,jb) = yld(ic,jc)
          shr(ic,jb) = shr(ic,jc)
          ind(ic,jb) = ind(ic,jc)
          mpn(ic,jb) = mpn(ic,jc)
          ign(ic,jb) = ign(ic,jc)
          bfs(ic,jb) = bfs(ic,jc)
          act(ic,jb) = act(ic,jc)
          qda(ic,jb) = qda(ic,jc)
          ex1(ic,jb) = ex1(ic,jc)
          ex2(ic,jb) = ex2(ic,jc)
          ex3(ic,jb) = ex3(ic,jc)
          ex4(ic,jb) = ex4(ic,jc)
          ex5(ic,jb) = ex5(ic,jc)
          ex6(ic,jb) = ex6(ic,jc)
          ex7(ic,jb) = ex7(ic,jc)
          ex8(ic,jb) = ex8(ic,jc)
          ex9(ic,jb) = ex9(ic,jc)
          xd0(ic,jb) = xd0(ic,jc)
          yd0(ic,jb) = yd0(ic,jc)
c
c         energy check
c
          fac = zms(ic,jb) / rdn
          tie = tie + fac * zie(ic,jb)
          tde = tde +fac * zde(ic,jb)
          tke = tke + zke(ic,jb)
          tms = tms + zms(ic,jb)
          txm = txm + zms(ic,jb) * (xvl(ic,jb) + xvl(il,jb) +
     *                             xvl(ic,jw) + xvl(il,jw))
          tym = tym + zms(ic,jb) * (yvl(ic,jb) + yvl(il,jb) +
     *                             yvl(ic,jw) + yvl(il,jw))
          teg = tie + tke
c
          call timpro
```

```
c
*i propro2/58
c
&matvar&
c
&gptary2&
c
*i propro2/182
c
c     save the old activity check
c
      noro=nor(ic,jc)
      if(noro.gt.4)actblc=actsav
      if(noro.gt.3)actsav=act(ic,jb)
c
c     only test interior points
c
      if(nccyc.le.3)go to 27
      if(noro.ne.5)go to 27
c
c     test for activity
c
      actsum = act(il,jt) + act(ic,jt) + act(ir,jt)
     *       + act(il,jc) + act(ic,jc) + act(ir,jc)
     *       + actblc     + act(ic,jb) + act(ir,jb)
      if(abs(actsum).gt.1.0e-15) go to 27
c
c     no activity - set variables in /gptvar/
c
c     write(6,8027)nccyc,i,j,actsum
c8027 format('act...nccyc=',i3,' i,j',2i3,' actsum=',1pe10.3)
      xpnotl = xpnotr
      ypnotl = ypnotr
      xpnobl = xpnobr
      ypnobl = ypnobr
      xpnotr = xpn(ic,jc)
      ypnotr = ypn(ic,jc)
      xpnobr = xpn(ic,jb)
      ypnobr = ypn(ic,jb)
c
c     set variables in /gptary/
c
      xpn(ic,jb) = xpn(ic,jc)
      ypn(ic,jb) = ypn(ic,jc)
      zpn(ic,jb) = zpn(ic,jc)
      xvl(ic,jb) = xvl(ic,jc)
      yvl(ic,jb) = yvl(ic,jc)
      zvl(ic,jb) = zvl(ic,jc)
      xac(ic,jb) = 0.0
      yac(ic,jb) = 0.0
      zac(ic,jb) = 0.0
      gxk(ic,jb) = gxk(ic,jc)
      gyk(ic,jb) = gyk(ic,jc)
      nor(ic,jb) = nor(ic,jc)
      nbm(ic,jb) = nbm(ic,jc)
      nbv(ic,jb) = nbv(ic,jc)
c
c     set variables in /zonary/
c
      dll(ic,jb) = dll(ic,jc)
```

```
      delx=0.5*(xpn(iz,jz)-xpn(iz-1,jz)+xpn(iz,jzb)-xpn(iz-1,jzb))
      dely=0.5*(ypn(iz,jz)-ypn(iz-1,jz)+ypn(iz,jzb)-ypn(iz-1,jzb))
c
c      get sound speeds
c
      sssprh = sqrt(sss(iz,jz))
      if(j.eq.1) rdn=1750.
      rhoref=1900.
      sssshr = sqrt(shr(iz,jz)/rhoref)
c
c      set x and y direction dll and ssp
c
      dllx=abs(delx)
      dlly=abs(delx)
      sspx=sssprh
      sspy=sssshr
c
c      compute lysmer boundary terms
c
  200 trmx1 = sspx * dnsb / dnso * dlto / dllx
      trmy1 = sspy * dnsb / dnso * dlto / dlly
      trmx2 = 1.0-trmx1
      trmy2 = 1.0-trmy1
      trmx3 = 1.0+trmx1
      trmy3 = 1.0+trmy1
c
c      compute motion
c
  300 xvlh=(xvlm*trmx2+xaco*dlto)/trmx3
      yvlh=(yvlm*trmy2+yaco*dlto)/trmy3
      if(abs(xvlh).lt.xvlmin) xvlh=0.0
      if(abs(yvlh).lt.yvlmin) yvlh=0.0
      if(j.eq.ncrow) yvlh=0.0
c
c      recompute accelerations
c
       xaco=(xvlh-xvlm)/ dlto
       yaco = (yvlh - yvlm ) / dlto
c
c     lysmer boundary diagnostics
c
c     write(6,500)i,j,sspx,sspy,xaco,yaco,xvlh,yvlh
c 500 format('mybdy...i,j',2i3,' sspx,y',1p2e10.3,' x,yaco',1p2e10.3,
c 500+       ' x,yvlh',1p2e10.3)
c
*/ *************************************************************
*/ **                                                        ***
*/ **              file: actxxx                              ***
*/ **                                                        ***
*/ *************************************************************
*/
*/
*/     activity check based on volumetric strain rate
*/
*i zonstn2/130
c
c     set activity switch in zonstn
c
      actn=0.0
      if(abs(vsrh).gt.1.0e-15)actn=vsrh
```

```
*d myfno/26-27
      go to (100,200) iftyp
c
c            dihest pressure function
c
  100 if(var.gt.fca(3))go to 130
c
  120 val=fca(1)*exp(-fca(2)*var)*(1.0-var/fca(3))
      go to 900
c
  130 val=0.0
      go to 900
c
c     speicher-brode overpressure
c
  200 call spbrode(fca(1),fca(2),fca(3),fca(4),nccyc,var,val)
      go to 900
c
  900 continue
*/
*/ *************************************************************
*/ **                                                        ***
*/ **            file: lysxxx                                ***
*/ **                                                        ***
*/ *************************************************************
*/
*/
*/       lysmer non-reflecting boundary
*/
*d mybdy2/14
c
c      compute motion of lysmer non-reflecting boundary
c
c
&matvar&
c
&gptvar&
c
&zonvar&
c
&gptary2&
c
&zonary2&
c
&timvar&
*d mybdy2/20-21
c
c      set appropriate zone indices
c
      iz=ir
      if(ic.eq.ncgpt) iz=ic
      jz=jt
      jzb=jc
      if(noro.ge.7) jz=jc
      if(noro.ge.7) jzb=jb
c
c      get density and zone length
c
      dnso=dns(iz,jz)
      dnsb=dnso
```

```
c
c       dihest points may never have negative x-coordinates
c
      if(i.gt.1)go to 108
      if(j.ge.5.and.j.le.17)go to 110
  108 continue
*/
*/    control of boundaries for pseudo-1d calculations
*/
*/ *d gptbdy2/51
*/ c
*/ c     a pressure boundary has been specified
*/ c     lnbv = 1 for bottom-side pressure history (y-dir prop)
*/ c     lnbv = 4 for right-side pressure history (x-dir prop)
*/ c
*/    120 continue
*/      if(lnbv.eq.4) call gptprh(val,timo,lnbv)
*/      if(lnbv.eq.4) ex7n=val
*/ c
*/ *i gptmot2/225
*/ c
*/ c     no x-velocity at bottom-right wall-interacting grid point
*/ c
*/      if(noro.eq.3) xvlh=0.0
*/ c
*/ *i gptmot2/240
*/ c
*/ c     no y-velocity at top-left pressure-boundary grid point
*/ c
*/      if(noro.eq.7) yvlh=0.0
*/ c
*/ c     no y-velocity at bottom-left pressure-boundary grid point
*/ c
*/      if(i.eq.1 .and. j.eq.1) yvlh=0.0
*/ c
*/ c
*/ *i gptmot2/247
*/ c
*/ c     pressure bdy points may never have negative x-coordinates
*/ c
*/ c     if(i.eq.1)go to 110
*/ c
*d gptnew2/102-103
c
c      don't zero out zone interior variables used
c      for storing applied pressure and impulse
c
      ex7(ic,jb)=ex7n
      ex8(ic,jb)=ex8(ic,jb)+ex7n*dlth
c
*/ ****************************************************************
*/ **                                                           ***
*/ **                 file: prpxxx                              ***
*/ **                                                           ***
*/ ****************************************************************
*/
*/
*i myfno/21
      data iftyp /1/
*/
```

```
c
*d zonsss/112-116
c
c     sound speed squared
c
      sssprh = eos0*(eos0-1)*(zien/dnsn)
c
*/
*/
*/ ****************************************************************
*/ **                                                          ***
*/ **                file: bswxxx                              ***
*/ **                                                          ***
*/ ****************************************************************
*/
*/
*/       control of boundaries for simquake ii ff problem
*/
*i gptbdy2/25
c
&zonary2&
&zonvar&
c
*d gptbdy2/51
c
c     a pressure boundary has been specified
c     lnbv = 1 for bottom-side 1 atmosphere pressure application
c     lnbv = 2 for right side non-reflective boundary
c     lnbv = 5 for left-side pressure history
c
  120 continue
      if(lnbv.eq.1) val=101379.
      if(lnbv.eq.2) val=ex9(i,jx)
c     if(lnbv.eq.2) write(6,9000)i,j,val
c9000 format('gptbdy...i,j',2i3,' val=',1pe10.3)
      if(lnbv.eq.5) call gptprh(val,timo,lnbv)
      if(lnbv.eq.5) ex7n=val
      go to 121
  121 continue
c
*d gptmot2/226
c
c     no x-velocity at top-left grid point
c
      if(noro.eq.7) xvlh=0.0
      if(j.eq.45)yvlh=0.0
      if(j.eq.45)ypnn=ypno
   79 go to 400
c
*i gptmot2/240
c
c     non-reflective boundary along right side
c
      if(i.eq.ncgpt) call mybdy
c
c     no x-velocity at top-left grid point
c
      if(noro.eq.7) xvlh=0.0
c
*i gptmot2/247
```

```
     *           txxn,tyyn,tzzn,prhn,comi)
      sxxn=txxn+prhn
      syyn=tyyn+prhn
      szzn=tzzn+prhn
      if(grvy.gt.0.0)ex9n=-txxn
      if(grvx.gt.0.0)ex9n=-tyyn
      epsn=sqrt(amax1(atmo/100.,-2./3.*(sxxn*syyn+syyn*szzn+szzn*sxxn)))
      rlvn = comi + 1.0
 9340 do 9350 ii=1,nsvar(ieos)
      jj=ii*2-1
      exg(jj)=state(ii)
 9350 exg(jj+1)=state(ii)
      rlv(i,jt) = rlvn
      tyy(i,jt) = tyyn
      txx(i,jt) = txxn
      tzz(i,jt) = tzzn
      prh(i,jt) = prhn
      sxx(i,jt) = sxxn
      syy(i,jt) = syyn
      szz(i,jt) = szzn
      ex1(i,jt) = ex1n
      ex2(i,jt) = ex2n
      ex3(i,jt) = ex3n
      ex4(i,jt) = ex4n
      ex5(i,jt) = ex5n
      ex6(i,jt) = ex6n
      ex7(i,jt) = ex7n
      ex8(i,jt) = ex8n
      ex9(i,jt) = ex9n
      eps(i,jt) = epsn
      xd0n=0.5*((xpnntr-xpnnbl)+(xpnnbr-xpnntl))
      yd0n=0.5*((ypnntr-ypnnbl)+(ypnntl-ypnnbr))
      xd0(i,jt)=xd0n
      yd0(i,jt)=yd0n
c     if(i.eq.2)write(6,8001)i,jt,ieos,xpnntr,ypnntr,xd0n,yd0n,
c    *                  trefy,ttempy,grp,txxn,tyyn
c8001 format('i,jt,ieos',3i3,' x,ytr',1p2e10.3,' x,y0',1p2e10.3,
c8001+      /,'trefy,tty,grp',1p3e10.3,' txx,yy',1p2e10.3)
*d genchk2/357
      if(mmdl.lt.0) go to 380
*d genchk2/378-389
c
  380 continue
c
*/
*/
*/ ***********************************************************
*/ **                                                      ***
*/ **              file: gamxxx                            ***
*/ **                                                      ***
*/ ***********************************************************
*/
*/
*/        substitution of gamma-law gas for jwl eos
*/
*d zonprh/189-191
c
c     pressure-density-energy relationship
c
      prhn = (eos0-1)*zien
```

```
*/ **                                                            ***
*/ ****************************************************************
*/
*/
*/                 updates for overburden initializationy using sem models
*/                   assuming: i-lines are oriented in the y-direction
*/                             j-lines are oriented in the x-direction
*/                             application of gravity stress is uniaxial,
*/                              either in x or y direction, but not both
*/
*/
*i genchk2/58
&number&
&allmod&
&prop0&
*i genchk2/60
      dimension exg(18)
      equivalence (exg(1),exlo)
*/
*i genchk2/103
c
c     increment y-stress on row loop
c
      trefy = trefy + ttempy*2.0
c
c     initialize x-stress
c
      trefx = 0.0
      ttempx = 0.0
c
*i genchk2/104
c
c     increment x-stress on column loop
c
      trefx = trefx + ttempx*2.0
c
*i genchk2/262
c     note: gravity stresses only calculated once per depth(j-line)
      if(grvy.gt.0.0 .and. i.ne.2)go to 9340
      mnum = mpn(i,jt)
c     assume soil properties for explosive
c     if(mnum.eq.1) mnum=2.0
      ieos=-mmmdl(mnum)
      rdn = ardn(mnum)
      rhoref=rdn
      grp=acoh(mnum,1)
c     set matvar properties
      do 9310 ii=1,50
      rskip=(ii-1)/10
      iiskip=ifix(rskip)
      if(iiskip.eq.4)iiskip=5
      locary=10*(ii-1+iiskip)+mnum
 9310 prop(mloc(ieos)+ii)=aeos0(locary)
c     determine vertical stress due to gravity at zone mid-depth
      ttempy = -rdn*grvy*(ypnnbr-ypnntr)*0.5
      ttempx = -rdn*grvx*(xpnnbl-xpnnbr)*0.5
c     determine complete gravity induced state of stress
      if(grvy.gt.0.0)call gload(-grp,-grp,-grp,-(trefy+ttempy+atmo),
     *           tyyn,txxn,tzzn,prhn,comi)
      if(grvx.gt.0.0)call gload(-grp,-grp,-grp,-(trefx+ttempx+atmo),
```

```
  225 state(ii)=exg(jj)
c
c     initialize stresses
c
  230 ep=prho
      p =prho
      s(1)=sxxo
      s(2)=syyo
      s(3)=szzo
      sigxy=sxyo
      sigyz=syzo
      sigxz=sxzo
c
  240 call model
c
  250 prhn=ep
      sxxn=s(1)
      syyn=s(2)
      szzn=s(3)
      sxyn=sigxy
      syzn=sigyz
      sxzn=sigxz
c     track invariant shear stress in eps (zonary)
      epsn=sqrt(amax1(atmo/100.,(-2./3.*(s(1)*s(2)+s(2)*s(3)+s(3)*s(1)-
     *                sigxy**2/2.+sigyz**2/2.+sigxz**2/2.))))
c
c     calculate total stress at time n+1
      call zonstr
c
c     calculate change in distortional energy density
      call zonzde
      prhh=(prhn+prho)/two
c     calculate change in internal energy density
      zien=ziec-(prhh+avsh)*dlrlvh+dlzdeh
c
c     update material model state variables
  300 do 305 ii=1,nsvar(ieos)
      jj=ii*2
  305 exg(jj)=state(ii)
c
c     calculate sound speed squared at time n+1
  400 if(ieos.eq.9)go to 490
      sssn=(bmodn+4./3.*gmodn)/rhoref
      go to 500
  490 sssn= exa*exp(-ejr1*exv)*(ejr1*exv*exv*(1-exw/(ejr1*exv))
     *     -exw/ejr1)
     *     +  exb*exp(-ejr2*exv)*(ejr2*exv*exv*(1-exw/(ejr2*exv))
     *     -exw/ejr2)
     *     +  exw*(exe+prhn*exv)
c
c     save current bulk and shear modulii in zonary
c
  500 yldn=bmodn
      shrn=gmodn
```

END
DTIC
9- 86